HELSINKI UNIVERSITY OF TECHNOLOGY
Department of Computer Science and Engineering

Hannu Pulakka

Analysis of Human Voice Production Using Inverse Filtering, High-Speed Imaging, and Electroglottography

Master's Thesis submitted in partial fulfillment of the requirements for the degree of Master of Science in Technology.

Espoo, 14 February 2005

Supervisor: Professor Paavo Alku

HELSINKI UNIVERSITY OF TECHNOLOGY Department of Computer Science and Engineering		ABSTRACT OF MASTER'S THESIS	
Author:	Hannu Pulakka	**Date:**	14 February 2005
		Pages:	104 + 7
Title of thesis:	Analysis of Human Voice Production Using Inverse Filtering, High-Speed Imaging, and Electroglottography		
Professorship:	Language technology	**Professorship code:**	S-89
Supervisor:	Professor Paavo Alku		
Instructor:	Professor Paavo Alku		

Human voice production was studied using three methods: inverse filtering, digital high-speed imaging of the vocal folds, and electroglottography. The primary goal was to evaluate an inverse filtering method by comparing inverse filtered glottal flow estimates with information obtained by the other methods. More detailed examination of the human voice source behavior was also included in the work.

Material from two experiments was analyzed in this study. The data of the first experiment consisted of simultaneous recordings of acoustic speech signal, electroglottogram, and high-speed imaging acquired during sustained vowel phonations. Inverse filtered glottal flow estimates were compared with glottal area waveforms derived from the image material by calculating pulse shape parameters from the signals. The material of the second experiment included recordings of acoustic speech signal and electroglottogram during phonations of sustained vowels. This material was utilized for the analysis of the opening phase and the closing phase of vocal fold vibration.

The evaluated inverse filtering method was found to produce mostly reasonable estimates of glottal flow. However, the parameters of the system have to be set appropriately, which requires experience on inverse filtering and speech production. The flow estimates often showed a two-stage opening phase with two instants of rapid increase in the flow derivative. The instant of glottal opening detected in the electroglottogram was often found to coincide with an increase in the flow derivative. The instant of minimum flow derivative was found to occur mostly during the last quarter of the closing phase and it was shown to precede the closing peak of the differentiated electroglottogram.

Keywords: speech production, glottal flow, vocal fold vibration, digital high-speed imaging, inverse filtering, electroglottography

TEKNILLINEN KORKEAKOULU		DIPLOMITYÖN TIIVISTELMÄ
Tietotekniikan osasto		
Tekijä:	Hannu Pulakka	**Päiväys:** 14.2.2005
		Sivumäärä: 104 + 7
Työn nimi:	Ihmisen äänentuoton analysointi käänteissuodatuksen, suurnopeuskuvauksen ja elektroglottografian avulla	
Professuuri:	Kieliteknologia	**Koodi:** S-89
Työn valvoja:	professori Paavo Alku	
Työn ohjaaja:	professori Paavo Alku	

Ihmisen puheentuottoa tutkittiin kolmella menetelmällä: käänteissuodatuksella, äänihuulten digitaalisella suurnopeuskuvauksella ja elektroglottografialla. Päätavoitteena oli tarkastella erään käänteissuodatusmenetelmän toimintaa vertailemalla näillä menetelmillä saatua informaatiota äänihuulten värähtelystä. Lisäksi tutkittiin tarkemmin eräitä äänilähteen käyttäytymisen yksityiskohtia.

Tutkimuksessa analysoitiin aineistoa kahdesta koejärjestelystä. Ensimmäisessä kokeessa tallennettiin samanaikaisesti äänisignaali, elektroglottogrammi ja suurnopeuskuvamateriaalia äänihuulista koehenkilöiden tuottaessa pitkiä vokaaleita. Käänteissuodatuksella saaduista glottisvirtausestimaateista sekä kuvamateriaalin ilmaisemasta ääniraon pinta-alavaihtelusta laskettiin pulssiparametreja, joiden avulla vertailtiin virtauksen ja ääniraon pinta-alan käyttäytymistä. Toisen koejärjestelyn aineisto koostui äänisignaalista ja elektroglottogrammista, jotka oli tallennettu vokaaliääntöjen aikana. Tämän materiaalin perusteella analysoitiin ääniraon avautumis- ja sulkeutumisvaihetta.

Tarkastellun käänteissuodatusmenetelmän todettiin tuottavan enimmäkseen luotettavia virtausestimaatteja edellyttäen, että menetelmän parametrit asetetaan tarkoituksenmukaisesti, mikä vaatii käyttäjältä kokemusta käänteissuodatuksesta ja ihmisen puheentuotosta. Glottisvirtauksen avautumisvaiheen havaittiin olevan useissa virtausestimaateissa kaksivaiheinen siten, että virtauksen kasvu voimistuu nopeasti kahdessa kohdassa sulkeutumisen ja maksimivirtauksen välillä. Virtauksen kasvun todettiin usein voimistuvan elektroglottogrammista tunnistetun ääniraon avautumishetken lähellä. Virtauksen derivaatan minimikohdan havaittiin sijoittuvan enimmäkseen virtauksen sulkeutumisvaiheen viimeiseen neljännekseen, ja sen osoitettiin esiintyvän ennen elektroglottogrammin derivaatan minimikohtaa.

Avainsanat: puheentuotto, glottisvirtaus, äänihuulten värähtely, digitaalinen suurnopeuskuvaus, käänteissuodatus, elektroglottografia

Acknowledgements

This Master's thesis was carrier out in the Laboratory of Acoustics and Audio Signal Processing and Helsinki University of Technology. The research was supported by the Academy of Finland (project no. 205962).

In the first place, I want to thank my supervisor professor Paavo Alku for providing me the possibility to do my Master's thesis on this interesting topic. His professional knowledge and ideas as well as the encouraging feedback from him have been essential in this work.

I am also grateful to Svante Granqvist and Hans Larsson from KTH and the Huddinge University Hospital of the Karolinska Institute in Stockholm, Stellan Hertegård and Per-Åke Lindestad from the Huddinge University Hospital, Anne-Maria Laukkanen from the University of Tampere, Erkki Vilkman from the Helsinki University Central Hospital, and Paavo Alku, who carried out the data recording session at the Huddinge University Hospital. Especially, I want to thank Svante Granqvist for answering numerous technical questions regarding the material that was analyzed in this study. Svante Granqvist and Hans Larsson also allowed me to use computer programs they had developed for the analysis of high-speed image recordings.

Finally, I would like to thank Matti Airas for technical support and valuable comments on the work, Eva Björkner and Laura Lehto for their contribution, and Juho Kontio for proposing improvements to several graphical illustrations.

Otaniemi, 14 February 2005

Hannu Pulakka

Contents

Abbreviations

ClQ	Closing quotient (glottal pulse shape parameter)
DAP	Discrete all-pole modeling
DAT	Digital audio tape
DC	Direct current
DEGG	Differentiated electroglottogram
EGG	Electroglottography, electroglottogram
EMGG	Electromagnetic glottography
FFT	Fast Fourier transform
FGG	Flow glottogram
FM	Frequency modulation
GCI	Glottal closure instant
HUT	Helsinki University of Technology
IAIF	Iterative adaptive inverse filtering
LPC	Linear predictive coding
NAQ	Normalized amplitude quotient
OQ	Open quotient
PGG	Photoglottography
SEM	Standard error of the mean
SPL	Sound pressure level
SQ	Speed quotient

List of Figures

List of Tables

Chapter 1

Introduction

1.1 Background

The vocal folds are located in the larynx and they are an essential part of the human speech mechanism. During speech, the vibration of the vocal folds converts the air flow from the lungs into a sequence of short flow pulses. This pulse train, the glottal flow, provides the excitation signal of voiced speech sounds.

The vocal fold vibration cannot be directly measured with non-invasive methods because the larynx is not accessible during phonation. However, there are several indirect means of studying the function of the vocal folds. One of the methods is called inverse filtering, which is used to estimate the pulsating air flow produced by the vibrating vocal folds. At a minimum, only the speech signal captured with a microphone is required for the procedure. Electroglottography is another voice analysis method. It measures impedance variations across the neck of the subject during speech. This yields information about vocal fold vibration because the varying amount of contact between the vocal folds causes impedance fluctuation. Inverse filtering and electroglottography are non-invasive methods: they do not require surgery or internal examination of the body, nor do they prevent the subject from speaking normally.

High-speed video recording of the larynx provides visual information about the movements of vocal folds. It is, however, more invasive than inverse filtering and electroglottography because an endoscope has to be inserted into the nasal or the oral cavity of the subject. The endoscope is used to illuminate the larynx and to deliver the visual image of the vocal folds to a special high-speed camera.

The human voice production and especially the voice source has been an active research topic at the Laboratory of Acoustics and Audio Signal Processing at Helsinki University of Technology. One concrete outcome of the research has been the inverse filtering method

developed by professor Paavo Alku in the early 1990's. The method has been used in the laboratory and by other researchers. However, due to the complexity of measuring the physiological processes at the larynx, the validity of the method has not been thoroughly assessed.

The Huddinge University Hospital of the Karolinska Institute in Stockholm, Sweden, has a digital high-speed camera system that is capable of recording the vibration of vocal folds at a rate of nearly two thousand frames per second via an endoscope inserted to the subject's mouth. Experience on using the equipment for the imaging of human larynx is also available at the hospital. These facilities provide an excellent possibility to compare the air flow between the vocal folds, estimated by inverse filtering, with a simultaneously recorded high-speed image sequence. Moreover, electroglottography can also be combined with these two methods.

Based on this idea, a data collection session was organized as a co-operation project of Finnish and Swedish voice researchers at the Karolinska University Hospital in April 2003. High-speed video of the vocal folds, electroglottogram, and speech sound were recorded synchronously during several sample phonations from three subjects. The material was collected partly for the evaluation of the inverse filtering method, but the data were also meant to serve more general research on the voice source behavior as well as other future research projects.

At this point, it still took several months until the analysis of this material was decided as the topic of this Master's thesis and the work on the data began. Originally, the primary goal of the study was to evaluate the inverse filtering method. However, interesting phenomena of the voice source behavior were encountered during the study, which shifted the focus slightly. Studying the voice source behavior itself finally constituted an important part of this study.

Some analysis of existing data from another experiment was also included in the thesis. This data set allowed more exact comparison of inverse filtered flow waveform and electroglottogram, and provided some interesting results about the relationship between these two signals.

1.2 Structure of the Thesis

This chapter has presented some background about the work described in this thesis. Chapter 2 provides an introduction to the physiology of the human voice production mechanism as well as the fundamental source-filter theory of speech production. Chapter 3 introduces methods for analyzing the activity of the vocal folds during phonation. Chapter 4 describes how research material was obtained for this study and how data was processed.

In Chapter 5, both qualitative and quantitative results are derived from the material. Finally, Chapter 6 draws conclusions from the results and relates them to the findings of previous research.

Chapter 2

Physiological and Theoretical Background

This chapter describes the basic physiology of human speech production mechanism and presents the fundamental source-filter theory of voice production.

2.1 Physiology of Voice Production

The human voice production mechanism can be roughly divided into three parts: lungs, vocal folds, and vocal tract. The lungs function as a source of air flow and pressure. When voiced speech sound is being produced, the vocal folds (vocal cords) open and close periodically and thus convert the air flow from the lungs into a train of flow pulses, which functions as an acoustic excitation and the source of voiced speech. The vocal tract is a set of cavities above the vocal folds up to the mouth and nostrils. It functions as an acoustic filter that shapes the spectrum of the sound. Finally, sound is radiated to the surrounding air at the lips and nostrils. The human voice production mechanism is illustrated in Figure 2.1.

In addition to voiced sounds, human speech contains also unvoiced sounds, such as the fricative /s/, during which the vocal folds are not vibrating. These are, however, outside the scope of this thesis.

2.1.1 Vocal Folds

The vocal folds are soft, elastic tissue structures that are located horizontally in the larynx. The airspace between the vocal folds is called the *glottis* (Karjalainen, 2000). According to another definition, glottis refers to the structures that surround this space (Merriam-Webster, 2004).

The mechanism is supported and controlled by a large number of cartilages and muscles.

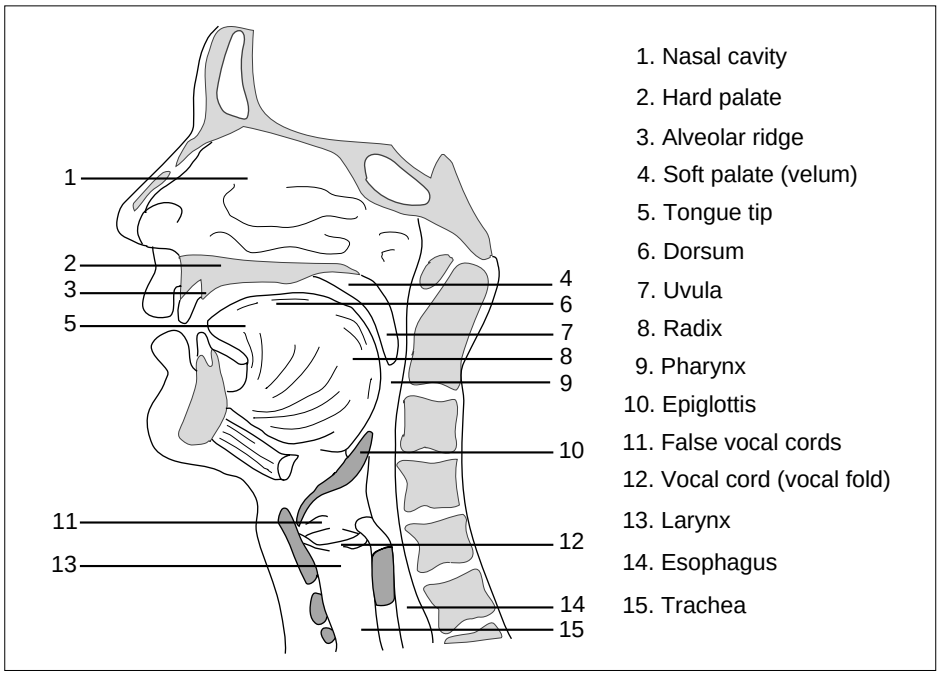

Figure 2.1: The human speech production mechanism. (Karjalainen, 2000)

The vocal folds are attached to the thyroid cartilage in their anterior ends and to the arytenoid cartilages at the posterior ends. The arytenoid cartilages can be moved by muscles in the larynx, which allows the width of the opening between the vocal folds to be varied. During respiration, the vocal folds are widely separated, or *abducted*, but in the phonation setting they are brought close to each other, *adducted*. Figure 2.2 shows images of the human glottis taken from above during respiration and voicing.

When air flows from the lungs through the narrow opening, the vocal folds start to oscillate. This vibration converts the air flow into a periodic train of flow pulses. These pulses are referred to as the *glottal flow*, or the *voice source*, and the process of generating the voiced excitation is called *phonation*.

The length and tension of the vocal folds can also be controlled by muscle action in order to regulate the oscillation frequency and voice quality. The vibrating vocal fold length is about 16 millimeters in an adult male and about 10 millimeters in an adult female, and the vocal folds can be stretched by a few millimeters by the action of the muscles in the larynx (Laukkanen & Leino, 1999).

The frequency of glottal vibration determines the fundamental frequency of speech, which is commonly denoted by f_0. The average speaking f_0 is approximately 120 Hz for men, 200 Hz for women, and even higher for children (Karjalainen, 2000). The range of

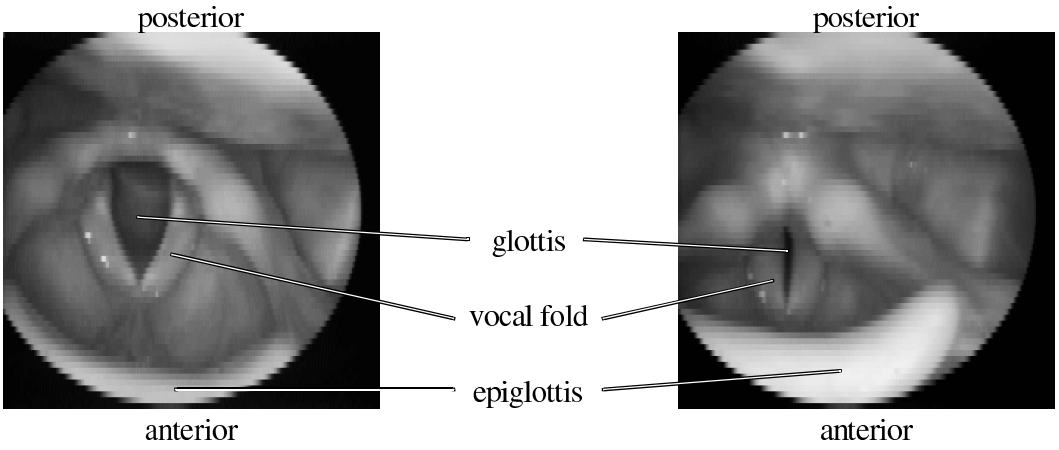

Figure 2.2: The larynx of a female subject seen from above during respiration (left) and phonation (right).

variation is large: Fundamental frequencies well below 100 Hz are not uncommon for men, but tenor singers may reach frequencies above 600 Hz. Women's lowest fundamental frequencies are below 150 Hz while the upper limit of a soprano's singing range may exceed 1300 Hz (Titze, 1994).

The vocal folds are composed of several layers with different stiffness properties. The topmost layer (*epithelium*) is a cover layer on top of mucosal tissue (*lamina propria*), which can be divided into three layers. The stiffness of the mucosal layers increases with depth. The innermost layer of the vocal folds is an elastic muscle (*musculus thyroarytenoideus*). Vibration occurs mainly in the mucosal part of the tissue. The oscillation itself does not require muscular work. It is maintained by air pressure variations and the elasticity of the tissues. However, muscles are used to bring the vocal folds together and to control their vibration properties. (Laukkanen & Leino, 1999)

Observations of vocal fold vibration using several techniques have revealed that the lower and upper portions of the vocal folds do not oscillate in phase. A wave propagates from the lower margins of the vocal folds towards the upper margins, which creates a wave-like motion traversing upwards in the vocal fold cover layer. This phenomenon is referred to as the *mucosal wave* and is illustrated in Figure 2.3. (Story, 2002).

Furthermore, opening and closure often do not occur simultaneously along the entire length of the vocal folds in the horizontal plane either. Instead, opening and closure often proceed from one end to the other in a zipper-like motion (Baken, 1992).

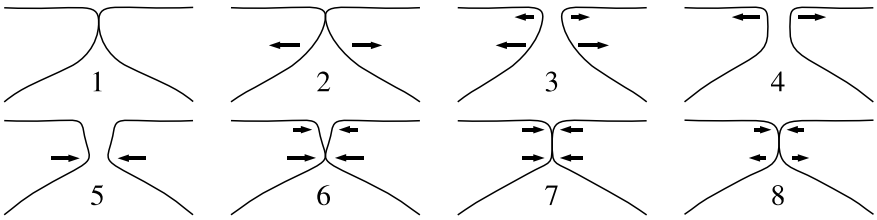

Figure 2.3: Cross profile of an idealized cycle of vocal fold vibration. The figure shows the mucosal wave, i.e., the phase difference between the upper and lower margin of the vocal folds. (Based on (Story, 2002))

2.1.2 Vocal Tract

The vibration of the vocal folds provides a spectrally rich acoustic excitation that is shaped by the cavities above the glottal source. The tube formed by larynx, pharynx, and oral cavity, is called the *vocal tract* (Karjalainen, 2000). Its average length is approximately 17 cm for men, 15 cm for women, and 14 cm for children (Claes *et al.*, 1998). According to another definition, the nasal cavity may also be included in the definition of vocal tract (Laukkanen & Leino, 1999).

The vocal tract is an adjustable acoustic filter that modifies the spectrum of the excitation signal. Each vowel sound has its characteristic spectral profile produced by vocal tract resonances, or *formants*. The formant frequencies depend on the shape of the vocal tract, which in turn is determined by the positions of the soft palate, tongue, jaw, and lips.

Vocal fold vibration and the glottal air flow are not affected much by the vocal tract shape. Therefore, the vocal tract is not considered in more detail in this thesis.

2.1.3 Registers and Phonation Modes

The vocal folds can vibrate in different configurations that differ in the length and thickness of the vocal folds and the muscular tensions involved. These modes are called *registers* or *laryngeal mechanisms* (Henrich *et al.*, 2004). Many different terms are used to describe them, which may lead to confusion. The two commonly used registers in speech and singing are often called *chest* or *modal* register, and *falsetto* register. Speech is normally produced in the modal register. The vocal folds are thick and vibrate along their entire length, the glottis is tightly closed during each cycle, and there is a vertical phase difference in vibration. In the falsetto register, the vocal folds are thin, the glottis is not necessarily completely closed, and there is no vertical phase difference. Higher fundamental frequencies can be obtained in the falsetto register than in the modal register. (Laukkanen & Leino, 1999)

Another type of variation in voice quality is caused by the degree of glottal adduction.

If the vocal folds are tightly pressed together, the resulting voice is referred to as being *pressed* or *hyperfunctional*. On the other hand, if the adduction is loose, the voice is called *breathy* or *hypofunctional*. Moderate level of adduction produces what is referred to as *normal* phonation. The different voice qualities reflecting the degree of glottal adduction are referred to as *phonation modes*. The phonation mode is relatively independent of fundamental frequency, loudness, and, to some degree, register of phonation. However, pressed voice tends to be louder than breathy voice. (Laukkanen & Leino, 1999)

Figure 2.4 shows a picture of a male speaker's larynx in breathy, normal, and pressed phonation. As seen in the figure, not only vocal folds are affected by the phonation mode but also surrounding tissues become more adducted as pressedness is increased.

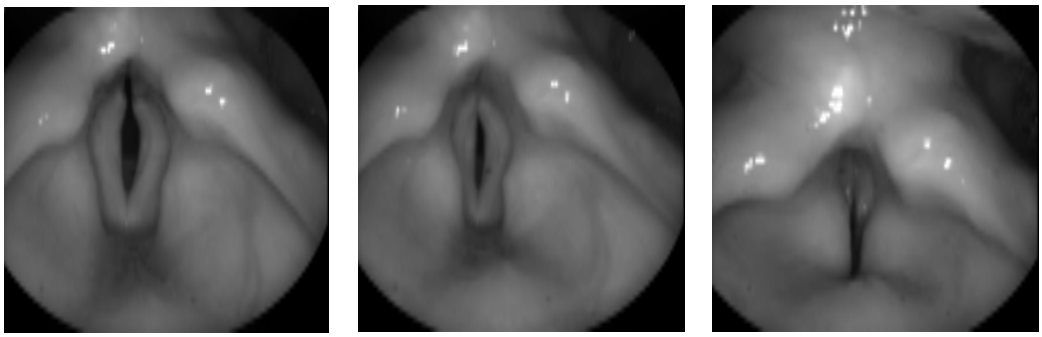

Figure 2.4: The larynx of a male speaker in breathy (left), normal (middle), and pressed phonation (right).

2.2 Source-Filter Theory

Fant (1960) introduced the source-filter theory of human speech production. The theory states that the voice production mechanism can be modeled as a series connection of an excitation source and a filter system. The source and filter are considered independent of each other. In the case of voiced speech sounds, the excitation is provided by the air flow through the vibrating vocal folds, the voice source. The vocal tract functions as a phone-dependent filter.

The independence assumption of voice source and vocal tract filter is not perfectly valid in reality because the glottal flow is actually influenced to some degree by the vocal tract configuration. Nevertheless, the validity of the theory can be considered sufficient for most cases of interest and the assumption is very common in speech processing systems. There are some cases where it cannot be used such as transient speech sounds (Rabiner & Gold,

1975) but, in most cases, the simplicity provided by the independence assumption overrides the minor inherent inaccuracy.

Acoustic analysis of the speech production mechanism commonly utilizes two physical variables: sound pressure and volume velocity of air flow. The glottal flow is usually expressed in terms of volume velocity, whereas speech is typically recorded at some distance from the speaker using a pressure microphone. The volume velocity waveform at the mouth determines the pressure signal propagating into the surrounding free field. The radiation at the lips is considered in detail by Fant (1960) and Flanagan (1972), but it is commonly reduced to a simple differentiation operation (Flanagan, 1972; Javkin *et al.*, 1987; Veldhuis, 1998).

Figure 2.5 illustrates the speech processing mechanism as a series connection of three separate and independent processes: glottal excitation, vocal tract filter, and lip radiation. Figure 2.6 shows the effect of these three processes in the frequency domain.

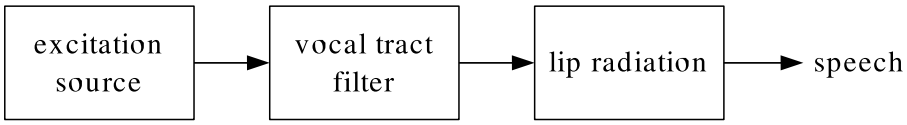

Figure 2.5: Source-filter model.

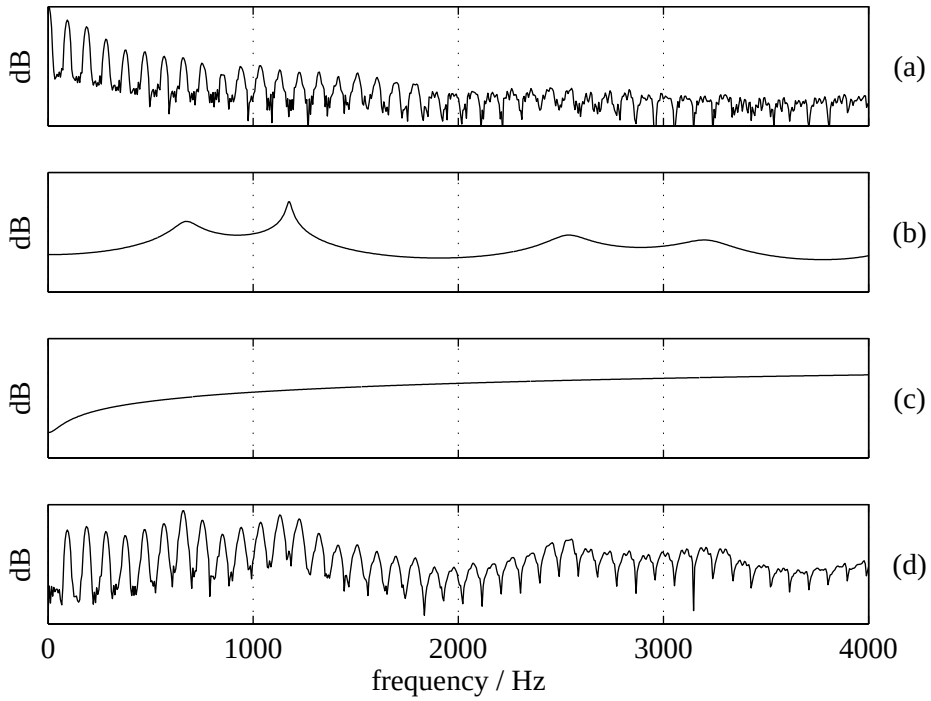

Figure 2.6: The effect of the components of the source-filter model in the frequency domain. (a) Spectrum of the glottal excitation. (b) Amplitude response of the vocal tract filter. (c) Amplitude response of the lip radiation. (d) Spectrum of the speech signal.

Chapter 3

Analysis Methods

Analysis of the vibrating vocal folds during phonation is challenging because the larynx is not easily accessible. However, several techniques have been developed that allow the examination of the laryngeal activities during voicing.

In general, an analysis technique should reflect the vibratory pattern of the vocal folds or indicate the related acoustic phenomena. It should also be reliable, accurate, and verifiable. Additionally, it is generally desirable that an analysis method be non-invasive, which means that no clinical operations are necessary to attach the required measurement equipment in place, and that the measurement setting interferes with normal speech of the subject as little as possible. Examination methods of the glottal source differ with respect to these desired characteristics—each method has its advantages and weaknesses.

This chapter describes the voice source analysis techniques that were used in this study. Some background is provided about the history of these methods. Other related techniques are described briefly as well. Finally, parameters for quantifying the shape of pulses related to the glottal activity are introduced.

3.1 Inverse Filtering

The source-filter theory of speech production provides theoretical background for the inverse filtering technique. If the transfer function of the vocal tract filter is known, an inverse filter can be constructed. In principle, the glottal excitation signal can then be reconstructed by feeding the speech signal through the inverse of the vocal tract filter.

In practice, the transfer function of the vocal tract filter can be approximated based on the speech signal and general knowledge about the voice production mechanism. An approximate inverse filter can then be constructed. Applying the inverse filter to the speech signal yields an estimate of the excitation signal, the glottal volume velocity waveform. This signal

is also known as the *flow glottogram* (FGG) (Hertegård *et al.*, 1992; Hertegård & Gauffin, 1995).

Inverse filtering was first presented by Miller (1959), who applied analog electronic filters to cancel two lowest formants and the lip radiation effect from a speech signal captured by a microphone.

Rothenberg (1973) introduced a different inverse filtering technique that uses the air flow at the mouth as the source signal. The subject's mouth and nose are surrounded by a special mask for measuring the flow waveform. This method allows the estimation of absolute flow values including the DC component, as opposed to the inverse filtering of the pressure signal captured by a microphone, which loses the absolute zero level of flow due to the lip radiation effect. Rothenberg's technique is also less sensitive to low-frequency noise. However, the flow measurement mask causes an upper bound on the useful frequency range at approximately 1.6 kHz (Hertegard & Gauffin, 1992).

Successful inverse filtering is sensitive to phase distortion in the speech signal in the frequency range of interest. Traditional tape recorders are problematic for signal storage in this sense since they cause substantial phase distortion, which must be compensated for (Childers *et al.*, 1983). This problem has been overcome by tape recorders utilizing frequency modulation (FM), which fulfills the requirement of phase linearity (Miller, 1959).

Digital filtering techniques provide obvious advantages over analog techniques. According to Hunt *et al.* (1978), a digital inverse filtering approach was applied to speech already by Holmes (1962). Since the 1970's, inverse filtering has been increasingly realized using digital techniques (Hunt *et al.*, 1978; Javkin *et al.*, 1987). Nowadays, practically all inverse filtering methods in use are digital due to the flexibility, repeatability, and ease of implementation of the digital techniques compared to analog filters. Digital sampling and storage techniques also do not have the phase distortion problem, provided that the equipment is of high quality and the frequency range of flat amplitude response and linear phase response extends to low frequencies.

Digital inverse filtering methods can be categorized to manual and automatic techniques. Manual methods require the human operator to manually adjust filters to match the formants of the speech signal, whereas automatic methods build a vocal tract model and automatically find filter parameters, often by means of LPC analysis (Hertegård *et al.*, 1992). There are also semiautomatic methods that lie somewhere between these two extremes. For example, the method proposed by Alku (1992) basically finds the vocal tract filters automatically but the user still controls a few parameters that affect the resulting flow signal. Södersten *et al.* (1999) compared an automatic and a manual inverse filtering method and reported high agreement between the airflow parameters calculated from the flow signals of these two methods. However, noticeable differences were also encountered.

Inverse filtering basically involves extracting two signals, the volume velocity waveform at the glottis, and the effect of the vocal tract filter, from a single source signal. The technique thus implies strong assumptions about the glottal volume velocity waveform and the transfer function of the acoustic vocal tract filter. Consequently, the result of inverse filtering has to be regarded as an estimate of the glottal flow. The actual volume velocity waveform at the glottis is not known exactly.

Furthermore, the accuracy of inverse filtering deteriorates if the fundamental frequency of speech is high because the sparse harmonic structure of the excitation spectrum interferes with formants, which are local resonances in the spectrum. Nasalized vowels are also not suitable for inverse filtering because their spectra contain antiformants that are difficult to compensate for properly (Hertegård *et al.*, 1992).

Despite these limitations of the method, inverse filtering has proved to be a valuable tool both for clinical use and for fundamental research of the voice production mechanism (Fritzell, 1992). It is a non-invasive technique that does not require bulky or expensive equipment. The restrictions of an application may make inverse filtering the only practical means of examining the voice source of a subject.

Figure 3.1 shows a typical example of a speech pressure signal and the corresponding inverse filtered glottal flow waveform.

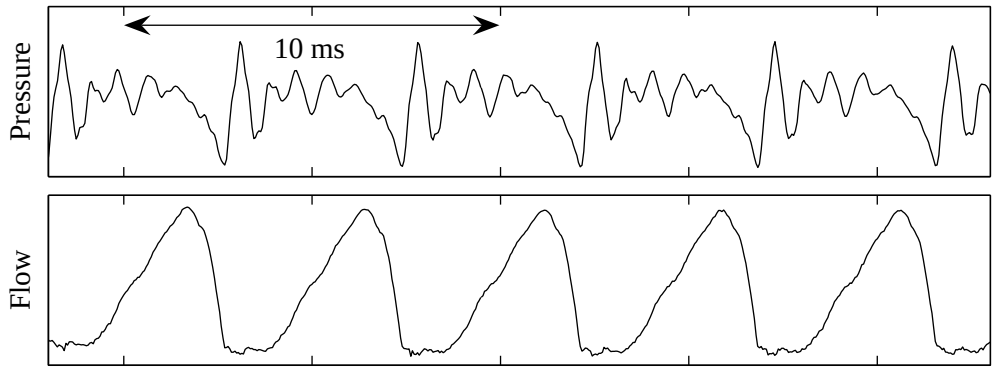

Figure 3.1: Speech pressure waveform of a female speaker's sustained /a/ vowel and the corresponding inverse filtered glottal flow waveform.

3.2 Videostroboscopy and Videokymography

Image recording of the larynx provides valuable information about the physiological movements of laryngeal structures during phonation. The experimental setting is shown in Figure

3.2. A solid endoscope is inserted into the subject's mouth. A bright light source is used to illuminate the target via the endoscope, and a special camera is attached to the endoscope to record a sequence of images. This procedure allows the examination of the glottal behavior during sustained vowels.

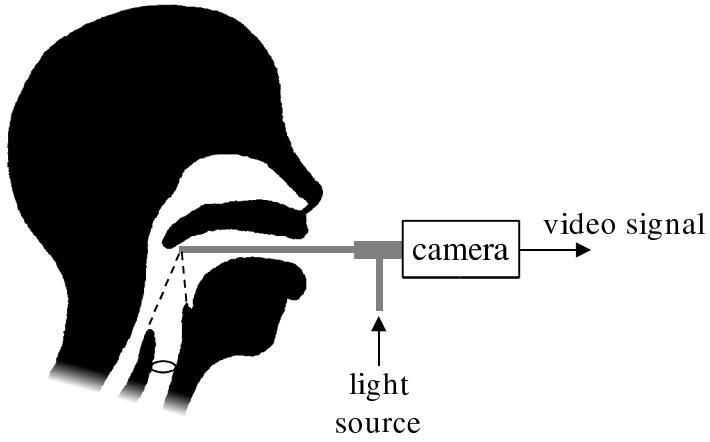

Figure 3.2: Simplified diagram of vocal fold imaging with a solid endoscope.

Another imaging setup uses a flexible fiberscope that is inserted through the nasal cavity to the pharynx. This allows the examination of the vocal fold vibration also during running speech including consonants. However, solid endoscope gives brighter image and better image quality. (Kiritani *et al.*, 1990)

High frequency of vocal fold vibration, typically 120 Hz for males and 200 Hz for females, makes the imaging task challenging. The international video standards PAL and NTSC provide 50 and 60 interlaced half frames per second, respectively Hertegård *et al.* (2003). Thus, ordinary video techniques are obviously insufficient for the observation of vocal fold vibration because the frame rate is far too low.

Stroboscopy is a commonly used technique for obtaining a video sequence of the vocal fold vibration. A flashing light source is used to illuminate the glottis. The frequency of flashing is adjusted slightly below that of the vocal fold vibration, so each flash occurs at a slightly later phase of the vibration period than the previous one. An ordinary video camera system can be used for recording. This technique is called video stroboscopy. Relatively low-cost equipment is sufficient but the method has certain limitations. Since at most one frame is obtained from each period of vibration, no information about any transient phenomena within a single cycle is obtained, and stable, periodic, and regular vocal fold vibration is required to achieve high-quality video. If the vibration is irregular, it is impossible to observe the precise pattern of vibration (Kiritani *et al.*, 1986).

Videokymography provides means to obtain visual information of the vocal fold vibration at much higher temporal resolution than videostroboscopy. Instead of covering the view of image with several hundreds of scan lines, the brightness along only a single scan line is recorded repeatedly. Scanning frequencies of almost 8000 Hz can be attained using relatively inexpensive systems based on ordinary video technology (Švec & Schutte, 1996). The resulting data sequence represents the behavior of the glottal source at one section of the vocal folds. It provides relatively high time resolution but does not give information about the vibration along the entire length of the vocal folds. An example of a kymogram is shown in Figure 3.3.

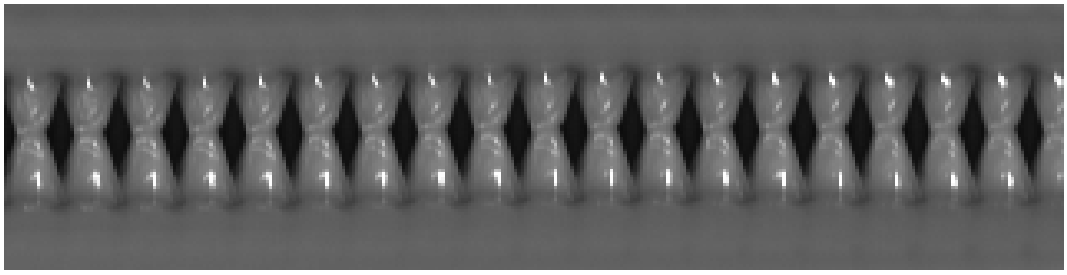

Figure 3.3: Kymogram displaying the vibration of the vocal folds along a single line. The vertical dimension represents time increasing from left to right.

3.3 High-Speed Imaging

Precise visual observation of the vocal fold vibration pattern requires an imaging system capable of full images and sufficiently high frame rate. Such systems were initially realized using high-speed cinematography. Pictures were exposed on a light-sensitive film using a high-speed shutter camera. According to various authors (e.g. Švec & Schutte (1996); Eysholdt *et al.* (1996); Wittenberg *et al.* (2001)), the method was first developed at the Bell Telephone Laboratories in the 1930's and described by Farnsworth (1940).

This approach had its limitations: large-scale equipment was required, real-time observation of the obtained material was not possible due to the required film processing procedure, and frame-by-frame measurements of the vocal fold movements were time-consuming (Kiritani *et al.*, 1986). Furthermore, mechanical noise generated by the system made simultaneous recording of speech sound impossible (Eysholdt *et al.*, 1996) or at least required special sound shielding (Kiritani *et al.*, 1986).

Digital high-speed camera systems were introduced in the 1980's (Kiritani *et al.*, 1986, 1990). They provide significant benefits over traditional filming techniques: The physical size of the required equipment is modest, simultaneous sound recording is possible since practically no noise is generated by the equipment, the imagery is instantly accessible, and computer-based analysis of the image data is possible.

Temporal and spatial resolution has been a limiting factor with digital devices. In general, there is a trade-off between image resolution and frame rate due to limited data transfer speed. Another limitation on shortening the recording duration of a single image frame is the illumination of the target. The light has to be fed to the larynx through an endoscope with a limited diameter, and the power of the light source cannot be increased endlessly because this might cause the equipment to heat too much and cause burns in the subject's oral cavities. (Wittenberg *et al.*, 2001)

Image resolutions of 100–300 pixels in each direction and frame rates of approximately 2 kHz are common in systems in use. The amount of memory in the high-speed device also commonly limits the duration of continuous recording to a few seconds. Most high-speed systems are capable of only gray-scale imaging. Color cameras are also available but using several color channels implies higher data rates and also increased requirement on the amount of light. (Wittenberg *et al.*, 2001)

Modern digital high-speed cameras reach frame rates of up to 10,000 frames per second at reasonable resolutions (Weinberger Vision, 2004).

Figures 2.2 and 2.4 show examples of digital high-speed images recorded at a frame rate of 1900 frames per second and a resolution of 256x64 pixels using a Weinberger Speedcam high-speed camera and an endoscope that was inserted to the mouth of the subject.

3.3.1 Detection of Vocal Fold Edges and Glottal Area

A widely used method to quantify the image information about the vibrating vocal folds is to detect the edges of the vocal folds and to calculate the area of glottal opening. The sequence of detected glottal areas of successive image frames is called the *glottal area function*. The vocal fold edges and thus the glottal area can be detected using manual computer-aided methods (Childers *et al.*, 1983), but automatic computer-based algorithms are also available, see e.g. Krishnamurthy & Childers (1981); Eysholdt *et al.* (1996); Larsson *et al.* (2000).

Usually the material obtained by laryngeal high-speed imaging does not provide absolute distance measures. However, additional equipment can be used to obtain depth information in the image, e.g. by using laser triangulation (Hertegård *et al.*, 2003) or stereo imaging (Wittenberg *et al.*, 2000). Depth information also makes it possible to determine absolute distances from the image.

3.4 Electroglottography

Electroglottography (EGG) is a non-invasive method for the examination of the vocal fold vibration. According to several authors (e.g. Colton & Conture (1990); Baken (1992); Henrich *et al.* (2004)), the method was first reported by Fabre (Fabre, 1940, 1957). Now it has been used for clinical and research purposes for decades.

Electroglottography is based on measuring impedance across the neck of the speaker. When the vocal folds are closed, electric current can pass through them. When the folds are apart, an insulating air gap separates them, and the impedance across the larynx is higher. Thus, the impedance changes across the larynx indicate the variation of the contact area between the focal folds.

Electrodes are placed on the subject's skin on each side of the larynx and a high-frequency alternating current is fed through them in order to measure the impedance between the electrodes. The frequency is typically in the megahertz region and the current is limited to a few milliamperes to ensure that the electric current is imperceptible and harmless to the subject (Baken, 1992). The voltage between the electrodes is typically about 0.5 volts (Marasek, 1997). Figure 3.4 shows the measurement setting with the electrodes on a subject's skin.

The resulting electroglottographic signal, the electroglottogram, shows the impedance variation as a function of time. Impedance variation due to vibrating vocal folds is relatively small, typically only 1–2 percent of the total measured impedance (Baken, 1992). Furthermore, the impedance varies considerably due to changing skin moistness and vertical movements of the larynx. Therefore, high-pass filtering is applied to the obtained electroglottographic signal in order to eliminate low-frequency noise and to extract only the variations caused by vocal fold vibration. Additionally, automatic gain control is often built into EGG devices to maintain appropriate signal level despite considerable impedance changes between subjects and also during a single recording session. These techniques cause phase and amplitude distortion that may influence the EGG waveform (Scherer *et al.*, 1988, page 291). Consequently, the EGG signal cannot be considered an absolute measure of vocal fold contact, and care must be taken when interpreting the signal.

Despite its limitations, EGG yields useful information about the behavior of the vocal folds during phonation. Electroglottography has been studied widely and its validity has been assessed by numerous studies comparing EGG with stroboscopic methods, high-speed imaging, photoglottography, subglottal pressure measurements, and inverse filtering, see Henrich *et al.* (2004) for references. The results show convincingly that the EGG signal is related to the contact area between the vocal folds.

Figure 3.5 shows a typical example of a high-quality electroglottogram recorded during

Figure 3.4: EGG measurement setting. Electrodes have been placed on the subject's skin and a band has been adjusted around the neck to hold the electrodes in place. The electroglottograph (Glottal Enterprises MC2-1) is on the right on top of the oscilloscope. (Photograph by Anne-Maria Laukkanen)

phonation. It has been high-pass filtered to eliminate the low-frequency components that are not related to the vibration of the vocal folds.

Rothenberg (1981b) presented a model of the different phases of the EGG signal period and their relations to the physiological events occurring in the larynx. This model is presented in Figure 3.6. Other similar models exist, see e.g. Childers *et al.* (1983). Such models are, however, idealized simplifications that must not be interpreted literally. Many authors have pointed out that the EGG signal does not allow exact determination of the instant of closure, and locating the instant of glottal opening from the EGG signal alone is even much more inaccurate, see e.g. (Colton & Conture, 1990) and (Baken, 1992).

Titze introduced a mathematical model that describes the vibration pattern of the vocal folds and predicts the contact area variation, see e.g. Titze (1990). A number of geometric

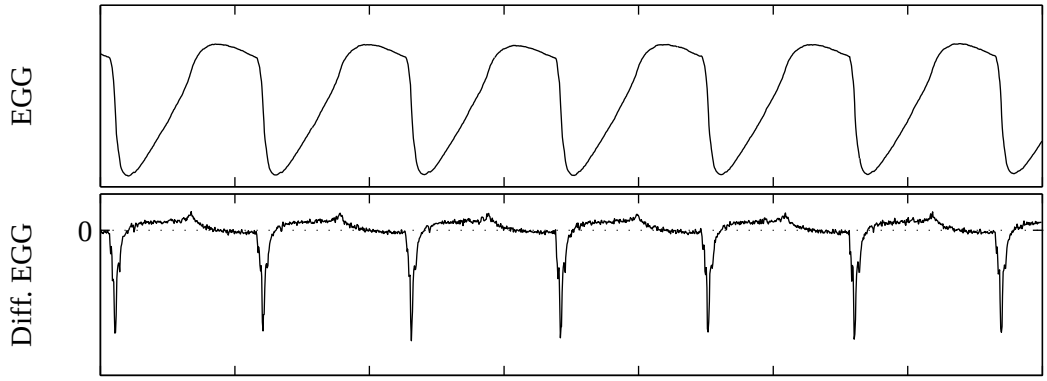

Figure 3.5: Electroglottogram of the normal phonation of a male subject. The upper panel shows the EGG signal and the lower panel its first derivative. Upward change in the signal represents decreasing impedance and thus reduced contact between the vocal folds.

and kinematic parameters are used to describe the shape and movements of the vocal folds, and the model gives the corresponding contact area waveform. The model explains many features of the contact area waveform by relating them to the physiological pattern of vocal fold vibration: EGG pulse widening is caused by adduction of the vocal folds, and peak skewing is related to wedge-shaped vocal folds and vertical phase difference. A knee in rising and falling edges of an EGG pulse corresponds to the bulging of the contact surfaces of the vocal folds. Vertical phasing also explains the variation of the pulse waveform between a triangular and a rectangular shape. Varying characteristics of real EGG pulses can be explained as combinations of these effects.

By comparing the EGG waveform with high-speed filming, Childers *et al.* (1983) related the initial point of vocal fold contact to a break in the negative slope of the EGG waveform, and the glottal opening to the instant at which the differentiated EGG (DEGG) waveform has its absolute maximum. Such peaks of DEGG are clearly visible in Figure 3.5. This approach was carried on by Henrich *et al.* (2004), who regarded the peaks of the DEGG signal as reliable indicators of glottal opening and closing instants defined by reference to the glottal air flow. However, often such peaks are imprecise or absent, or double peaks occur. All these cases make this approach unusable.

In addition to resistance across the neck, the impedance measurement is also influenced by reactance (capacitance or inductance) of the examined load. Varying capacitance may be hypothesized to exist in the glottis when the two vocal folds are separated by a thin insulating layer of air, as pointed out by Rothenberg (1981b). This hypothesis can be checked

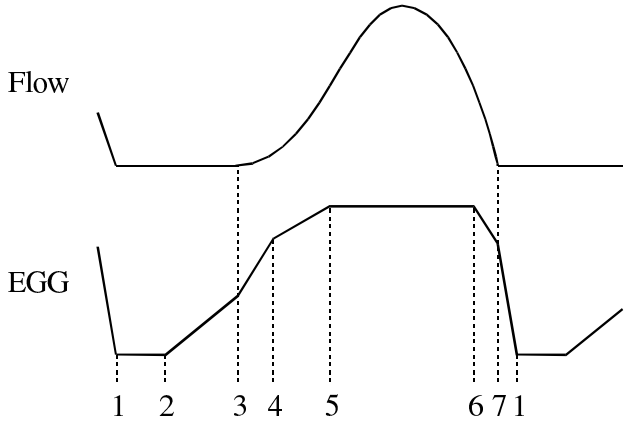

Figure 3.6: The phases of the EGG signal period and their relations to the glottal air flow and physiological events. The figure illustrates the Rothenberg model (Rothenberg, 1981b). 1–2: Vocal folds are maximally closed. 2–3: Vocal folds are separating from lower margins towards upper margins. 3–4: Upper margins are opening. 4–5: Upper margins are still opening. Changed slope is due to phase differences along the length of the vocal folds. 5–6: Vocal folds are fully parted. The distance between the vocal folds is varying but there is little change in contact area. 6–7: Lower margins are closing with a phase difference along the length of the vocal folds. 7–1: Vocal folds are closing from lower margins towards upper margins. The flow pulse begins closely after point 3 and terminates closely before point 7.

by changing the frequency of the alternating current used for impedance measurement: the current remains unchanged only if the load is purely resistive. According to Gauffin (Scherer *et al.*, 1988, page 291), the impedance is essentially resistive in a wide frequency range.

3.5 Other Analysis Methods

Other analysis techniques are also used. For example, photoglottography (PGG) is a method that measures the degree of glottal opening by illuminating the glottis from above or below and monitoring the light intensity on the other side in order to get an estimate of the glottal area (Baer *et al.*, 1983).

Titze *et al.* (2000) described a relatively new technique for examining the glottal source, the electromagnetic glottography (EMGG). It utilizes high-frequency electromagnetic

waves to measure tissue motions and does not require skin contact. EMGG may be a viable alternative to traditional electroglottography.

Subglottal pressure is another quantity that is sometimes measured or estimated to examine the laryngeal function. For example, Lecluse *et al.* (1975) included subglottal pressure measurements in their study of EGG devices and the behavior of vocal folds using excised human larynxes, and Hertegård *et al.* (1995) measured subglottal pressure of a subject during phonation by means of tracheal puncture.

3.6 Studies Combining Several Analysis Methods

The analysis methods described above are commonly used for validating or evaluating the results of each other. For example, Henrich *et al.* (2004) provided a list of comparative studies that analyze the EGG signal using videostroboscopy, high-speed imaging, inverse filtering, and other methods. Some interesting studies utilizing several analysis techniques are mentioned below but the list is by no means complete.

Rothenberg (1981b) recorded simultaneously electroglottogram and oral airflow, which was then inverse filtered to get an estimate of glottal flow. A seven-stage model of the EGG waveform with physiological interpretations (see Figure 3.6) was presented as a result.

Baer *et al.* (1983) compared information obtained by simultaneous and synchronized high-speed filming, acoustic recording, photoglottography, and electroglottography. The results indicated high agreement between photoglottography and film measurements with respect to peak glottal opening and glottal closure, and EGG appeared to indicate vocal fold contact reliably.

Childers *et al.* (1983, 1984) recorded synchronously electroglottogram, speech signal, and high-speed film. Glottal flow was obtained by inverse filtering the speech signal. Glottal area as well as vocal fold contact area were measured from the film. The material was used to evaluate the validity of electroglottography as an analysis method and to relate the phases of the EGG waveform to laryngeal events.

Kiritani *et al.* (1986) compared digital high-speed image sequences with simultaneously acquired synchronized speech pressure and EGG signals.

Hertegård *et al.* (1992) and Hertegård & Gauffin (1995) analyzed simultaneously obtained videostroboscopy, inverse filtered flow waveform, and electroglottogram. They provided a schematic illustration of the correspondence between the phases of the glottal vibration cycle as seen in the inverse filtered flow waveform and in the laryngeal image.

Schutte & Miller (2001) registered simultaneously electroglottogram, microphone signal, and videokymography. They reported substantial agreement between the information achieved by EGG and videokymography and showed how videokymography could help

avoiding misinterpretations of the EGG signal.

Granqvist *et al.* (2003) examined the relationship between vocal fold vibration and the glottal flow by comparing simultaneous, synchronized recordings of oral pressure and air flow, sound pressure, inverse filtered glottal flow, EGG, and glottal area function extracted from digital high-speed image sequences.

Henrich *et al.* (2004) evaluated the validity of the differentiated EGG signal as an indication of glottal opening and closure by comparing a simultaneously obtained EGG and high-speed recording.

Studies combining inverse filtering, digital high-speed imaging, and electroglottography are rare. A search for publications of such studies was performed using search engines accessing several databases of scientific articles in February 2005. Relevant publications were found from only two research groups: Granqvist *et al.* (2003) utilized all these analysis methods synchronously but did not analyze the EGG signal in detail. Sakakibara *et al.* (2001, 2004) studied throat singing by means of inverse filtering, electroglottography, and digital high-speed imaging.

3.7 Parametrization of Glottal Flow and Area

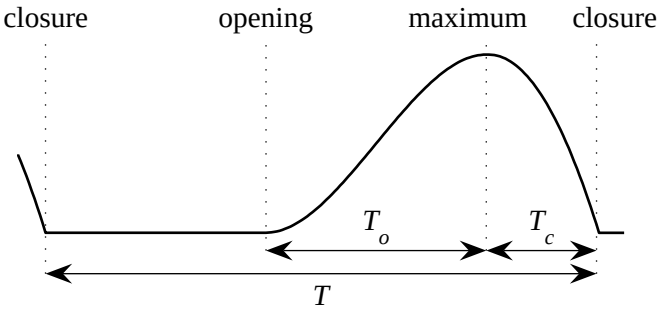

Figure 3.7: Schematic diagram of flow pulse phases. The waveform is generated by the polynomial pulse shape model proposed by Rosenberg (1971). The length of the glottal cycle is denoted by T, the length of the opening phase by T_o, and the length of the closing phase by T_c.

The glottal cycle can be divided to a few phases that are illustrated on the glottal flow pulse in Figure 3.7. Related terminology is introduced below.

Closed phase is the part of the glottal cycle when the vocal folds are in contact along their entire length and the area of glottal opening is thus zero. There is no air flow between the vocal folds during the closed phase.

Opening phase is the phase during which the vocal folds are at least partly separated and the area of opening between them is increasing. The duration of the opening phase is denoted by T_o in Figure 3.7.

Closing phase is the phase during which the vocal folds are separated and the area of opening between them is decreasing. The duration of the closing phase is indicated by T_c in Figure 3.7.

Open phase is the part of the glottal cycle during which the vocal folds are separated and air flows through the glottis. Using the symbols of Figure 3.7, the duration of the open phase is $T_o + T_c$.

Closure refers to the instant when the vocal folds come into contact along their entire length, or when the area of opening between them reaches zero.

Period length, or the length of the glottal cycle, is the time between the corresponding instants of two successive cycles. This is denoted by T and is the reciprocal of the fundamental frequency f_0.

These time measures are used as the basis for time-domain parameters that describe the pulse shape. The parameters used in this work are open quotient, closing quotient, and speed quotient (Holmberg *et al.*, 1988).

Open quotient (OQ) is defined as the ratio of the open phase length to the total length of the glottal cycle.

$$\mathrm{OQ} = \frac{T_o + T_c}{T} \tag{3.1}$$

A related measure is the closed quotient (CQ), which is the ratio of the closed phase length to the glottal cycle length. Thus, CQ = $1-$ OQ. In this work, OQ is used exclusively instead of CQ.

Closing quotient (ClQ) is the ratio of the closing phase duration to the glottal cycle length.

$$\mathrm{ClQ} = \frac{T_c}{T} \tag{3.2}$$

Speed quotient (SQ) is defined as the ratio of the opening phase length to the closing phase length.

$$\mathrm{SQ} = \frac{T_o}{T_c} \tag{3.3}$$

Figure 3.8 illustrates how these parameters reflect typical changes in the glottal flow waveform. The same parameters can be calculated also from other glottal signals than the air flow waveform, e.g. the area of opening between the vocal folds. The resulting parameter values may not necessarily reflect exactly the same properties of the glottal behavior

because, for example, the maximum of air flow does not necessarily occur simultaneously with the maximum glottal area.

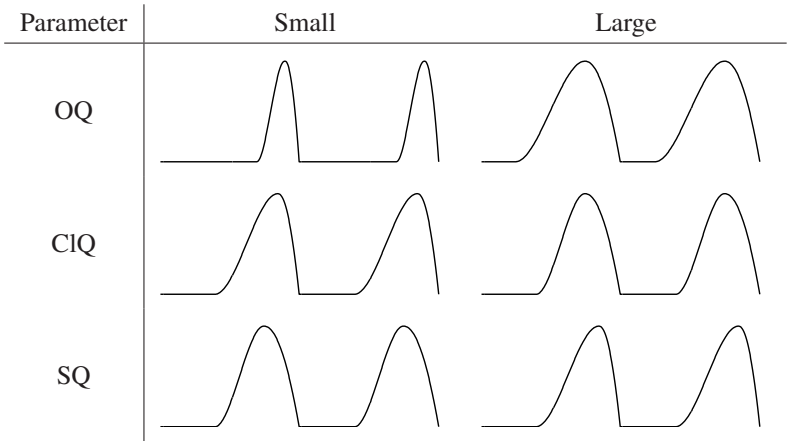

Figure 3.8: Synthetic glottal flow pulses that illustrate how the parameters reflect changes in the pulse waveform. Pulses have been generated using the polynomial glottal pulse model introduced by Rosenberg (1971).

Other parameters exist for describing the shape of a glottal pulse waveform. For example, the Normalized Amplitude Quotient (NAQ) (Alku *et al.*, 2002) can be used to parametrize the closing phase of the flow pulse.

A completely different approach to the parametrization of the flow pulse is to use a parametric model for describing the glottal volume velocity waveform. A mathematical model is fit to the observed waveform by finding the most suitable values for the model parameters. These parameters contain information about the most relevant properties of the pulse shape, and they can also be used to reconstruct an approximation of the original pulse waveform. Synthetic glottal pulses can be used for e.g. speech synthesis.

The most commonly used model of glottal volume velocity waveform is the LF model (Fant *et al.*, 1985). It has four parameters that, together with the length of the glottal cycle, uniquely determine the pulse shape. To reconstruct the pulse waveform, a couple of construction parameters have to be solved from these specification parameters. This requires a numerical, iterative procedure that is computationally heavy. The computational complexity limits the usefulness of the LF model for practical applications (Veldhuis, 1998).

In general, parameters describing the glottal flow waveform can be used for a variety of purposes including fundamental research on speech production, clinical use, speech analysis, coding, and synthesis, automatic speech recognition, and automatic speaker verification and identification (Strik, 1998). An example of the utilization of time-based pulse shape parameters is the research reported by Lauri *et al.* (1997) and Vilkman *et al.* (1997), in which

the effects of vocal loading were studied by means of inverse filtering and the glottal flow pulse parameters OQ, ClQ and SQ. Glottal flow parameters can also be used for quantifying the role of the glottal flow waveform in communicating emotion (Gobl & Chasaide, 2003; Airas & Alku, 2004).

Chapter 4

Material and Methods

This chapter describes the material that was studied in this research as well as methods and techniques for processing the data. The material originates from two separate experiments that are referred to as the Huddinge experiment and the HUT experiment. They are described in detail in this chapter. But first, the inverse filtering method IAIF is introduced.

4.1 Matlab Signal Processing and Programming Environment

All digital signal processing, programming, and data visualization was done using the Matlab software (The MathWorks, 2004). Matlab versions 6.5, 7.0, and 7.1 were used. The Matsig signal processing class library for Matlab (Airas, 2004) was also utilized. Custom scripts, functions, and user interfaces were developed for the purposes of the work.

4.2 Iterative Adaptive Inverse Filtering (IAIF)

Iterative Adaptive Inverse Filtering (IAIF) is a semi-automatic inverse filtering method developed by Paavo Alku (Alku, 1992; Alku *et al.*, 1999). The method takes a speech pressure signal as input and generates an estimate of the corresponding glottal flow signal. Block diagram of the IAIF procedure is shown in Figure 4.1.

The IAIF algorithm has been improved from that described by Alku (1992) by replacing the conventional linear predictive coding (LPC) technique with the discrete all-pole (DAP) modeling method (El-Jaroudi & Makhoul, 1991). DAP gives more accurate estimates of vocal tract formants than the conventional LPC method (Bäckström *et al.*, 2002).

The method operates in two repetitions, hence the word *iterative* in the name of the method. These two phases are indicated by gray outlines in Figure 4.1. The first phase generates an estimate of the glottal excitation, which is subsequently used as input of the

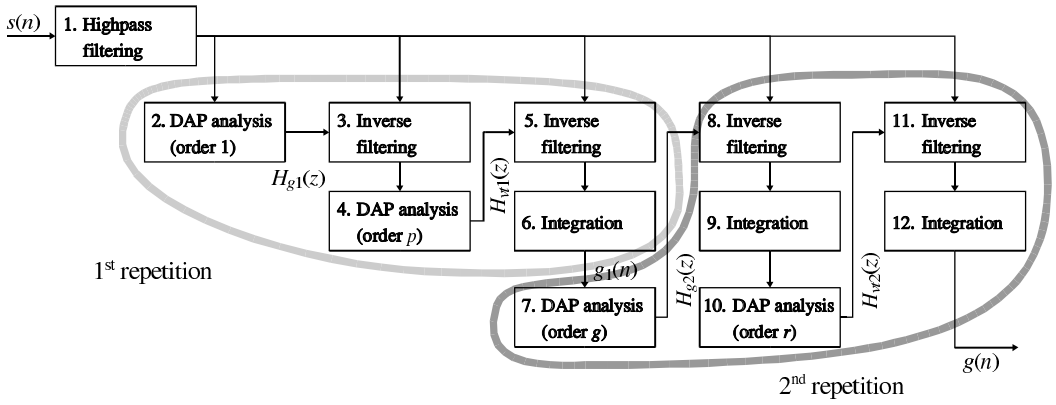

Figure 4.1: Block diagram of the steps of the IAIF method. (Diagram by Matti Airas, MSc(Tech))

second phase to achieve a more accurate estimate. The steps of the method are described in detail below.

1. The input signal is first high-pass filtered to remove disturbing low-frequency fluctuations. The high-pass filtered signal is used as the input of subsequent stages. The cut-off frequency can be adjusted. It should be lower than the fundamental frequency of the speech signal in order to avoid filtering out relevant information.

2. A first-order DAP analysis is calculated. This step gives an initial estimate of the combined effect of the glottal flow and the lip radiation effect on the speech spectrum.

3. The input signal is inverse filtered using the filter obtained in step 2. This step effectively removes the spectral tilt caused by the spectrum of the excitation signal and the lip radiation effect.

4. The output of the previous step is analyzed by DAP to obtain a model of the vocal tract transfer function. The order p of the DAP analysis is related to the number of formants to be modeled in the analysis frequency band, and it can be adjusted by the operator of the IAIF method. As a rule of thumb, p should be an even integer that is obtained by adding a small number to the sampling frequency of the analyzed signal in kHz (Markel & Gray, 1976).

5. The input signal is inverse filtered using the inverse of the pth-order model from step 4.

6. The output of the previous step is integrated in order to cancel the lip radiation effect. This yields the first estimate of the glottal flow and completes the first repetition.

7. The second repetition starts by calculating a gth-order analysis of the obtained glottal flow estimate. This gives a spectral model of the effect of glottal excitation on the speech spectrum. The value of g is usually between 2 and 4.

8. The input signal is inverse filtered using the model of the excitation signal to eliminate the glottal contribution.

9. Lip radiation is canceled by integrating the output of the previous step.

10. A new model of the vocal tract filter is formed by an rth order DAP analysis. The value of r can be adjusted by the user but it is commonly set equal to the value of p in step 4.

11. The effect of the vocal tract is removed from the input signal by inverse filtering it with the vocal tract model obtained in the previous step.

12. Finally, the lip radiation effect is canceled by integrating the signal. This yields the final estimate of the glottal flow, which is the output of the IAIF method.

The conversion from volume velocity at the mouth to the radiating pressure signal is commonly modeled by a simple differentiation operation, which in the digital signal processing domain is represented by the following transfer function:

$$L(z) = 1 - z^{-1} \tag{4.1}$$

When the source for inverse filtering is the pressure signal, this lip radiation effect has to be canceled by the inverse filtering procedure in order to obtain the glottal flow waveform. The inverse of $L(z)$ above amounts to integration. However, this cannot be directly used in practice since integration implies infinite gain at zero frequency and great amplification at low frequencies. This would lead to instability and undesired behavior in practical implementation. (Javkin *et al.*, 1987)

Consequently, inverting the effect of lip radiation is typically realized by the following leaky integrator

$$IL(z) = \frac{1}{1 - \rho z^{-1}} \tag{4.2}$$

where ρ is an adjustable parameter whose value is slightly below unity.

The integration blocks of the IAIF method are realized using the leaky integrator. The constant ρ can be varied within a small range below 1. The closer the value is to unity, the more exactly the leaky integration corresponds to the inverse effect of differentiation.

Decreasing ρ makes the integrator more leaky, which decreases low-frequency amplification and makes the output signal value approach the zero level faster. The parameter ρ is controlled by the user of the IAIF method to make the flow waveform most plausible by adjusting the waveform approximately horizontal in the closed phase.

IAIF applies the same filtering procedure to the entire signal to be processed, so the input signal is assumed to exhibit a stable vocal tract configuration. The method can be used to inverse filter a lengthy segment of speech in so far as this assumption holds. However, typically the inverse filtered signal is no longer than a couple of hundreds of milliseconds to ensure minimal changes in the vocal tract transfer function. The signal should not be too short either: a minimum of a few periods is recommended to get reliable results.

4.2.1 HUT IAIF Toolbox

HUT IAIF Toolbox is a Matlab implementation of IAIF developed mainly by Matti Airas at the Laboratory of Acoustics and Audio Signal Processing at Helsinki University of Technology. The inverse filtering procedure is controlled through the graphical interface shown in Figure 4.2.

First, a WAV audio file is chosen and a portion of it is selected for inverse filtering. Then, IAIF parameters are tuned to get a plausible glottal flow signal as a results. Controls for setting the most relevant parameters are located in the `IAIF parameters` box of the user interface. The `Max # of formants` slider adjusts the order of the DAP models: p and r are set to twice the chosen number of formants. g is 4 by default. Another settings window allows setting p and r individually and also changing g, but typically this possibility is not used.

`Lip radiation` is the ρ parameter used in the integrating stages of IAIF. The cut-off frequency of the high-pass prefiltering stage is controlled by the `Highpass` slider but the cut-off can also be chosen to be automatically set to a slightly lower frequency than the fundamental frequency in the selected speech segment. The toolbox determines the fundamental frequency automatically by calling the Matsig implementation of the YIN algorithm (de Cheveigné & Kawahara, 2002).

The input signal as well as the resulting flow estimate are shown in the signal window, see Figure 4.3. The upper panel shows the high-pass filtered speech signal and indicates the portion of it selected for inverse filtering. The lower panel displays the resulting flow estimate in blue. The gray signal is obtained by simply integrating the input signal. This signal window is updated automatically when the IAIF parameters are modified or the input signal selection is changed.

Additional features of HUT IAIF Toolbox include spectral display of signals and DAP models, automatic determination of inverse filtering parameters, and automatic NAQ pa-

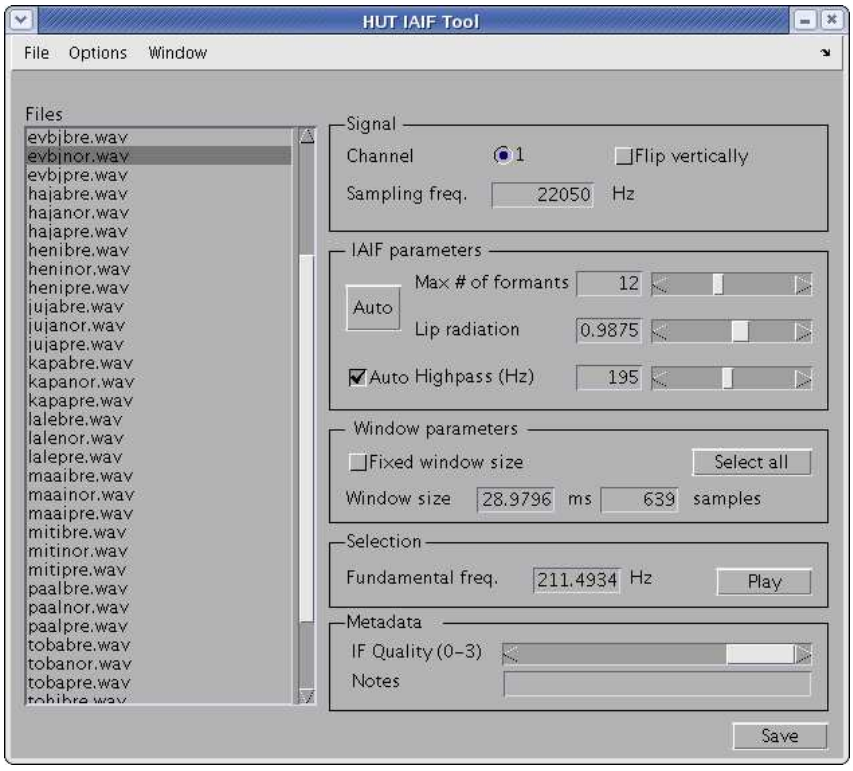

Figure 4.2: The graphical user interface of HUT IAIF Toolbox, which is a Matlab implementation of the IAIF method.

rameter calculation.

4.3 Huddinge Experiment

4.3.1 Recording Setup

The first set of data to be analyzed in this study was collected in an experiment that was carried out at the Huddinge University Hospital of the Karolinska Institute in Stockholm, Sweden, in April 2004. There were three subjects, one female and two males. They all were adults with healthy voices and long experience in voice research.

The experiment consisted of two parts. In the first part, the subjects produced sustained /æ/ vowels in three phonation modes: breathy, normal, and pressed. The duration of each phonation was approximately one second. The phonations were produced in rapid succession so that the entire sequence of three phonations took no longer than four seconds. Each subject repeated this at least three times.

In the second part, four sustained /æ/ vowels were produced with loudness increasing

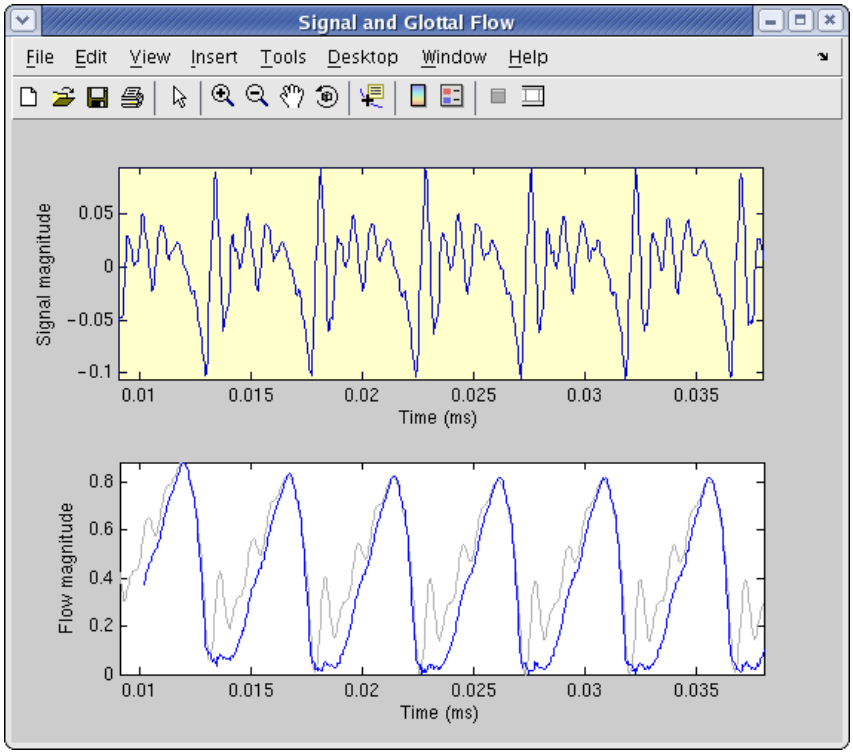

Figure 4.3: The signals window of HUT IAIF Toolbox. The upper panel shows the high-pass filtered speech pressure signal. The yellow rectangle on background indicates the signal segment selected for inverse filtering. In this case, the entire visible signal is selected. The lower panel displays the integrated pressure signal in gray and the inverse filtered flow signal in blue. The inverse filtering settings are shown in Figure 4.2.

from phonation to phonation. These vowels were slightly less than one second in duration and they were also produced in rapid succession to fit the whole sequence in a four-second time window. The subjects repeated this task three times.

The voice production in all these phonations was measured using three techniques simultaneously. See also Figure 4.4.

1. Speech pressure signal was captured using a Brüel & Kjær condenser microphone 4192 and a Brüel & Kjær microphone amplifier 2669. The microphone was placed at a distance of 10 centimeters from the subject's mouth. The distance was controlled in the beginning of each recording.

2. Electroglottogram was recorded by means of a Glottal Enterprises MC2-1 electroglottograph. The electrodes were placed on the subject's neck and conducting paste

was applied between the electrodes and the skin. A flexible band was adjusted around the neck over the electrodes to hold them in place.

3. Digital high-speed image sequence of the vocal folds was obtained via a rigid endoscope and recorded by a Weinberger Speedcam +500 high-speed camera. A 300 W xenon lamp (R. Wolf) was used as the light source. The endoscope was inserted into the subject's mouth and the operating physician held the subject's tongue.

   The video image sequence was digitized by a frame grabber card on a computer. A sequence of digital grayscale images with 256 gray levels was obtained. The resolution was 64x256 pixels and the frame rate approximately 1900 frames per second. The maximum length of continuous video recording was limited by the memory size (128 MB) of the frame grabber device to 8192 frames, or 4.3 seconds.

   At the end of each phonation, the high-speed image capturing process was stopped by pressing a foot pedal. The last 8192 frames before the instant of this pedal press were then saved on hard disk without any compression.

   The image from the high-speed camera was also shown in real time on a computer screen.

For the synchronization of the microphone and EGG signals with the video image sequence, an additional synchronization channel was included. Synchronization was arranged by recording the state of the pedal, which stopped the imaging, on the synchronization channel. The beginning of the pedal pulse thus indicated the instant of the last image and provided the primary means of synchronization.

Due to the lack of synchronization between the video frame rate and the sound card sampling rate, the pedal pulse alone would provide sufficient synchronization accuracy only in a relatively short time window at the end of the image sequence. Therefore, an improvement was made to the synchronization method used in e.g. the study by Granqvist *et al.* (2003). The video signal from the high-speed camera was summed to the synchronization channel at a low amplitude. No image information could be obtained from this synchronization signal, but the frame synchronization pulses in the video signal caused a strong spectral peak at the frequency of the frame rate. Consequently, this arrangement allowed exact extraction of the frame rate from the synchronization signal.

The three signals—pressure captured by the microphone, EGG, and the synchronization signal—were digitized by a multichannel sound card using 16 kHz sample rate and 16 bits per sample. The data was then stored in a sound file on a computer hard disk. The durations of these recordings varied between 8 and 40 seconds. The 4.3-second time span of the high-speed image sequence was completely covered in all recordings.

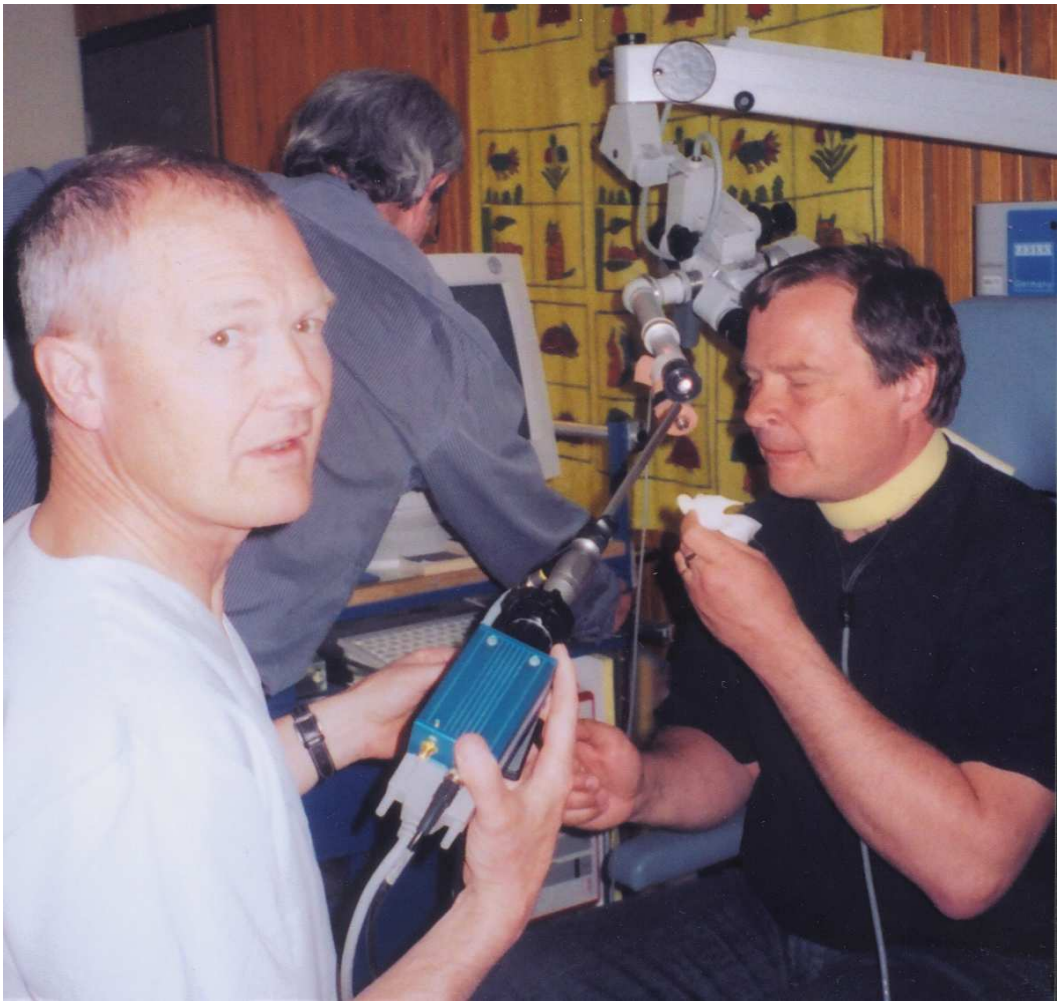

Figure 4.4: The Weinberger high-speed camera with the endoscope attached. The microphone is attached to the stand and is positioned in front of the subject's mouth. EGG electrodes are placed on the subject's neck below a supporting band. (Photograph by Anne-Maria Laukkanen)

Each sequence of three phonations in different phonation modes or four phonations with increasing loudness was stored separately. One sound file with three channels and one image sequence file was created for each such recording. Additional data files were also produced containing information about the camera frame rate, resolution, etc.

Figure 4.5 shows an example of a recorded sound file of breathy, normal, and pressed phonation. The pedal pulse is clearly visible on the synchronization channel, and the raw video signal is seen as low-amplitude ripple on this channel.

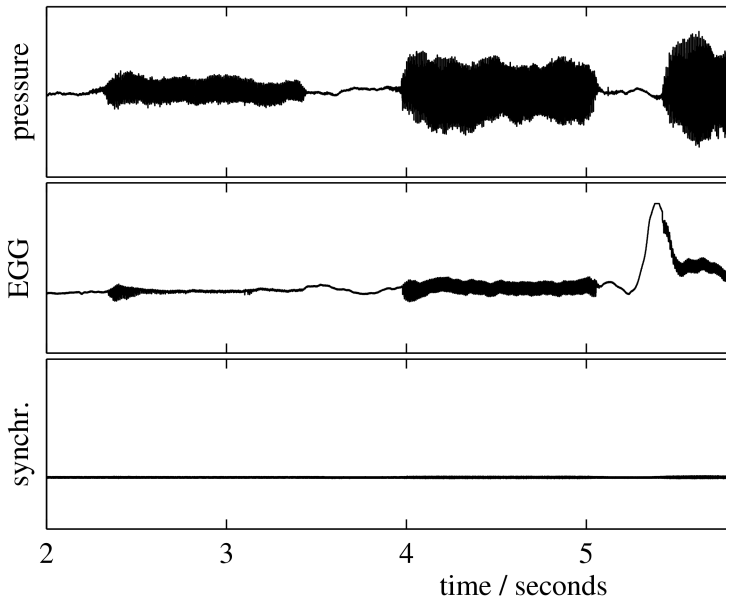

Figure 4.5: Three-channel recording of breathy, normal, and pressed phonation. The video signal is seen as low-amplitude ripple on the synchronization channel. The pedal pulse indicating the instant of the last high-speed image is clearly visible.

4.3.2 Data Selection and Preprocessing

The quality of the EGG signals turned out to be inconsistent. In many cases, the EGG signal was too noisy to be used as a reliable source of information about the glottal behavior. Figure 4.6 shows an example of such a noisy EGG signal. Due to the apparently unreliable signal quality, the EGG recordings of the Huddinge data were not used in this study, except for the analysis of the signal synchronization accuracy as described in Section 4.3.7.

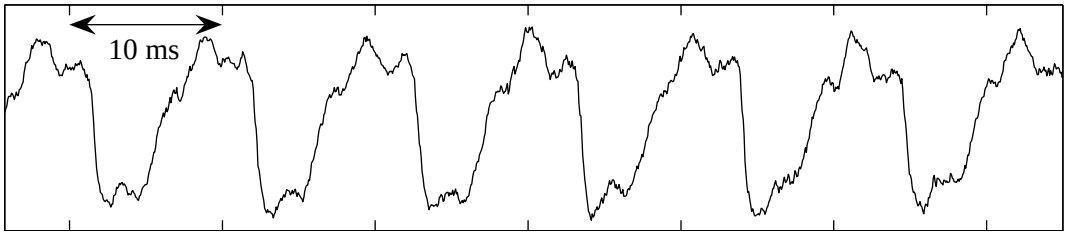

Figure 4.6: Example of a noisy EGG signal.

An obvious discontinuity was detected in two of the high-speed image recordings. This indicated that something unexpected had happened to the image data. Consequently, these two recordings were discarded altogether. Three to four recordings of each subject remained for the analysis of the different phonation modes, and three recordings of each subject were available for the loudness variation cases.

In the loudness variation recordings, the first phonation was found to be too soft in many cases. Therefore, the weakest phonation was omitted and only the last three phonations were examined in each recording.

A sequence of five consecutive glottal periods was then chosen for examination in each of the phonations to be analyzed. Primarily, the periods were chosen approximately at the middle of the phonation. However, this requirement was relaxed if, e.g., the signal was not stationary in the middle part of the phonation or if the high-speed image sequence began at a later time instant for the first phonation in a recording.

An analysis window was then marked around each five-cycle sequence. The window extended up to a couple of periods to both directions from the sequence of five analysis periods. The durations of the windows varied between 30 and 80 milliseconds depending on the fundamental frequency of phonation.

4.3.3 Calculation of the Sound Pressure Level

The sound pressure level (SPL) of each analysis window was estimated from the microphone signal recording. A calibration signal for the SPL calculation was recorded at the data collection session prior to starting the phonation measurements. Any changes in the recording setup, e.g. adjusting the gain setting, were followed by the recording of a new calibration signal. Annotations were made indicating the calibration signal to be used with each data recording.

The calibration signals were obtained by placing a calibrator device tightly against the microphone and recording the microphone output in the same way as phonations were recorded. A Brüel&Kjær Sound Level Calibrator, Type 4231, was used as the calibrator. It provided a sinusoidal pressure signal whose frequency was 1000 Hz $\pm$ 0.1 % and sound pressure level 94.00 dB $\pm$ 0.20 dB.

Sound pressure level is defined as

$$\begin{aligned} L_p &= 20 \log_{10} \frac{p}{p_0} \\ &= 10 \log_{10} \frac{p^2}{p_0^2} \end{aligned} \tag{4.3}$$

where p is the effective root-mean-square (RMS) sound pressure, and the reference pressure is p_0 = 20 μPa. Since the microphone signal is directly proportional to the sound pressure,

the sound pressure level can be expressed in terms of the digitized microphone signal $x[n]$ as follows:

$$L_p \quad = \quad 10 \log_{10} \frac{x_{rms}^2}{x_0^2} \tag{4.4}$$

where x_0 is the root-mean-square value of the microphone signal corresponding to the reference pressure p_0, and x_{rms} is the root-mean-square value of the microphone signal in the time range of interest:

$$x_{rms} = \sqrt{\frac{1}{N} \sum_{n=k+1}^{k+N} (x[n])^2} \tag{4.5}$$

Since applying this to the calibration signal $x_c[n]$ has to yield $L_p = 94$ dB, the reference value x_0 can be eliminated and the formula for the SPL is

$$L_p = 10 \log_{10} \frac{\frac{1}{N} \sum (x[n])^2}{\frac{1}{N_c} \sum (x_c[n])^2} + 94 \text{ dB}. \tag{4.6}$$

The calibration signals were high-pass filtered using a digital 2048-tap linear-phase FIR filter to remove low-frequency noise components. The choice of the exact cut-off frequency had very little effect on the RMS value of a filtered calibration signal as long as the cut-off was above a few herz and well below the calibration signal frequency 1 kHz. This was verified by a simple experiment in which the cut-off frequency was varied between 20 Hz and 700 Hz. Less than 0.05 % variation was found in the RMS values. Based on this result, a cut-off frequency of 100 Hz was chosen. It seemed safe to assume that the filtering removed disturbing low-frequency noise sufficiently without affecting considerably the actual calibration signal.

The calibration signals were then examined visually and auditorily. A stable sequence was cut from each signal and its root-mean-square value was computed and stored. The durations of these calibration sequences varied between 2.5 and 4.5 seconds.

Equation 4.6 was then applied to calculate the sound pressure levels of the analysis windows marked in the phonations. No frequency weighting was applied.

The correctness of the SPL calculation procedure was verified by two tests. First, a portion of each calibration signal was run through the same steps as the phonation recordings, including the high-pass filtering stage in the HUT IAIF Toolbox software. The obtained SPL values were within 0.01 dB from 94 dB. Second, the signal values of one calibration signal were divided by two and the same test was repeated. The SPL dropped by 6 dB as expected.

4.3.4 Inverse Filtering

Each analysis window was inverse filtered using the HUT IAIF Toolbox, which was described in Section 4.2.1. The cutoff frequency of the high-pass filter was set a few percent below the fundamental frequency of each phonation. The parameters of the IAIF method were adjusted manually as follows. The goal was to obtain a plausible flow waveform with approximately constant value in the closed phase if possible. The number of formants, which controls the IAIF parameters p and r described in Section 4.2, was set to the lowest value that gave a reasonable result. It was varied between 6 and 11. The lip radiation coefficient, indicated by ρ in Equation 4.2, was then adjusted to give an approximately horizontal closed phase. The range of values was from 0.972 to 0.997.

Other parameters of the HUT IAIF Toolbox were not altered from their default values. Thus, p and r were always equal and g was 4. See section 4.2 for a detailed description of IAIF and its parameters.

Parametrization of Flow Pulses

The flow waveforms obtained by inverse filtering were parametrized using open quotient (OQ), closing quotient (ClQ), and speed quotient (SQ), which were introduced in Section 3.7. The instants of closure, opening, and maximum flow were marked manually in the flow pulses.

It turned out that the flow often showed pulse waveforms similar to the one shown in Figure 4.7. The instant of closure is followed by a relatively short closed phase with nearly constant flow. Then, the flow starts to increase gently. This phase ends abruptly at a knee that begins a segment with more rapid flow increase. Thus, there are two instants that could be considered instants of glottal opening. From now on, these instants are referred to as the *primary opening*, which is the end of the horizontal phase, and the *secondary opening*, which is the instant of abrupt increase of flow derivative.

To study this phenomenon and its relation to the glottal behavior visible in the image sequence, the two opening instants were marked in flow pulses in which this phenomenon appeared. Two open quotients (OQ_1 and OQ_2) and speed quotients (SQ_1 and SQ_2) were then calculated correspondingly:

$$\mathrm{OQ}_1 = \frac{T_{o1} + T_c}{T} \tag{4.7}$$

$$\mathrm{OQ}_2 = \frac{T_{o2} + T_c}{T} \tag{4.8}$$

$$\mathrm{SQ}_1 = \frac{T_{o1}}{T_c} \tag{4.9}$$

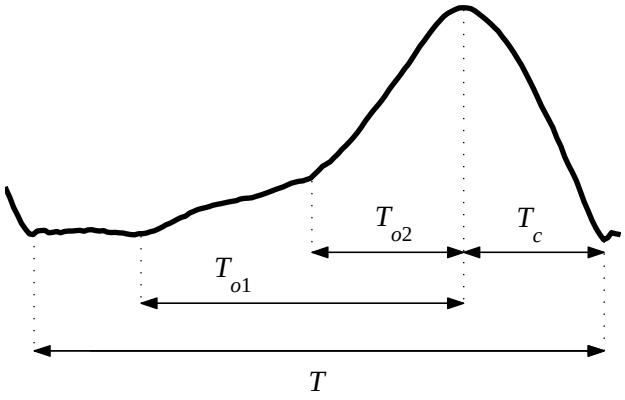

Figure 4.7: Flow pulse with primary and secondary opening. The length of the glottal cycle is denoted by T. The interval from the primary opening to the instant of maximum flow is indicated by T_{o1} and the interval from the secondary opening to the instant of maximum flow by T_{o2}. The closing phase length is denoted by T_c.

$$\mathrm{SQ}_2 = \frac{T_{o2}}{T_c} \tag{4.10}$$

If a flow pulse did not show two opening instants, the two opening marks were positioned at the same instant. In this case, $\mathrm{OQ}_1 = \mathrm{OQ}_2$ and $\mathrm{SQ}_1 = \mathrm{SQ}_2$.

4.3.5 Glottal Area Function

Automatic Detection of Glottal Area

The glottal area waveform in each high-speed video sequence was extracted automatically using the custom-made software High-speed Toolbox, version 2.0. The software has been developed by Hans Larsson. (Larsson *et al.*, 2000)

The user interface of the software consists of several windows. The main window, shown in Figure 4.8 (a), is used for adjusting the video display and for controlling the analysis procedure. The video image is displayed in a separate window as shown in Figure 4.8 (b).

The detection of glottal area is performed in the following steps:

1. The desired high-speed video file is opened, the file position slider is moved to the portion of interest, and the area calculation mode is activated.

2. The software detects automatically the range of interest within the image area based on brightness variations in a sequence of successive frames. This area can be dis-

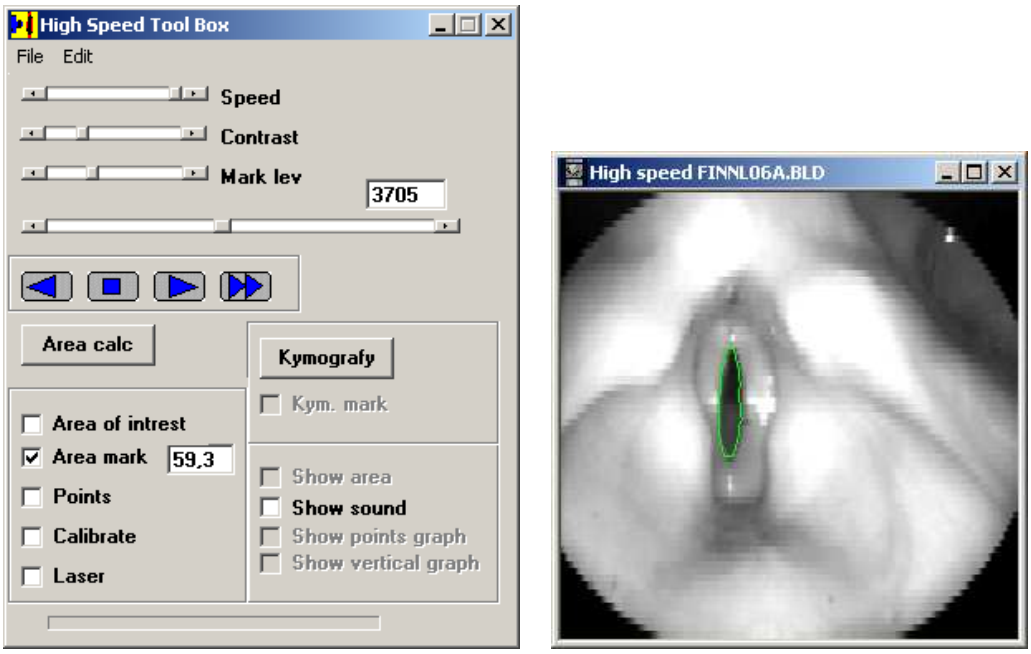

(a) (b)

Figure 4.8: The High-Speed Toolbox software (Larsson *et al.*, 2000). (a) The main window with user controls. (b) The related video frame display. The detected edge of glottal opening is also displayed on top of the video image.

played in the video window, and its borders can be manually dragged to desired locations.

3. Now, the software tries to detect the edges of the glottis in the active frame. It first high-pass filters the selected range of interest in horizontal direction. Edge tracking is then performed based on maximal derivative in the image, an adjustable gray level, and the detected edge in the previously analyzed frame (Larsson *et al.*, 2000). The detected edges of the glottis can be displayed on top of the video image, as shown in Figure 4.8 (b). The gray level utilized by the algorithm is adjusted using the `Mark lev` slider in the main window in order to obtain correct edge positions. Moving in the video sequence is possible, so the results of edge detection can be checked in different phases of the vibration cycle.

4. After setting the area of interest and the gray level optimally, the area calculation is started. It takes a couple of minutes to process the entire sequence of eight thousand frames on a machine with AMD Athlon(tm) XP 2400+ processor.

5. The detected edges can now be examined for each frame, and the obtained area function can be shown in a separate window. The edges can also be adjusted manually for each frame individually using the mouse.

6. Finally, the resulting area function is saved to file.

The area detection procedure does not give an absolute area measure since the dimensions of the glottis in the image are generally not known. The software supports absolute area measurement by using a laser triangulation technique (Hertegård *et al.*, 2003). However, this capability was not utilized in this study because no laser triangulation equipment was used in the data recording setting.

Additionally, the High-Speed Toolbox software is capable of generating a kymogram over a selected portion of the file at a specified scan line in the image, but this feature was not used in this study.

Limitations of the Area Function

Care must be taken when interpreting the glottal area waveforms acquired by the High-Speed Toolbox software. Several issues limit the reliability of the obtained area function:

- The actual borders of the vocal folds are not easy to distinguish in the figure even by a human observer. The task is complicated by suboptimal illumination conditions, relatively low spatial resolution of the video image, and physiological phenomena. The mucosal wave, or the vertical phase difference of the vocal fold vibration, makes the vocal fold edge often hard to follow accurately, especially because the lower margin is often not well illuminated. Also, the opening phase is often gradual: The middle of the glottis starts to get darker but it is not easy to determine the instant when a gap actually opens between the vocal folds. Finally, a minor chink is frequently observed, especially in the case of the female subject, in either the posterior or the anterior part of the glottis or in both parts. See Figure 4.9 for an example. However, there is no clear-cut boundary between cases where a chink exists and where the vocal folds close completely.

- The automatic area detection is highly sensitive to the gray level adjustment made by the operator of the software. Finding an optimal level setting often involves a compromise: If the gray level is set too low, dark areas surrounding the glottis are often erroneously detected as part of the glottal opening in some of the frames. If the level is set too high, the ability of the software to detect a narrow glottal opening deteriorates.

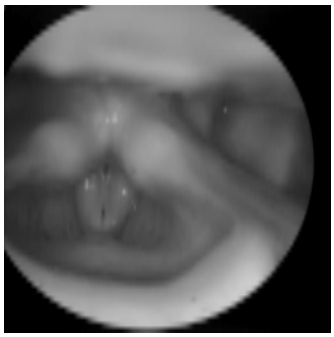

Figure 4.9: Anterior and posterior chink in the most closed phase of the glottal cycle in female subject's normal phonation.

- High-Speed Toolbox is relatively poor at detecting the edges of the vocal folds when the opening is narrow. Often, the instant of glottal opening would be placed manually at the previous frame compared to what the automatic algorithm yields. The same applies to the instant of closure, so the manual examination would commonly give open phases that are a couple of frames longer. Unfortunately, High-Speed Toolbox does not seem to allow setting the glottal area easily by hand for frames in which no opening has been found.
- Especially in pressed phonations, the vocal folds are often partially hidden by other structures above the glottis. An example is shown in Figure 4.10. In such cases, it is impossible to measure the actual area of opening between the vocal folds from the image data. The visible opening can be measured with some accuracy, but this measure does not necessarily correspond to the actual glottal opening that determines the air flow to the vocal tract.

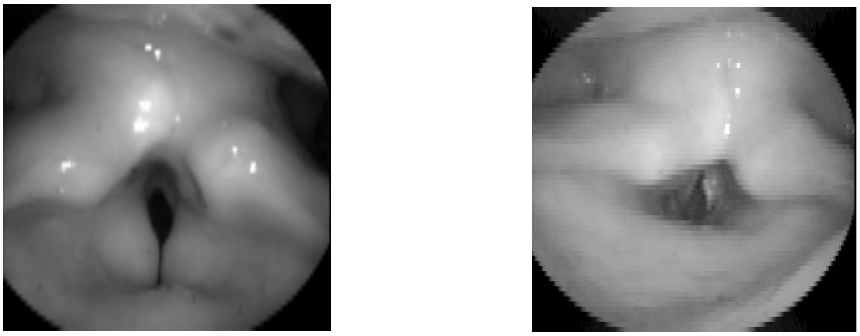

Figure 4.10: Two examples of the glottis being partially hidden by supraglottal structures in pressed phonation.

- The distance between the endoscope and the vocal folds varies between recordings and also during a four-second recording. Since this distance is not compensated for, the area calculated from the image data is highly dependent on this distance. The illumination conditions change as well, which also causes variation in the area detection. Therefore, the absolute values of the glottal area function can be compared only within a small time window, during which no substantial changes are assumed to occur in distance or illumination.

- The temporal resolution of the video image sequence, approximately 1900 frames per second, is quite low for accurate examination of vocal fold behavior. Especially for female phonations, with fundamental frequency of about 200 Hz, less than ten frames are obtained of each complete glottal cycle. In particular, pressed phonation of the female speaker may yield no more than four images of the open phase of a glottal period. It is evident that the low time resolution limits the precision of parameters based on the image data.

- Finally, if manual corrections of the glottal edges are necessary, it is very difficult to mark the edges consistently with the surrounding frames. This fact was noticed very clearly in a different experiment, where a fully custom-made user interface was experimented for examining the possibility of manually marking the edges of the vocal folds, frame by frame, on top of the video image. Even though the edges were drawn very carefully, the comparison of the area markings of two successive, almost identical glottal periods showed differences in the resulting glottal area pulses.

These limitations and inaccuracies must be borne in mind when interpreting the obtained area functions.

Parametrization of the Area Function

The area detection parameters in High-Speed Toolbox were adjusted individually for each five-period segment to be examined. The area detection process was then run on the entire video file, and the resulting area function was examined in the five-cycle time range of interest.

The glottal area function was parametrized using the pulse parameters introduced in Section 3.7: open quotient (OQ), closing quotient (ClQ), and speed quotient (SQ). The instants of opening, maximum area, and closure were detected in the area signal. The instant of opening was marked at the last frame of the closed phase where no opening could be seen. Correspondingly, the instant of closure was set at the first frame where the vocal folds were completely closed after the open phase. This is illustrated in Figure 4.11. In case of no

complete closure, the instants of opening and closure were set at the frame with minimum area of opening.

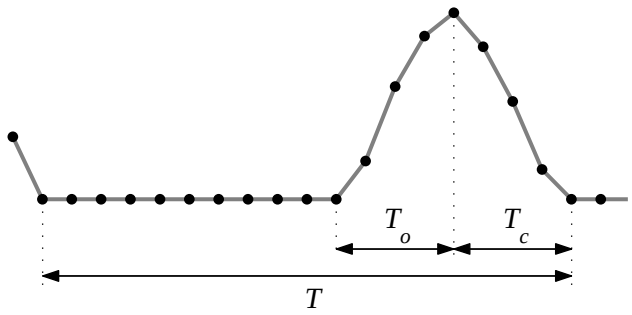

Figure 4.11: Phases of a glottal area pulse. The figure shows glottal cycle length T, opening time T_o, and closing time T_c derived from the area waveform.

All instants of opening, maximum area, and closure were checked manually by visual inspection of the image sequence. If necessary, the marks based on the automatically acquired area function were corrected. Indeed, changes were made in this manual checking stage. The most frequent reason was the inability of High-Speed Toolbox to detect a narrow slit between the vocal folds. Therefore, the opening marks were often moved backward and the closure marks forward by one frame.

Consequently, the automatically obtained area function was not directly used for parametrization or analysis of the glottal behavior. The area function provided, however, an important visualization that improved the understanding of the glottal behavior and also served as a basis for the manual corrections.

4.3.6 Error Estimates of Individual Pulse Parameters

Due to the limited frame rate of the high-speed imaging system, samples of the glottal area can be obtained relatively sparsely. If the closing, opening, and maximum instants of the area function are assumed to be located correctly, each such instant is marked to the frame closest to the true instant of the event. The maximum error of each measured time instant is thus one half of the time between two successive video frames.

This limits the precision of the pulse parameters OQ, ClQ, and SQ that are derived from the image material. It is important to assess the precision of these parameters to avoid making conclusions of minor variations that may actually be caused by measurement uncertainty.

The same source of uncertainty applies to the microphone and EGG signals, but the errors are much smaller because the sample rate (16 kHz) is almost ten times higher than the frame rate of the high-speed image sequence (1900 Hz).

Error Propagation

Suppose that a parameter y is calculated from measured quantities x_1, x_2, ..., x_n.

$$y = f(x_1, x_2, \ldots, x_n) \tag{4.11}$$

Also suppose that absolute limits Δx_i of measurement errors are available. The true value of each measured quantity is thus known to be in the range $x_i \pm \Delta x_i$. These errors will cause an error Δy in the calculated parameter y.

A general method for getting the formula of propagating error is based on the concept of total differential (Vaari, 1994). If each variable x_i changes by a small amount dx_i, the effect on y is given by the total differential

$$dy = \left(\frac{\partial f}{\partial x_1}\right) dx_1 + \left(\frac{\partial f}{\partial x_2}\right) dx_2 + \ldots + \left(\frac{\partial f}{\partial x_n}\right) dx_n. \tag{4.12}$$

The error in y caused by measurement errors is obtained by replacing the differentials dx_i by the corresponding error limits Δx_i. To get an upper bound for Δy, all error estimates as well as partial derivatives are assumed to be positive. This method gives the following formula for the error estimate of y:

$$\Delta y = \left|\frac{\partial f}{\partial x_1}\right| \Delta x_1 + \left|\frac{\partial f}{\partial x_2}\right| \Delta x_2 + \ldots + \left|\frac{\partial f}{\partial x_n}\right| \Delta x_n \tag{4.13}$$

If the error terms Δx_i are not considered absolute limits of error but statistical bounds, probable errors, or uncertainties, a different formula has to be used. According to Doebelin (1975), it can be shown (Scarborough, 1955) that a proper method for combining such errors is using the root-sum square formula:

$$E_{rss} = \sqrt{\left(\frac{\partial f}{\partial x_1}\Delta x_1\right)^2 + \left(\frac{\partial f}{\partial x_2}\Delta x_2\right)^2 + \ldots + \left(\frac{\partial f}{\partial x_n}\Delta x_n\right)^2} \tag{4.14}$$

This yields an error E_{rss} that has the same meaning as the individual errors Δx_i. The resulting error estimate is always smaller than that given by Equation 4.13 (Doebelin, 1975). In this work, however, this approach was not used.

Error Limits of Pulse Parameters

Figure 4.12 shows an idealized glottal pulse. The instants required for calculating pulse parameters from the waveform are indicated in the figure.

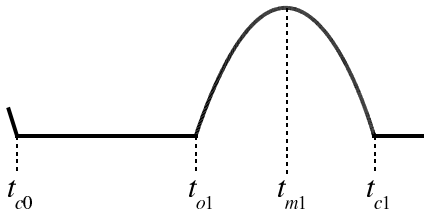

Figure 4.12: Idealized glottal pulse waveform. The instants required for calculating time-based pulse parameters are indicated: closure (t_{c0} and t_{c1}), opening (t_{o1}), and maximum (t_{m1}).

Let us denote the time intervals estimated from the pulse as follows:

- Cycle length $\hat{T} = t_{c1} - t_{c0}$
- Opening time $\hat{T_o} = t_{m1} - t_{o1}$
- Closing time $\hat{T_c} = t_{c1} - t_{m1}$

The instant of each event in the signal is assumed to be marked correctly to the sample closest to the actual event. Thus, the absolute limit of each time error can be assumed to be half the time between two successive samples. This is denoted by Δt.

$$\Delta t_{o1} = \Delta t_{c0} = \Delta t_{c1} = \Delta t = \frac{1}{2f_s} \tag{4.15}$$

An estimate of the fundamental frequency is obtained as the reciprocal of the cycle length estimate:

$$\hat{f_0} = \frac{1}{\hat{T}} = \frac{1}{t_{c1} - t_{c0}}. \tag{4.16}$$

An upper bound on the absolute error of f_0 can be obtained using the total differential method.

$$\Delta \hat{f_0} = \left| \frac{\partial \hat{f_0}}{\partial t_{c0}} \right| \Delta t_{c0} + \left| \frac{\partial \hat{f_0}}{\partial t_{c1}} \right| \Delta t_{c1} \tag{4.17}$$

Solving the partial differentials yields

$$\Delta \hat{f_0} = \left| \frac{1}{(t_{c1} - t_{c0})^2} \right| \Delta t_{c0} + \left| \frac{-1}{(t_{c1} - t_{c0})^2} \right| \Delta t_{c1}. \tag{4.18}$$

Using the notation introduced above, this can be rewritten as

$$\begin{aligned} \Delta \hat{f_0} &= \frac{1}{\hat{T}^2} \Delta t + \frac{1}{\hat{T}^2} \Delta t \\ &= \frac{2}{\hat{T}^2} \Delta t. \end{aligned} \tag{4.19}$$

This is a practical formula for the maximum error in the fundamental frequency estimate caused by the limited sampling frequency.

Open quotient (OQ) is defined as the ratio of the open phase length to the cycle length. The open quotient estimate acquired from the pulse in Figure 4.12 is thus

$$\widehat{\mathrm{OQ}} = \frac{t_{c1} - t_{o1}}{t_{c1} - t_{c0}}. \tag{4.20}$$

The total differential method gives the following upper bound on the absolute error propagated to the OQ estimate.

$$\Delta\widehat{\mathrm{OQ}} = \left|\frac{\partial\widehat{\mathrm{OQ}}}{\partial t_{o1}}\right|\Delta t_{o1} + \left|\frac{\partial\widehat{\mathrm{OQ}}}{\partial t_{c0}}\right|\Delta t_{c0} + \left|\frac{\partial\widehat{\mathrm{OQ}}}{\partial t_{c1}}\right|\Delta t_{c1} \tag{4.21}$$

Solving the partial differentials yields

$$\Delta\widehat{\mathrm{OQ}} = \left|\frac{-1}{t_{c1} - t_{c0}}\right|\Delta t_{o1} + \left|\frac{t_{c1} - t_{o1}}{(t_{c1} - t_{c0})^2}\right|\Delta t_{c0} + \left|\frac{t_{o1} - t_{c0}}{(t_{c1} - t_{c0})^2}\right|\Delta t_{c1} \tag{4.22}$$

which can be rewritten as

$$\begin{aligned}\Delta\widehat{\mathrm{OQ}} &= \frac{1}{\hat{T}}\Delta t + \frac{\hat{T}_o + \hat{T}_c}{\hat{T}^2}\Delta t + \frac{\hat{T} - \hat{T}_o - \hat{T}_c}{\hat{T}^2}\Delta t \\ &= \frac{2}{\hat{T}}\Delta t.\end{aligned} \tag{4.23}$$

Similarly, closing quotient (ClQ) is defined as the ratio of the closing phase length to the cycle length and is estimated from the time instants shown in Figure 4.12 by the formula

$$\widehat{\mathrm{ClQ}} = \frac{t_{c1} - t_{m1}}{t_{c1} - t_{c0}}. \tag{4.24}$$

The total differential method yields the following estimate of the upper bound on the absolute error of ClQ.

$$\begin{aligned}\Delta\widehat{\mathrm{ClQ}} &= \left|\frac{\partial\widehat{\mathrm{ClQ}}}{\partial t_{m1}}\right|\Delta t_{m1} + \left|\frac{\partial\widehat{\mathrm{ClQ}}}{\partial t_{c0}}\right|\Delta t_{c0} + \left|\frac{\partial\widehat{\mathrm{ClQ}}}{\partial t_{c1}}\right|\Delta t_{c1} \\ &= \left|\frac{-1}{t_{c1} - t_{c0}}\right|\Delta t_{m1} + \left|\frac{t_{c1} - t_{m1}}{(t_{c1} - t_{c0})^2}\right|\Delta t_{c0} + \left|\frac{t_{m1} - t_{c0}}{(t_{c1} - t_{c0})^2}\right|\Delta t_{c1} \\ &= \frac{1}{\hat{T}}\Delta t + \frac{\hat{T}_c}{\hat{T}^2}\Delta t + \frac{\hat{T} - \hat{T}_c}{\hat{T}^2}\Delta t \\ &= \frac{2}{\hat{T}}\Delta t\end{aligned} \tag{4.25}$$

Finally, the speed quotient (SQ) estimate is

$$\widehat{\mathrm{SQ}} = \frac{t_{m1} - t_{o1}}{t_{c1} - t_{m1}}. \tag{4.26}$$

and its error limit is obtained as follows.

$$\begin{aligned}
\Delta\widehat{\mathrm{SQ}} &= \left|\frac{\partial\widehat{\mathrm{SQ}}}{\partial t_{o1}}\right|\Delta t_{o1} + \left|\frac{\partial\widehat{\mathrm{SQ}}}{\partial t_{m1}}\right|\Delta t_{m1} + \left|\frac{\partial\widehat{\mathrm{SQ}}}{\partial t_{c1}}\right|\Delta t_{c1} \\
&= \left|\frac{-1}{t_{c1}-t_{m1}}\right|\Delta t_{o1} + \left|\frac{t_{c1}-t_{o1}}{(t_{c1}-t_{m1})^2}\right|\Delta t_{m1} + \left|\frac{-(t_{m1}-t_{o1})}{(t_{c1}-t_{m1})^2}\right|\Delta t_{c1} \\
&= \frac{1}{\hat{T}_c}\Delta t + \frac{\hat{T}_o+\hat{T}_c}{\hat{T}_c^2}\Delta t + \frac{\hat{T}_o}{\hat{T}_c^{\,2}}\Delta t \\
&= 2\frac{\hat{T}_o+\hat{T}_c}{\hat{T}_c^{\,2}}\Delta t \\
&= 2\frac{\frac{\hat{T}_o+\hat{T}_c}{\hat{T}}}{\frac{\hat{T}_c^{\,2}}{\hat{T}^2}\hat{T}}\Delta t \\
&= 2\frac{\widehat{\mathrm{OQ}}}{\widehat{\mathrm{ClQ}}^{\,2}\hat{T}}\Delta t
\end{aligned} \tag{4.27}$$

Error Limits of Averaged Pulse Parameters

Representative parameter values are commonly estimated by averaging the parameters calculated from a few successive glottal cycles:

$$\hat{y} = \frac{1}{N}\sum_{n=1}^{N}\hat{y}_n \tag{4.28}$$

Absolute error limits of the mean can be obtained from the error limits of individual parameter values y_n using the total differential method. Since

$$\frac{\partial\hat{y}}{\partial\hat{y}_n} = \frac{1}{N}, \tag{4.29}$$

Equation 4.13 implies that the error bound of the mean is the mean of the individual error bounds.

Applying this principle to the mean pulse parameters of successive glottal cycles gives the upper bound on the error of the mean caused by low temporal resolution. The approach assumes that the time instants are perfectly assigned to the respective signal samples and that all examined pulses are identical.

The glottal pulse parameters extracted from successive glottal periods are not completely independent. The closure instant is used as the end mark of one cycle and the beginning mark of the next cycle. Therefore, error in the timing of a closure instant affects both the preceding and the following cycle. This interdependency is ignored in this error analysis.

Another commonly used method for estimating the error limits of the mean of measured values is to calculate the standard error of the mean (SEM), which is derived from the

variance of individual measured values. It is calculated using the following formula (Vaari, 1994; Klaucke *et al.*, 2004; Pindyck & Rubinfeld, 1998):

$$\text{SEM} = \sqrt{\frac{\sum (y_i - \bar{y})^2}{N(N-1)}} \tag{4.30}$$

It can be stated with 95 percent confidence that the mean of the measured characteristic is between $\bar{y} - 1.96$ SEM and $\bar{y} + 1.96$ SEM (Pindyck & Rubinfeld, 1998).

According to Klaucke *et al.* (2004), the standard error of the mean can be used as an estimate of confidence if the characteristic to be measured is normally distributed, or if the distribution is not normal but the sample size is greater than 30. In this study, only five consecutive glottal cycles were averaged, and it is probably not safe to assume that the pulse parameters are normally distributed. Moreover, due to the relatively low frame rate of the imaging system, it is not uncommon that a pulse parameter estimation yields exactly the same value from five successive cycles of the glottal area waveform. In such cases, the SEM equals zero and fails to give any useful information about the real uncertainty of the parameter value. However, also in these cases, the error limits derived from the temporal resolution using the total differential method give an appropriate estimate of the uncertainty caused by the limited time resolution.

Consequently, two complementary error estimates were calculated for each average pulse parameter:

1. The uncertainty caused by the limited time resolution is quantified by the mean of the error bounds of individual parameter values. This does not take into account any variation between successive cycles nor errors in marking the time instants of events in the glottal waveforms.

2. The standard error of the mean (SEM) is calculated from the variance of individual parameter values and the 95 % confidence interval is derived from the SEM. Low temporal resolution of the glottal area data causes this measure to be useless in some cases, and the low number of samples in the calculation of mean also deteriorates the reliability of the SEM-based uncertainty estimate.

4.3.7 Synchronization

Pedal Pulse

Since the high-speed image sequence was stored separately from the other signals, explicit synchronization was required. For the comparison of glottal area waveform with the corresponding glottal flow signal, it was essential to find exactly which area pulse corresponds

to each flow pulse. Much more accurate synchronization of the flow and area signals would be necessary to assess temporal differences between the waveforms in detail.

The pedal pulse, which stopped the high-speed imaging, was recorded on the synchronization channel. The beginning of the pedal pulse was detected automatically from each recording by finding the position of maximum derivative of the synchronization signal. This indicated the instant of the last video frame.

An obvious source of uncertainty in this method is that the pedal pulse does not occur in synchrony with the video frames and, consequently, the time difference between the pulse and the last frame varies between 0 and 1 frames. Granqvist *et al.* (2003) examined the synchronization error between the pedal pulse and the last frame in a similar experimental setup. They recorded a periodically varying light signal simultaneously by a light diode and the high-speed camera. Comparison of these two recordings showed that the time shift between the pedal pulse and the last video frame was 0.27 frames on average with standard deviation of 0.39 frames.

Based on this result, the instant of the last frame was shifted backward from the beginning of the pedal pulse by 0.27 frames also in this study. Consequently, the timing of the last frame was set slightly prior to the pedal pulse. However, this procedure does not remove the uncertainty indicated by the standard deviation of the time shift in the measurements made by Granqvist *et al.* (2003).

If the error is assumed to be caused purely by the random timing of the pulse between two successive video frames, the theoretical standard deviation can be calculated easily. The probability density function of the pedal pulse $f(x)$ is supposed to be uniform in the time range from 0 to 1 frames and zero outside this range. Thus, the expected value of delay is

$$\mu = \int_0^1 x f(x)\,\mathrm{d}x = \frac{1}{2} \tag{4.31}$$

and the standard deviation

$$\sigma = \sqrt{\int_0^1 (x-\mu)^2 f(x)\,\mathrm{d}x} \approx 0.29, \tag{4.32}$$

which is less than the empirically measured value 0.39. Thus, there is more uncertainty related to the timing of the last frame and the pedal pulse than just the interval between two successive frames. In other words, the last frame may actually occur more than one frame time after the pedal pulse.

Video Frame Rate

Granqvist *et al.* (2003) also stated that the synchronization drifted as the distance from the pedal pulse increased because the sound card sample rate and the frame rate of the high-

speed camera were not synchronized. In this study, this source of timing error was reduced by including the video signal on the synchronization channel. This provided means to measure the video frame rate in the postprocessing stage. Figure 4.13 shows a short excerpt of the synchronization signal. Despite the relatively low sample rate, the frame rate is evident.

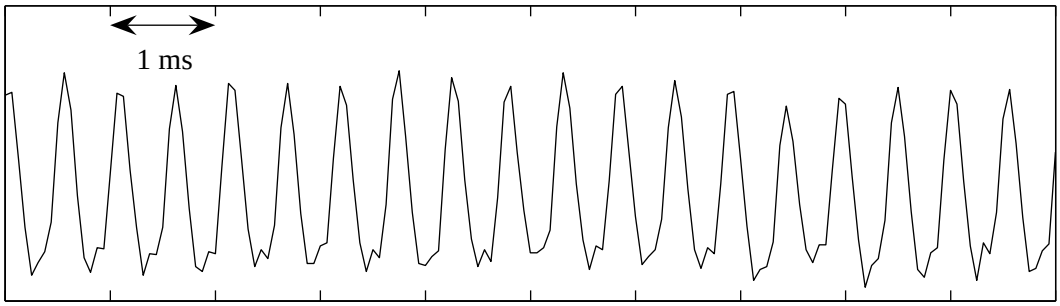

Figure 4.13: Video signal on the synchronization channel. The frame rate of approximately 1900 Hz can be obtained accurately from the signal.

The frame rate was estimated from each synchronization signal by the following procedure:

1. Hanning window was applied to the synchronization signal of the entire recording.
2. Fast Fourier Transform (FFT) of one million points was computed from the windowed signal to get the spectrum.
3. The highest peak of the amplitude spectrum in the frequency range from 1880 Hz to 1910 Hz was located. This was used as the estimate of frame rate.

Synchronization signals were examined by listening. This revealed that in many cases the the microphone signal was audible also on the synchronization channel at a level almost comparable to the video synchronization signal. The video synchronization tone at approximately 2 kHz varied in intensity and timbre between recordings and also within each recording. However, it was almost impossible to assess perceptually if there was also variation in the fundamental frequency of the synchronization signal.

The stability of the frame rate was examined by applying the frame rate estimation procedure to different parts of each recording: the entire file, the duration of the stored video sequence (4.3 s), the first half of the stored video sequence (2.1 s), and the last half of the stored video sequence (2.1 s). The results showed that differences between the frame rate estimates of different portions of a recording differed by less than 0.1 Hz in most cases. In

all but two cases, the maximum difference was less than 0.3 Hz. For two recordings, the maximum difference was almost one frame per second, but also in these cases the difference between the frame rate estimate of the entire file and the portion of the stored video recording was less than 0.3 Hz.

The frame rates estimated from the entire recordings were between 1891.7 Hz and 1892.3 Hz except for one recording whose frame rate was 1904.8 Hz. This deviant recording also had a break in the image sequence and was discarded. Another file showed an interesting phenomenon: very close to the moment of the pedal press, the frame rate jumped approximately from 1892 Hz to 1898 Hz. Since this happened at the end of the image sequence, it was considered harmless. Similar behavior was not found in any other recording.

As a result, the frame rate estimated from each entire recording was considered reliable enough to be used for the synchronization of high-speed images with the other signals. This was supposed to give more accurate synchronization than using the frame rate saved to a data file during the recording since this was given at the precision of one Hz only. Indeed, visual inspection showed no considerable synchronization drift between the area and flow waveforms during the 4.3-second time span of each image sequence. The uncertainty of the exact position of the pedal pulse relative to the last frame was considered larger than that caused by the inaccuracy of the frame rate estimate.

The video signal on the synchronization channel also opened up the possibility of more exact timing of the last video frame by means of the video signal phase. However, it was not known at which point of the video frame cycle the image was actually obtained from the photo sensors and whether this happened instantaneously for the entire image. Furthermore, there was no way or eliminating the uncertainty of whether one more frame occurs after the pedal pulse or not. Therefore, the video signal phase was not used for correcting the timing of the last frame relative to the pedal pulse.

Propagation Delay

Electroglottography and high-speed imaging indicate movements of laryngeal tissues practically instantly, whereas a significant delay is associated with the propagation of the acoustic signal from the vocal folds to the microphone. Therefore, to examine the laryngeal events originating in the larynx at the same instant of time, the microphone signal has to be shifted relative to the other signals. The propagation delay is determined by the distance from the sound source to the microphone and the speed of sound in the medium.

The length of the vocal tract is typically approximately 17 centimeters for men and 15 centimeters for women. During the recording, the distance from the subject's mouth to the microphone was tried to keep constant at 10 centimeters. Thus, the distance from the glottis to the microphone was 27 centimeters and 25 centimeters for male and female subjects,

respectively. The speed of sound was approximated to be 350 m/s, which is probably a relatively accurate approximation in the conditions where the air is warmed by the human body temperature.

Thus, the microphone signal was shifted for males by

$$\Delta t = \frac{0.27}{350\ \frac{\mathrm{m}}{\mathrm{s}}} = 0.771\ \mathrm{ms}. \tag{4.33}$$

Similarly for females, it was shifted by

$$\Delta t = \frac{0.25}{350\ \frac{\mathrm{m}}{\mathrm{s}}} = 0.714\ \mathrm{ms}. \tag{4.34}$$

This corresponds to 11–12 samples at the sample rate of 16 kHz.

Evaluation of Synchronization Accuracy

The accuracy of synchronization between the obtained signals was assessed by comparing the waveforms. Especially, the instant of glottal closure was detected in the signals because it can be detected most reliably. It corresponds to the instant of major excitation of the vocal tract system within a pitch period because the glottis closes abruptly and opens more slowly (Strube, 1974).

Several algorithms have been proposed for locating the glottal closure instant (GCI) in the acoustic signal automatically. One such method detects discontinuities of the differentiated speech signal (Ananthapadmanabha & Yegnanarayana, 1975). Many other methods are primarily based on the linear prediction error, which is large at the location of glottal closure (Strube, 1974; Ma *et al.*, 1994). Several improvements to this basic principle have been developed utilizing e.g. maximum-likelihood epoch determination and Hilbert transform (Cheng & O'Shaughnessy, 1989), Frobenius norm approach (Ma *et al.*, 1994), or the group delay function (Smits & Yegnanarayana, 1995). Since the detection of glottal closure was used only for the evaluation of synchronization in this study, the instant of major excitation was estimated manually based on the instant of an abrupt change in the microphone signal.

The instant of glottal closure occurs in the glottal flow signal at the position where the flow drops abruptly to the base level. This is illustrated in Figure 3.7.

In the electroglottographic signal, the glottal closure causes a steep, abrupt decrease in the waveform, as shown in Figure 3.6. According to Henrich *et al.* (2004), the peak in the derivative of the EGG signal can be regarded as a reliable indication of the instant of glottal closure in the modal register.

The glottal area signal, of course, drops to zero at the point of glottal closure.

These definitions of the glottal closure instant are based on different signals and may thus be related to slightly different physiological events during the closing phase. However, time differences between those instants should not be large.

The maximum acoustic excitation located in the microphone signal seemed to coincide with the glottal closure as detected from the inverse filtered flow signal. The peak of the DEGG waveform also matched well with the end of the glottal area pulse in general. However, the closure was consistently marked at an earlier instant of time in the microphone and flow signals as compared to the EGG or area signals. In several cases, the timing difference was as much as 0.5 milliseconds, which corresponds to more than 15 cm in distance, and the pressure signal never seemed to lag the EGG signal. Furthermore, the distance from the synchronization pulse was not found to have any consistent effect on the magnitude of the synchronization offset.

An example of the evaluation of synchronization accuracy is shown in Figure 4.14. The closure instant of the flow waveform coincides with the location of excitation in the pressure signal. Also, the DEGG peak occurs between the time instants of the last non-zero area sample and the following zero-valued area sample.

The observed synchronization shift has approximately the same magnitude as the uncertainty related to the alignment of the high-speed image sequence with the other signals. The instants of closure detected in the different signals are also related to different physiological phenomena and they may thus not occur exactly simultaneously, which causes some uncertainty in the evaluation of synchronization accuracy.

Due to the uncertainty of synchronization, accurate temporal within-period comparisons between the area function and the inverse filtered flow waveform were not considered reasonable. However, the synchronization error was small compared to the cycle length, and the area pulse corresponding to each flow pulse could thus be identified exactly. Consequently, pulse-by-pulse comparisons of signal waveforms were possible.

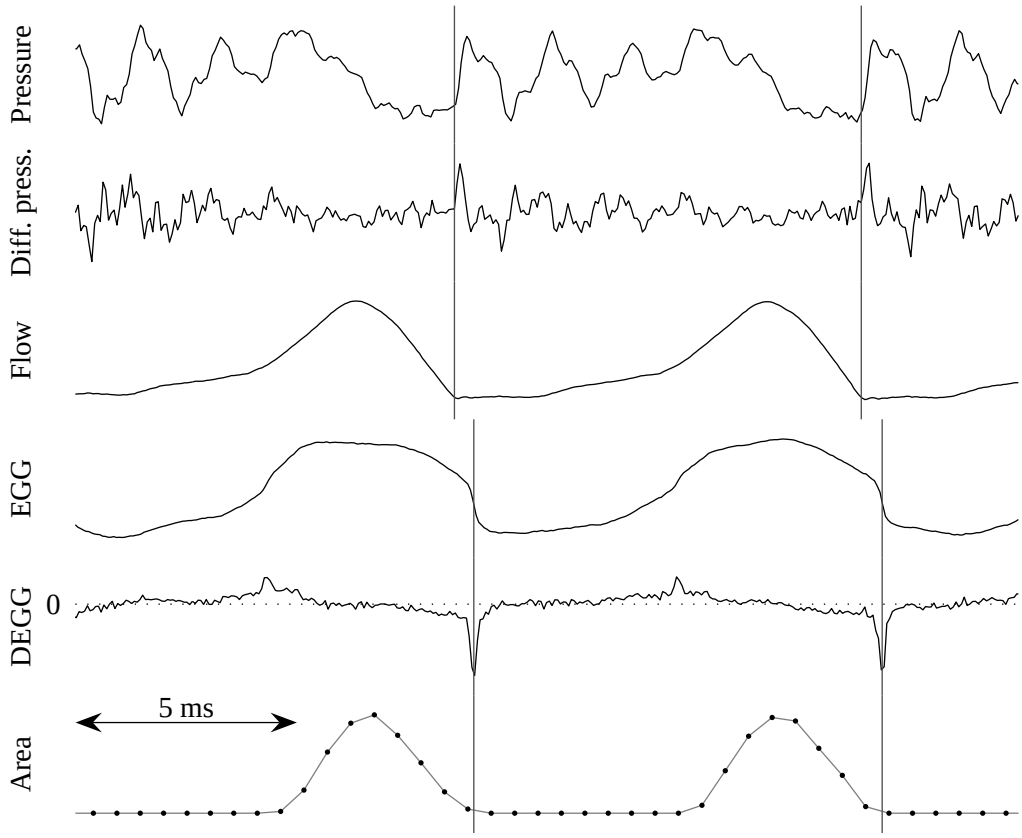

Figure 4.14: Evaluation of signal synchronization. The figure shows the following signals from top to bottom: pressure captured by microphone, differentiated pressure, inverse filtered glottal flow, EGG, differentiated EGG, and glottal area extracted from the high-speed image sequence. Propagation delay has been compensated for by shifting the pressure signal and the flow signal. Two instants of closure, indicated by gray vertical lines, have been located manually in the flow waveform and in the EGG signal. The acoustic signal shows an abrupt change at the closure instant found in the flow signal, whereas the closure in the area function matches well with the instant of closure detected in the electroglottogram. The mismatch between the two instants is approximately 0.4 milliseconds, which is similar in magnitude to the uncertainty of the alignment of the high-speed image sequence. The instants detected in different signals are related to different physiological phenomena, which causes some uncertainty in this comparison.

4.4 HUT Experiment

4.4.1 Recording Setup

The second experiment was conducted in the anechoic chamber of the Laboratory of Acoustics and Audio Signal Processing at Helsinki University of Technology in May 2003. There were 13 subjects, 6 females and 7 males. Most of them were young adults and none had voice disorders.

The subjects were asked to phonate sustained /a/ vowels five times in sequence, first in breathy, then in normal, and finally in pressed phonation. The duration of each phonation was approximately one second.

Phonations were captured by a Brüel & Kjær 4188 condenser microphone that was attached to a Brüel & Kjær Mediator 2238, which is a sound pressure level meter and also functions as a microphone amplifier. The signal was recorded on a DAT tape. The distance from the subject's mouth to the microphone was 40 cm, and special attention was paid to keeping it constant. The distance was controlled and, if necessary, corrected during the recording session.

Electroglottogram was recorded simultaneously with the acoustic signal. A Glottal Enterprises MC2-1 electroglottograph was used. Another channel of the DAT tape was used for storing the EGG signal.

The signals were stored on the digitally on the tape using 48 kHz sample rate and 16 bits per sample. The data were later moved to a computer hard disk.

The same material is used in another study that compares the flow waveforms obtained by several operators of two different inverse filtering methods (Lehto *et al.*, 2005).

4.4.2 Data Selection and Preprocessing

The sampling rate was reduced to 22.05 kHz using the downsampling feature of the Cool Edit Pro software version 1.2a.

A segment of ten successive glottal periods was selected for analysis from every subject's breathy, normal, and pressed phonation. Primarily, the segment was chosen from the third of the five phonations of the same phonation type, starting at 100 milliseconds after the beginning of the phonation. However, this rule was not followed strictly in some cases where a more stable and more representative sample was obtained at another position or where the subject had made more than five phonations.

4.4.3 Calculation of the Sound Pressure Level

Sound pressure level was measured from each window of interest in the same way as described in Section 4.3.3. The Brüel&Kjær Sound Level Calibrator of type 4231 was used also in this experiment. A calibration file was recorded in the beginning of the recording session. Gain settings were not altered during the experiment, so this calibration file applies to all recordings.

4.4.4 Inverse Filtering

The selected segments of the phonations were inverse filtered using the HUT IAIF Toolbox software, which was introduced in Section 4.2.1.

First, the cutoff frequency of high-pass filtering was set automatically eight percent below the fundamental frequency of the phonation. The number of formants was then set to the lowest value that gave a reasonable glottal flow waveform. The value of this parameter varied between 7 and 15 for these signals. Finally, the lip radiation term was adjusted in the range from 0.97 to 0.9975 so that a horizontal closed phase appeared in the flow waveform if possible. Other parameters had default values.

The high-pass filtering phase reduced the length of the analyzed signal segment from 10 periods by a couple of periods because part of the signal was required to fill the filter's internal memory, which is necessary for the filtering operation to stabilize.

4.4.5 Electroglottogram

The EGG signals obtained in this experiment were superior in quality to those obtained from the Huddinge experiment. The sample electroglottogram in Figure 3.5 was acquired from a normal phonation of a male subject in this experiment. It is a good example of a very clean EGG signal as compared to the one in Figure 4.6.

The EGG signals were high-pass filtered digitally using a 2048th-order linear-phase FIR filter with cutoff frequency at 70 Hz. This removed low-frequency fluctuations that were considerably large in the EGG signal.

4.4.6 Compensation of the Propagation Delay

The sound propagation from the glottis to the microphone was compensated in order to assess the glottal behavior at the same instant of time in both the inverse filtered flow waveform and the EGG. Therefore, the EGG signal was delayed relative to the sound pressure signal and the inverse filtered flow signal.

The vocal tract length was assumed to be 15 cm for female subjects and 17 cm for male

subjects. The distance from the subject's mouth to the microphone was 40 cm in the recording setting, so the total travel distance was 55 cm and 57 cm for women and men, respectively. The speed of sound was supposed to be 350 m/s. The delay was thus approximately 1.6 ms, or 35–36 samples at the sampling rate of 22.05 kHz.

After compensating for the sound propagation delay, the synchronization of the microphone and EGG signals was assessed by comparing the instants of closure detected manually from the microphone signals, inverse filtered flow waveforms, and differentiated EGG signals. Good agreement was found in these comparisons. Based on this observation and the fact that the microphone distance was repeatedly controlled in the recording session, the synchronization was considered accurate enough for temporal comparisons of instants detected in the inverse filtered flow waveforms and the corresponding EGG waveforms.

4.4.7 Parametrization of Glottal Flow and EGG

Detailed behavior of the inverse filtered flow pulses and the EGG waveforms in the opening and closing phases were of major interest for this data set. Also, it was assumed that the compensation of the sound propagation delay was quite accurate. Therefore, instead of the quotients introduced in Section 3.7, exact instants of significant events in the flow and EGG waveforms were detected. Automatic algorithms were developed and tuned for this purpose.

Glottal Flow Waveform

Locating instants of significant events in the flow waveform was based on three signals:

1. The inverse filtered flow itself.
2. The first derivative of the flow. This was constructed by simply calculating the difference of consecutive sample values.
3. A smoothed second derivative of the flow signal. Basically, this signal was produced by first applying a Gaussian mask to the signal to smooth it and then differentiating the result twice. Since these operations are linear, the same result can be obtained by differentiating the Gaussian mask twice and then applying it to the original signal. This procedure yields the mask shown in Figure 4.15. A similar mask shape can be obtained as a difference of two Gaussians with different standard deviations. This is known as the Difference of Gaussians (DoG) operator, or the Mexican Hat operator. It is used in edge detection applications. (Owens, 1997)

   The Gaussian mask was computed by

$$y = e^{-\left(\frac{t}{0.05T}\right)^2} \tag{4.35}$$

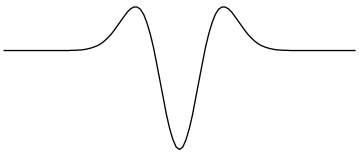

Figure 4.15: Mask for calculating the smoothed second derivative. The shape is obtained by differentiating a Gaussian mask twice.

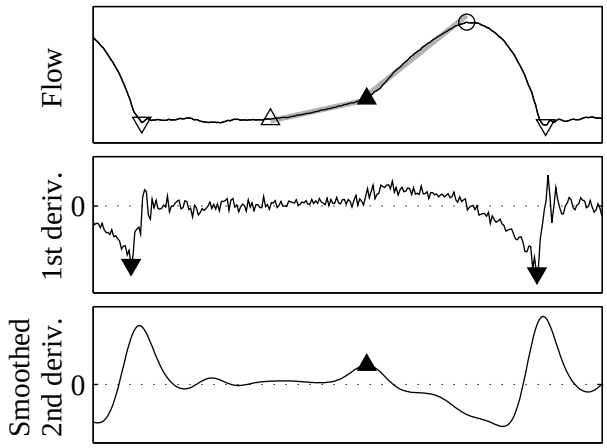

Figure 4.16: Significant instants detected from the glottal flow waveform. Inverse filtered flow is shown in the top panel, first derivative of the flow in the middle panel, and smoothed second derivative in the bottom panel. The detected instants are marked as follows: ○ maximum flow, ▼ negative peak of the flow derivative, ▽ closure, △ primary opening, and ▲ secondary opening. Gray lines illustrate the regression lines that have been fit to the opening phase of the flow waveform.

where T is the length of the glottal cycle.

Figure 4.16 shows an example of these three signals calculated from a single flow pulse. The following instants were detected from each flow period:

1. The instant of maximum flow was detected as the maximum of the inverse filtered flow signal within the cycle.

2. The instant of primary excitation was located as the minimum of the flow derivative between two successive flow maxima.

3. The range of flow variation during the cycle was defined as the range from the lowest flow level between two successive flow maxima to the flow level at the preceding maximum. A threshold was set at 15 % above the bottom of this flow range. The instant of closure was then determined by searching forward from the instant of negative peak of the flow derivative until a point was found where the flow was below the threshold and the flow derivative had a positive value.

4. For the detection of the primary opening instant, another flow range and threshold were defined. The minimum of the range was set at the average flow value during the 10 % of the period length after the instant of closure, and the maximum was the flow level at the next flow maximum. A threshold was defined at 10 % above the bottom of this range. The instant of primary opening was then found in two stages: First, the flow signal was scanned backward from the next flow maximum until the flow value dropped below the threshold. Then, the backward scanning was continued as long as either the flow derivative was positive or the preceding 5 % of the glottal period contained a flow value lower than 1 % of the flow range below the flow value at the current scanning position. The instant of primary opening was then set at the point where this search algorithm stopped. However, the opening instant was not allowed to occur before the instant of closure.

5. Finally, the instant of secondary opening was located at the largest local maximum of the smoothed second derivative of the flow signal in the time window starting 5 % of the period after the primary opening and extending up to the next flow maximum.

Furthermore, the sharpness of the knee in the flow waveform at the secondary opening was assessed quantitatively. Two regression lines were fit to the flow signal using the least-squares criterion, one between the primary opening and the secondary opening, and the other between the secondary opening and the following flow maximum. Such regression lines are shown in gray in Figure 4.16. The slopes of these two lines are denoted here by k_1 and k_2, respectively. The sharpness of the knee was quantified by

$$S = \frac{k_1 - k_2}{flow_{max} - flow_{min}} T \tag{4.36}$$

where $flow_{max}$ is the value of the flow at its maximum, $flow_{min}$ is the minimum flow value within the period, and T is the length of the glottal period.

Electroglottogram

Similarly, the instants corresponding to the glottal opening and closure were identified automatically in each cycle of the electroglottogram. The detection was based on the first

derivative of the EGG signal (DEGG). Figure 4.17 illustrates the EGG waveform and its derivative during one glottal cycle and also indicates the detected instants of closure and opening.

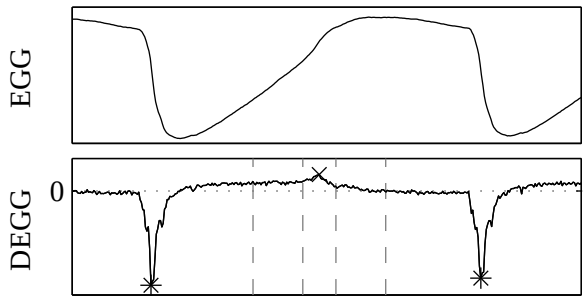

Figure 4.17: Glottal closure and opening detected from the EGG waveform: ✳ closure and $\times$ opening. The top panel shows the EGG waveform and the bottom panel its first derivative, the differentiated EGG.

1. The instant of glottal closure was determined in the time window between two successive flow maxima as the first local minimum of the DEGG signal that was less than 25 % above the global minimum in this time window.

2. The instant of glottal opening was located as the maximum of the DEGG signal in the time window between the EGG closure instant and the next flow maximum.

   The sharpness of the opening peak was also assessed by a quantitative measure. The maximum value of the DEGG signal was searched in a time window of 40 % of the glottal cycle length around the opening peak, excluding the 10 % of the glottal cycle in the middle of that window. This value, denoted by $DEGG_{win}$, was thus the maximum of the DEGG in the neighborhood of the peak excluding the very closest vicinity. The dashed vertical lines in Figure 3.6 indicate the borders of this window. The sharpness of the opening peak was then quantified by the measure

   $$P = \frac{DEGG_{max} - DEGG_{win}}{EGG_{max} - EGG_{min}} T \tag{4.37}$$

   where $DEGG_{max}$ is the maximum value of the opening peak in DEGG, EGG_{min} and EGG_{max} are the minimum and maximum values of the EGG signal between two successive flow maxima, and T is the cycle length. The purpose of the denominator in the formula is to normalize the measure to variations in the EGG amplitude, whereas T normalizes variations in the fundamental frequency.

Chapter 5

Results

This chapter reports the results obtained using the material and methods described in the previous chapter. Numerical data and graphical illustrations are provided. Special, unexpected findings are also reported. Further analysis and explanations of the results is the topic of Chapter 6.

5.1 Huddinge Experiment

The data files of the Huddinge experiment were numbered with consecutive numbers when the recordings were saved. Altogether, 20 recordings were successful and were examined. Each of them contained three phonations that were analyzed.

In this thesis, the three subjects are referred to as Female 1, Male 1, and Male 2. Each recording is denoted by a combination of subject and recording number, e.g. Male1-06. Individual phonations are indicated by the recording identification followed by the phonation type: breathy, normal, or pressed for phonation modes, and soft, normal, or loud in case of loudness variation. The loudness referred to as normal does not necessarily correspond to the subject's habitual way of speaking but it refers to the second last of the four phonations in this phonation task. See Sections 4.3.1 and 4.3.2 for details of the recording setting and data selection.

Table 5.1 lists all the recordings.

5.1.1 Sound Pressure Level Estimates

Sound pressure level estimates were calculated for each analyzed phonation from the signal in the analysis window as described in Section 4.3.3. Recording settings were changed several times during the experiment. Therefore, several calibration files were used for SPL calculation.

Table 5.1: Huddinge recordings. File numbers between 19 and 37 were used for another type of experiment which is not included in this work.

Recording	Subject	File	Phonation task
Male1-03	Male 1	finnl03a	breathy, normal, pressed
Male1-05	Male 1	finnl05a	breathy, normal, pressed
Male1-06	Male 1	finnl06a	breathy, normal, pressed
Male1-07	Male 1	finnl07a	breathy, normal, pressed
Male1-08	Male 1	finnl08a	soft, normal, loud
Male1-09	Male 1	finnl09a	soft, normal, loud
Male1-10	Male 1	finnl10a	soft, normal, loud
Male2-12	Male 2	finnl12a	breathy, normal, pressed
Male2-13	Male 2	finnl13a	breathy, normal, pressed
Male2-14	Male 2	finnl14a	breathy, normal, pressed
Male2-15	Male 2	finnl15a	breathy, normal, pressed
Male2-16	Male 2	finnl16a	soft, normal, loud
Male2-17	Male 2	finnl17a	soft, normal, loud
Male2-18	Male 2	finnl18a	soft, normal, loud
Female1-38	Female 1	finnl38a	breathy, normal, pressed
Female1-39	Female 1	finnl39a	breathy, normal, pressed
Female1-40	Female 1	finnl40a	breathy, normal, pressed
Female1-41	Female 1	finnl41a	soft, normal, loud
Female1-42	Female 1	finnl42a	soft, normal, loud
Female1-43	Female 1	finnl43a	soft, normal, loud

Tables 5.2 and 5.3 show the results of SPL calculation. For each recording, the SPL is shown for all three phonations. The difference in SPL between each pair of successive phonations is also presented. Additionally, the table indicates the calibration file that is related to each recording according to the annotations made during the recording session. Figures 5.1 and 5.2 illustrates the SPL estimates graphically.

A listening check revealed that the background noise level changes notably between recordings 07 and 08 but not between recordings 08 and 09 where the annotations indicate a change of the calibration signal. Similarly, listening indicated a change in noise level between recordings 16 and 17. According to the notes, however, the calibration file was not changed here. Since assigning calibration files to recordings by listening would involve too much guesswork, the results shown here are based on the annotations, but suspicious cases are marked by asterisks in Table 5.3. Fortunately, the SPL values are not salient results of this study.

In each recording, the SPL increases consistently from breathy to pressed phonation and

Table 5.2: Sound pressure level estimates of vowels in different phonation types in the Huddinge experiment. Sound pressure levels are given in dB with linear weighting.

Recording	Calibration file	Breathy	Δ	Normal	Δ	Pressed
Male1-03	kalib	81.3	*6.6*	87.9	*1.8*	89.7
Male1-05	kalib	82.7	*4.6*	87.3	*1.4*	88.7
Male1-06	kalib	81.9	*5.7*	87.6	*2.1*	89.7
Male1-07	kalib	80.3	*5.6*	85.9	*2.7*	88.6
Male2-12	kalib2	71.6	*3.1*	74.7	*4.3*	79.0
Male2-13	kalib2	73.3	*7.7*	81.0	*3.3*	84.3
Male2-14	kalib2	70.7	*10.5*	81.2	*3.5*	84.7
Male2-15	kalib2	77.0	*5.5*	82.5	*6.4*	88.9
Female1-38	kalib3	77.2	*5.0*	82.2	*15.0*	97.2
Female1-39	kalib3	72.7	*7.6*	80.3	*9.9*	90.2
Female1-40	kalib3	75.8	*3.5*	79.3	*2.7*	82.0

Table 5.3: Sound pressure level estimates of phonations at different loudness in the Huddinge experiment. Sound pressure levels are given in dB with linear weighting. Three recordings are marked with an asterisk (*) indicating a probable confusion with the calibration files.

Recording	Calibration file	Soft	Δ	Normal	Δ	Loud
Male1-08	kalib*	77.3	*10.0*	87.3	*6.9*	94.2
Male1-09	kalib2	95.6	*5.0*	100.6	*5.4*	106.0
Male1-10	kalib2	94.3	*6.8*	101.1	*4.8*	105.9
Male2-16	kalib2	88.7	*12.2*	100.9	*8.7*	109.6
Male2-17	kalib2*	74.0	*17.4*	91.4	*10.4*	101.8
Male2-18	kalib2*	80.1	*7.0*	87.1	*10.0*	97.1
Female1-41	kalib4	76.4	*13.1*	89.5	*12.2*	101.7
Female1-42	kalib4	79.6	*8.3*	87.9	*19.5*	107.4
Female1-43	kalib4	87.0	*12.9*	99.9	*2.8*	102.7

from soft to loud phonation as expected. Yet, there are considerable differences in SPL values between subjects but also between the phonations of the same subject within the same phonation type. Some of the within-subject variation may be explained by errors in the notes about calibration files, but remarkable variation still remains. This indicates that the phonations vary in their acoustic features even in consecutive recordings of the same subject and the same phonation task.

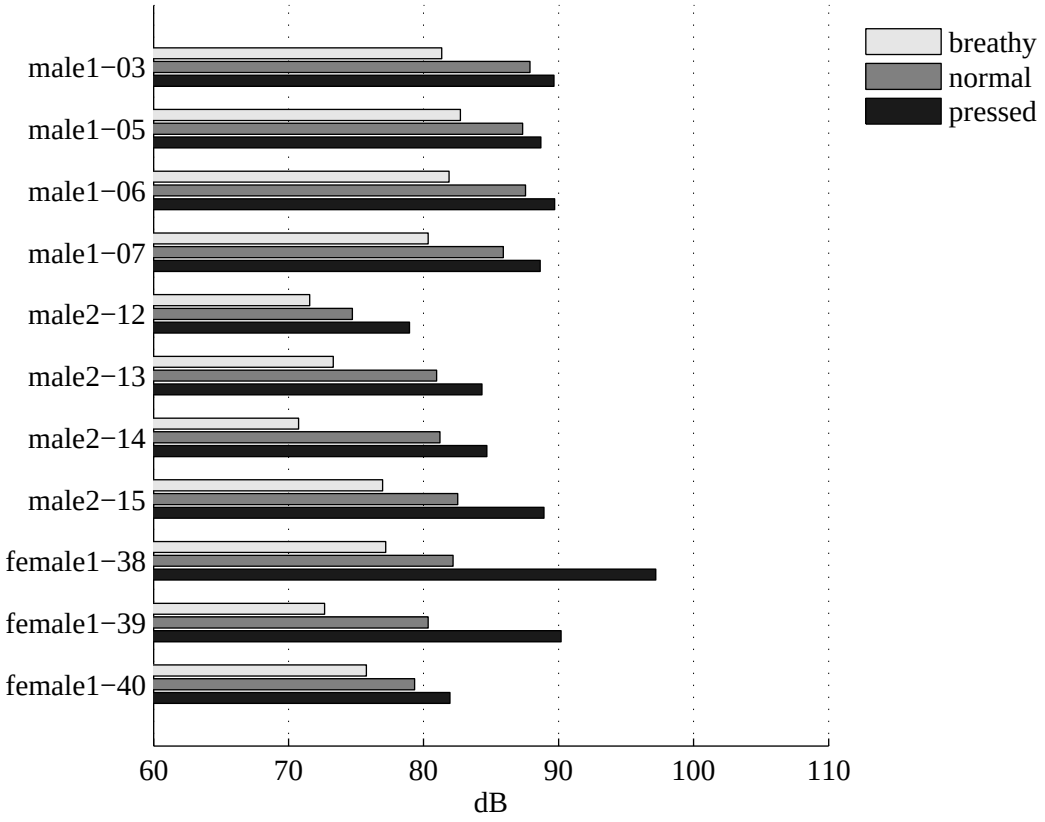

Figure 5.1: Sound pressure level estimates of vowels in different phonation types in the Huddinge experiment.

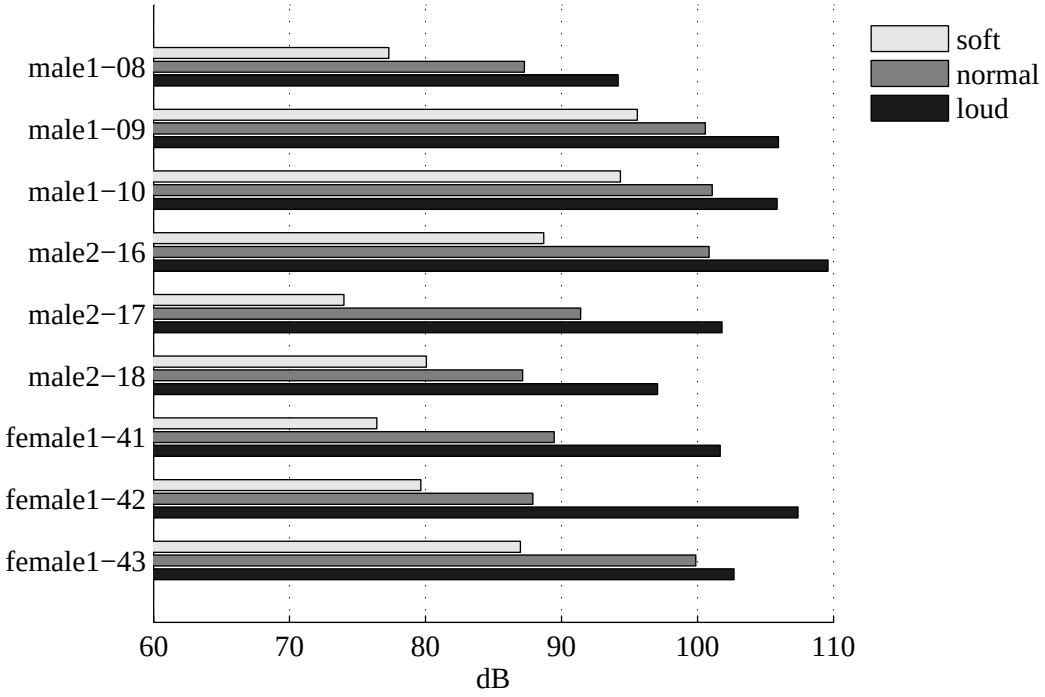

Figure 5.2: Sound pressure level estimates of phonations at different loudness in the Huddinge experiment.

5.1.2 Qualitative Observations

Figure 5.3 shows the pressure, flow, and area signals of phonation Male1-06-normal. The high-speed images from three instants are also shown. The flow signal exhibits a clear two-stage opening phase. However, no glottal opening can be seen in the image taken shortly prior to a secondary opening.

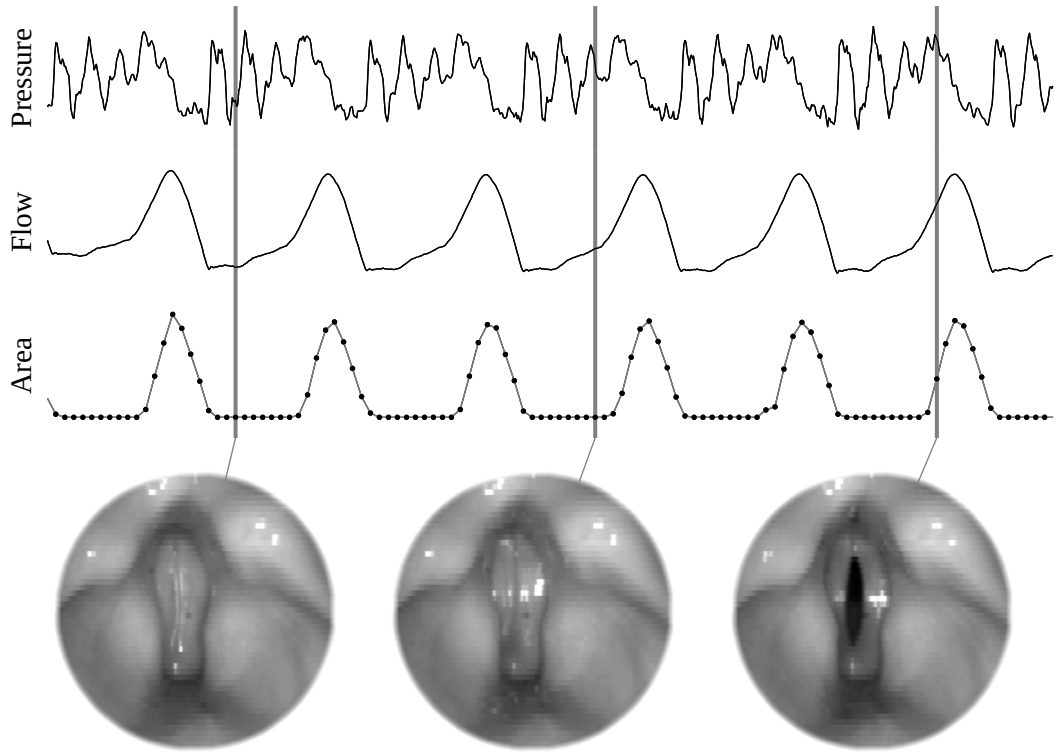

Figure 5.3: Phonation Male1-06-normal. No glottal opening can be seen in the vocal fold image in the middle even though the flow signal has increased from the base level.

Figure 5.4 is a similar illustration of the phonation Male2-12-breathy. The glottis is not completely closed in this example. This was typical of the breathy phonations examined in this study.

A minor opening between the vocal folds was commonly observed in the most closed phase of the glottal cycle in the female subject's normal phonations. Figure 4.9 shows an example of a chink at both the anterior and the posterior parts of the vocal folds. Occasionally, a probable chink was also seen in normal phonations of the subject Male 2 and in pressed phonations of the female subject. The existence of a minor chink complicated

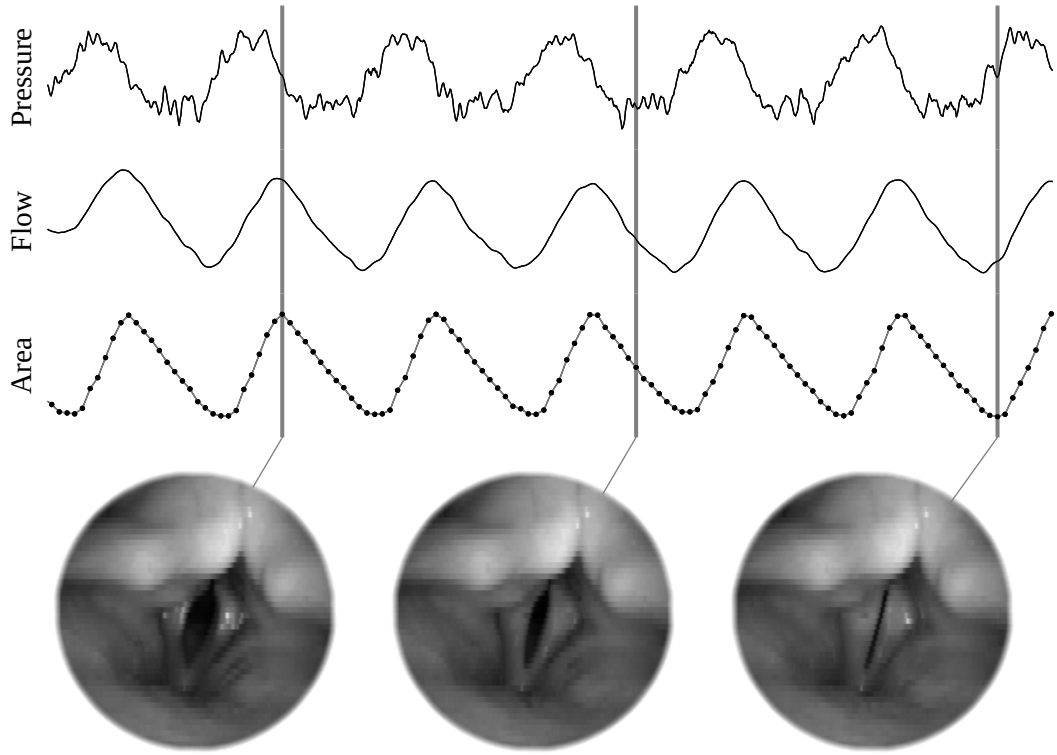

Figure 5.4: Phonation Male2-12-breathy. The vocal folds are not closed completely.

the determination of the instants of opening and closure in the image sequence. A small opening was not detected by the automatic area extraction software, but manual checking of the opening and closure instants required a frame-by-frame decision between open and closed glottis. This was not trivial because there did not seem to be any unambiguous criterion. Consequently, the glottis was considered closed in some cases where there might be evidence of a glottal chink in the image.

5.1.3 Pulse Parameters

Numerical parameters were calculated from each cycle of glottal flow and area within the analysis windows. Error bounds were estimated for each parameter as described in Section 4.3.6. Figure 5.5 shows the parameters obtained from the phonations of the subject Male 1 at normal loudness. Error limits are illustrated by vertical lines with horizontal end markers. An example of the flow pulse waveform and the area pulse waveform in each phonation is also shown. Appendix A contains similar figures of all examined cases.

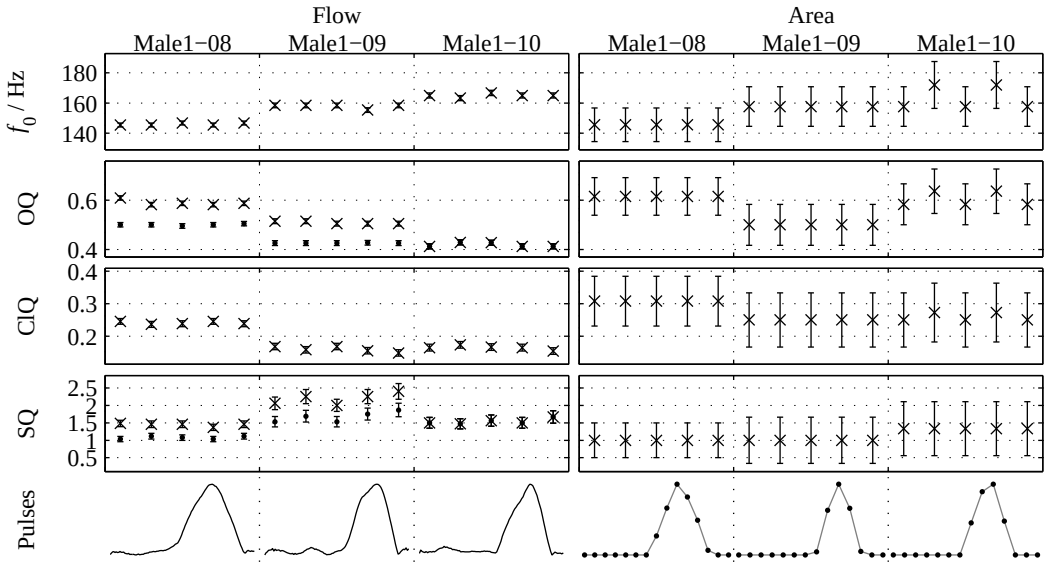

Figure 5.5: Parameters estimated from the phonations of the subject Male 1 at normal loudness. Each column with five values for each parameter corresponds to one recording from which five successive glottal periods have been analyzed. For OQ and SQ, cross ($\times$) denotes primary opening and dot ($\bullet$) denotes secondary opening. Vertical lines with horizontal end markers indicate estimated error boundaries due to limited time resolution. For each phonation, the flow waveform and the corresponding area pulse of one glottal cycle are also shown at the bottom of the figure.

Originally, the aim was to calculate a set of representative parameters for each subject in all phonation type and loudness categories by averaging the parameter values of all the analyzed periods of the subject and phonation task in question. However, successive recordings of the same subject and phonation type turned out to have quite different characteristics in

some cases. This is evident in Figure 5.5 where the fundamental frequency, pulse waveform, and pulse parameters vary considerably from recording to recording. However, the parameter values extracted from successive glottal periods within a single recording are much more consistent.

The observed variation of parameters is not surprising. The speaking conditions were far from normal in the recording situation because of the endoscope that was inserted into the subject's mouth. Furthermore, several minutes elapsed between successive recordings due to necessary preparations of the equipment.

Consequently, it seemed reasonable to apply averaging only to parameter values originating from quite similar glottal pulses. This was particularly true for parameters differentiating between primary and secondary opening: there was no point in averaging e.g. OQ_2 values over a collection of phonations that contained cases where a clear secondary opening was found and cases where it was not found. Therefore, only one representative phonation was chosen for each combination of speaker and phonation type, and the pulse parameters were averaged from the five consecutive cycles in this phonation.

The phonations selected for further analysis of parameters are listed in Table 5.4. The selection was based on the following criteria:

- Typical occurrence of the desired phonation type as assessed by subjective listening.
- High image quality and good visibility of the glottis.
- EGG signal quality.

Table 5.4: Phonations selected for parameter analysis.

Phonation	Male 1	Male 2	Female 1
Breathy	Male1-06-breathy	Male2-12-breathy	Female1-40-breathy
Normal	Male1-06-normal	Male2-14-normal	Female1-39-normal
Pressed	Male1-06-pressed	Male2-14-pressed	Female1-39-pressed
Loudness 1	Male1-09-soft	Male2-16-soft	Female1-42-soft
Loudness 2	Male1-10-normal	Male2-17-normal	Female1-42-normal
Loudness 3	Male1-09-loud	Male2-16-loud	Female1-41-loud

5.1.4 Mean Pulse Parameters

Phonation Modes

Average parameters of the selected phonations in different phonation modes are shown in Figure 5.6. Propagated uncertainties due to limited temporal resolution are shown as ver-

tical lines and SEM-based 95 % confidence intervals are shown as rectangles. Parameters derived from flow and area signals are drawn side by side using different colors.

Fundamental frequency (f_0) shows only minor variation between phonation modes within subject. Frequencies detected from area and flow are in agreement.

Open quotient decreases consistently with increasing pressedness. There are considerable differences between OQ values based on primary openings and those based on secondary openings. In general, OQ_2 seems to correspond more closely to OQ derived from the image data.

Closed quotient also decreases when the phonation type is changed from breathy to normal and pressed phonation. ClQ values derived from the image data are close to those derived from the flow signals, flow ClQ being slightly smaller.

Speed quotient is the most ambiguous of the parameters. The uncertainties of the detected time instants affect SQ more than the other pulse parameters. However, a rising tendency of SQ with increasing pressedness is observed. Flow SQ_2 is close to SQ derived from image data, whereas flow SQ_1 is generally higher.

Loudness Variation

Average parameters of the selected phonations in the loudness variation recordings are shown in Figure 5.6. Error bounds due to limited temporal resolution are shown as vertical lines and SEM-based 95 % confidence intervals are shown as rectangles. Parameters derived from flow and area signals are drawn side by side using different colors.

The fundamental frequency of all the subjects rises when loudness is increased. Especially Male 1 shows large relative increase of f_0.

Open quotient values of the flow pulses of Male 2 and Female 1 decrease with increasing loudness. Flow OQ of Male 1, on the other hand, remains almost constant. Only minor variation is observed in the area-based OQ values. Flow OQ_2 of all the subjects is lower than OQ based on the image data.

There are no clear tendencies in the behavior of the ClQ parameters with increasing loudness. However, flow ClQ seems to be lower than area ClQ.

Flow SQ_2 values are within the error bounds of area SQ values, whereas flow SQ_1 values are larger for Male 2 and Female 1.

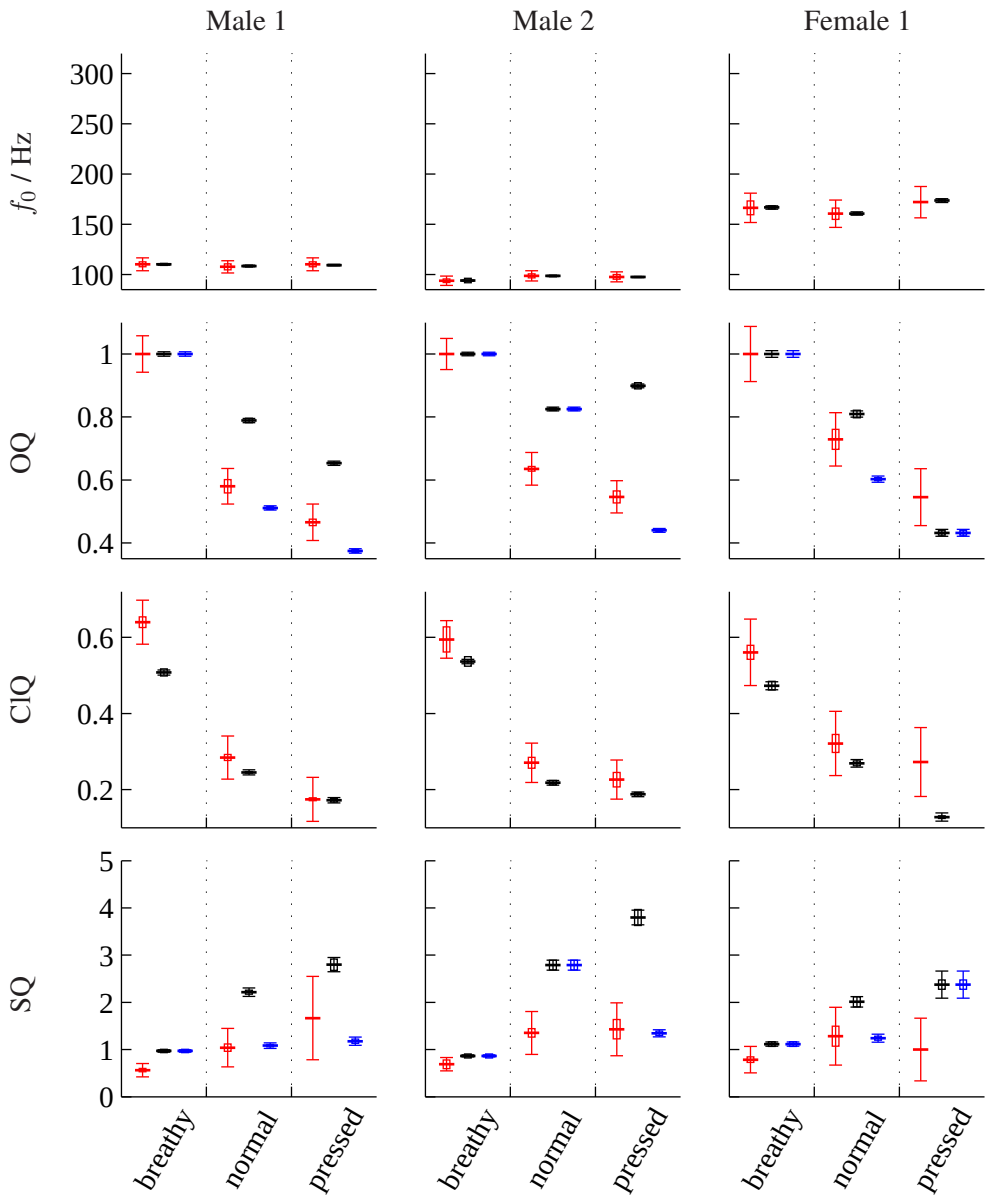

Figure 5.6: Pulse parameters estimated from breathy, normal, and pressed phonations. Area parameters are drawn in red, flow parameters based on the primary opening in black, and flow parameters based on the secondary opening in blue. Vertical line indicates the uncertainty caused by limited time resolution. Rectangle shows the estimate of uncertainty derived from the standard error of the mean.

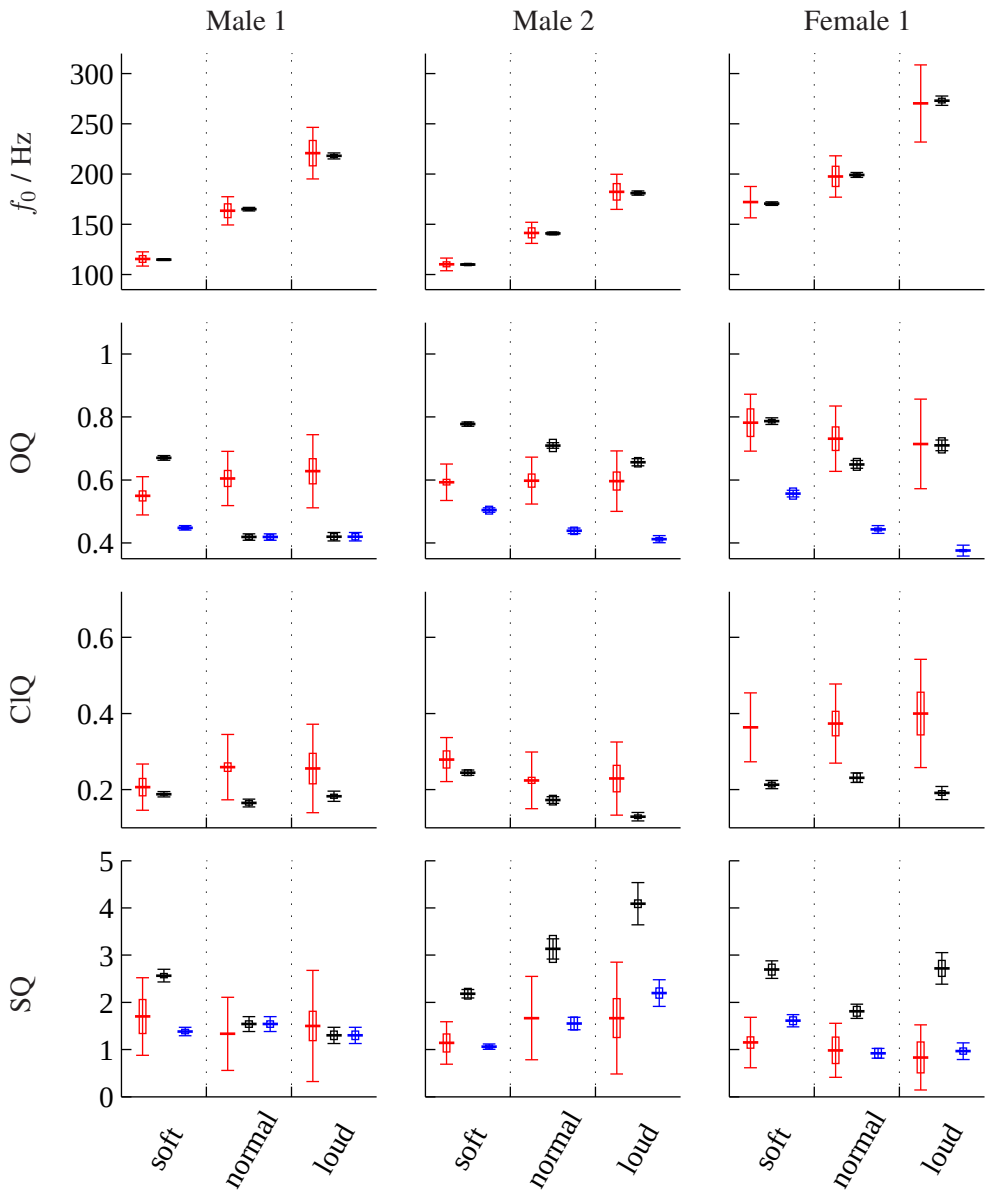

Figure 5.7: Pulse parameters estimated from the phonations in different loudness categories. Area parameters are drawn in red, flow parameters based on the primary opening in black, and flow parameters based on the secondary opening in blue. Vertical line indicates the uncertainty caused by limited time resolution. Rectangle shows the estimate of uncertainty derived from the standard error of the mean.

5.2 HUT Experiment

There were 13 subjects in the HUT experiment, six of which were women. One breathy, normal, and pressed phonation of each subject was examined. In this thesis, the subjects are denoted by an identification consisting of the gender and a running letter: from Female A to Female F and from Male A to Male G. The individual phonations are denoted by the identification of the subject followed by the phonation type, e.g. MaleC-normal.

5.2.1 Sound Pressure Level Estimates

Sound pressure level estimates were calculated for each analysis window using the procedure described in Section 4.3.3. The gain settings of the recording equipment were not altered during the recording session, so only one calibration signal was necessary. The resulting SPL values are listed in Table 5.5 and illustrated graphically in Figure 5.8.

Table 5.5: Sound pressure level estimates of phonations in different phonation types in the HUT experiment. Sound pressure levels are given in dB with linear weighting.

Recording	Breathy	Δ	Normal	Δ	Pressed
Female A	63.0	*6.0*	69.0	*11.0*	80.0
Female B	71.9	*0.6*	72.5	*7.5*	80.0
Female C	65.2	*13.1*	78.3	*7.4*	85.7
Female D	65.7	*6.4*	72.1	*12.3*	84.4
Female E	63.3	*6.5*	69.8	*12.4*	82.2
Female F	64.4	*3.1*	67.5	*14.0*	81.5
Male A	68.7	*11.1*	79.8	*10.7*	90.5
Male B	63.5	*13.4*	76.9	*4.9*	81.8
Male C	73.9	*0.1*	74.0	*4.2*	78.2
Male D	65.0	*5.9*	70.9	*-0.8*	70.1
Male E	60.3	*6.7*	67.0	*6.7*	73.7
Male F	72.4	*-2.2*	70.2	*5.6*	75.8
Male G	64.3	*7.4*	71.7	*13.0*	84.7

For most subjects, the SPL increases from breathy to pressed phonation, which is an expected result in general. Several exceptions of this rule exist in the data, but this is of course possible and does not imply any error in the measurements. There is considerable variation in the SPL values between subjects.

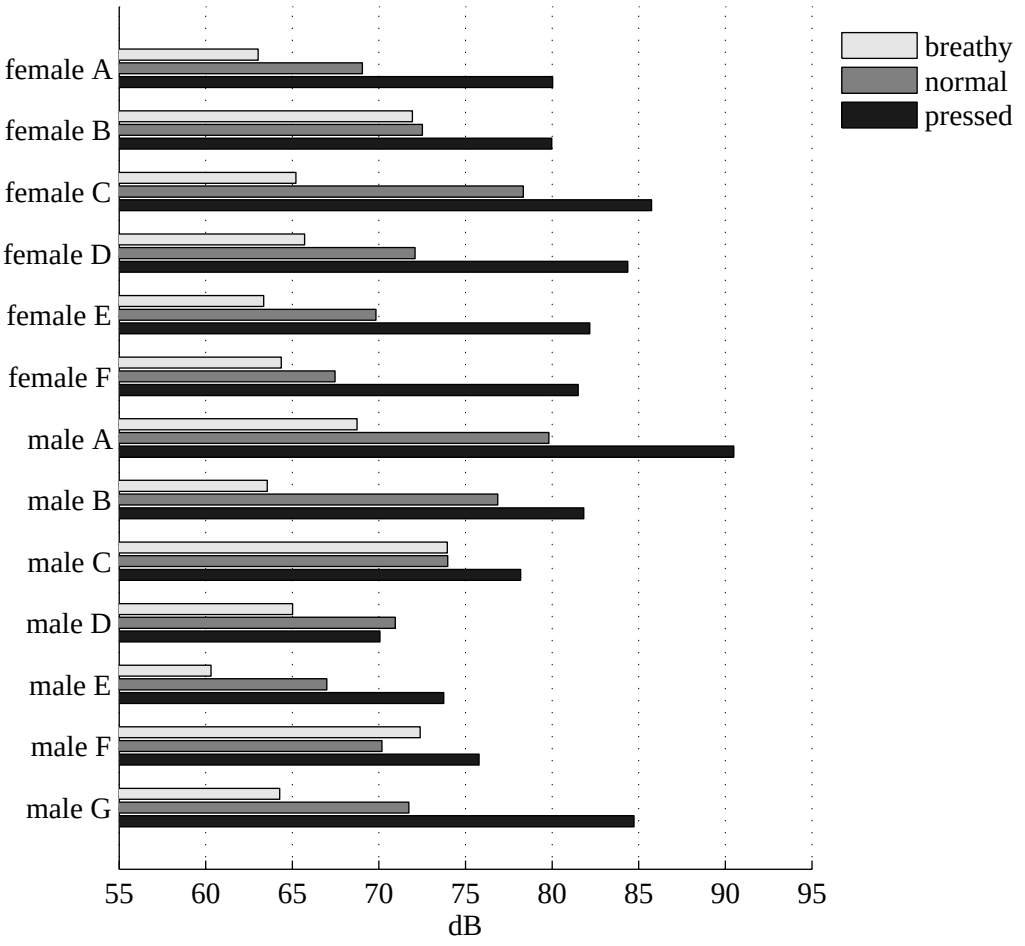

Figure 5.8: Sound pressure level estimates of vowels in different phonation types in the HUT experiment.

5.2.2 Opening Phase

The opening phase was examined with special emphasis on the two-stage opening behavior commonly observed in the Huddinge data. To compare the instants of interesting events within each glottal cycle, a normalized time scale was introduced as illustrated in Figure 5.9. The glottal cycle is defined as the interval between two successive maxima of the glottal flow, and a linear time scale from 0 % to 100 % is used to indicate the instants of events within this interval. Closure, primary opening, and secondary opening detected from the glottal flow waveform are indicated using respective symbols. The instant of the positive opening peak in the differentiated electroglottogram is also marked.

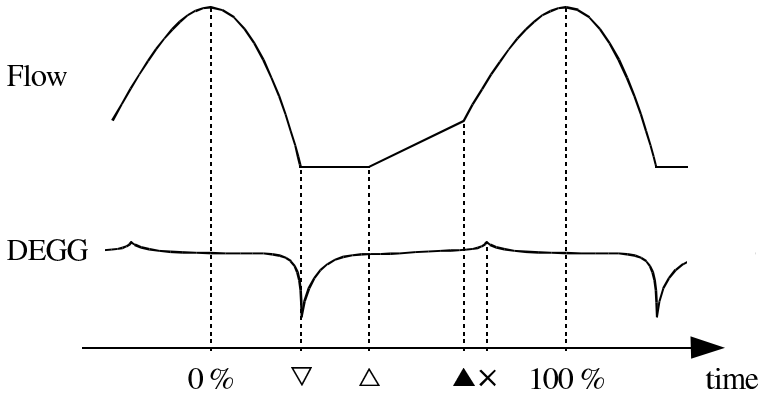

Figure 5.9: Illustration of the notation used in the examination of the opening phase: ▽ closure, △ primary opening, ▲ secondary opening, and × positive peak in the DEGG signal. The time scale is normalized to the interval between two flow maxima.

This notation is used in Figure 5.10 to illustrate the instants of interest in all the examined glottal cycles. Color coding is applied to the symbols of secondary opening instants and DEGG peak instants to indicate the sharpness of these features. The color varies between cyan indicating a very weak knee or peak and magenta indicating a strong knee or peak.

In most phonations, the automatically detected instants of events show good agreement between the cycles within the same phonation. Exceptions with high variance due to varying waveforms or detection errors exist, however. See e.g. FemaleB-normal and MaleC-pressed. In the sample FemaleD-normal there was a noise burst in the middle of the analysis window, which affected the EGG parameters in a couple of glottal periods.

Inverse filtered flow waveforms of breathy phonations are much more vague by nature than those of normal and pressed phonations. Therefore, one has to be especially careful when interpreting the results of breathy phonations.

In many cases, especially in the normal phonations of the male subjects, the instant of primary opening occurs very shortly after the closure. This suggests a flow waveform with a very short flat segment followed by a long, gently rising phase.

Some other cases show a very short distance between the primary and secondary opening, see e.g. FemaleA-breathy and MaleB-pressed. This indicates that the detection algorithm did not find any secondary knee at a later position in the opening phase.

Phonations with strong secondary opening knees and sharp DEGG opening peaks show good agreement between the instants of these phenomena. Strongest evidence of this is found in normal phonations of the male subjects A to D and pressed phonations of all male subjects except Male E.

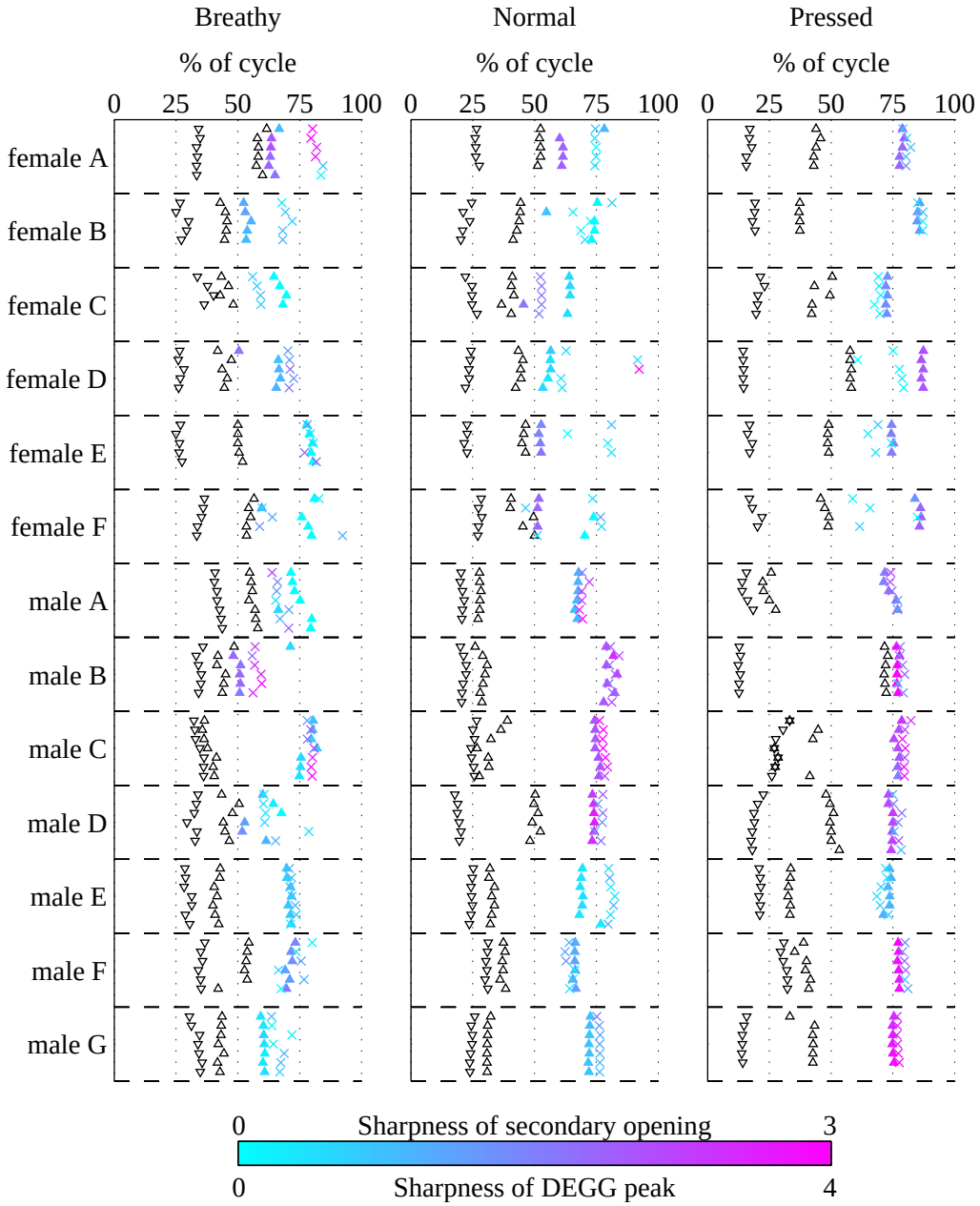

Figure 5.10: Significant instants detected from each glottal cycle: ▽ closure, △ primary opening, ▲ secondary opening, and × positive peak in DEGG. Time scale is normalized to the glottal cycle length between two successive flow maxima. Figure 5.9 illustrates the notation. Each row refers to one glottal cycle. Color coding indicates the sharpness of each DEGG peak and secondary opening knee in the flow waveform.

5.2.3 Closing Phase

The behavior of the glottal flow and the electroglottogram during the closing phase was studied using the normalized time scale illustrated in Figure 5.11. The instant of maximum flow is used as the origin and the instant of closure determines the 100 % point.

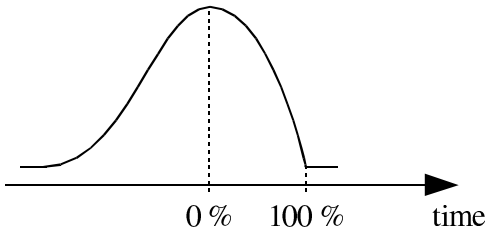

Figure 5.11: The definition of the time scale of the closing phase that will be used in subsequent illustrations. The instant of maximum flow determines the zero position and the instant of closure defines the 100 percent position.

Figure 5.12 illustrates the instant of the minimum in the flow derivative, or maximum excitation, and the instant of the negative closing peak in the differentiated EGG waveform in each examined glottal cycle.

It should be pointed out that the inverse filtered flow waveforms of breathy phonations and the time instants derived from them are less reliable than those acquired from the normal and pressed phonations. This can also be seen in Figure 5.12 as a higher variability of the detected instants.

The phonation FemaleC-pressed seems to deviate from the common pattern apparent in the column of pressed phonations. Visual examination of the waveforms revealed that the flow pulses of FemaleC-pressed showed a smooth closure whereas most other normal and pressed flow pulses had a very abrupt closure. This has shifted the detected instant of closure in FemaleC-pressed forward relative to the point of maximum excitation. A smooth closure of the flow waveform also causes the relatively early instants detected from the phonations FemaleC-normal and FemaleB-pressed.

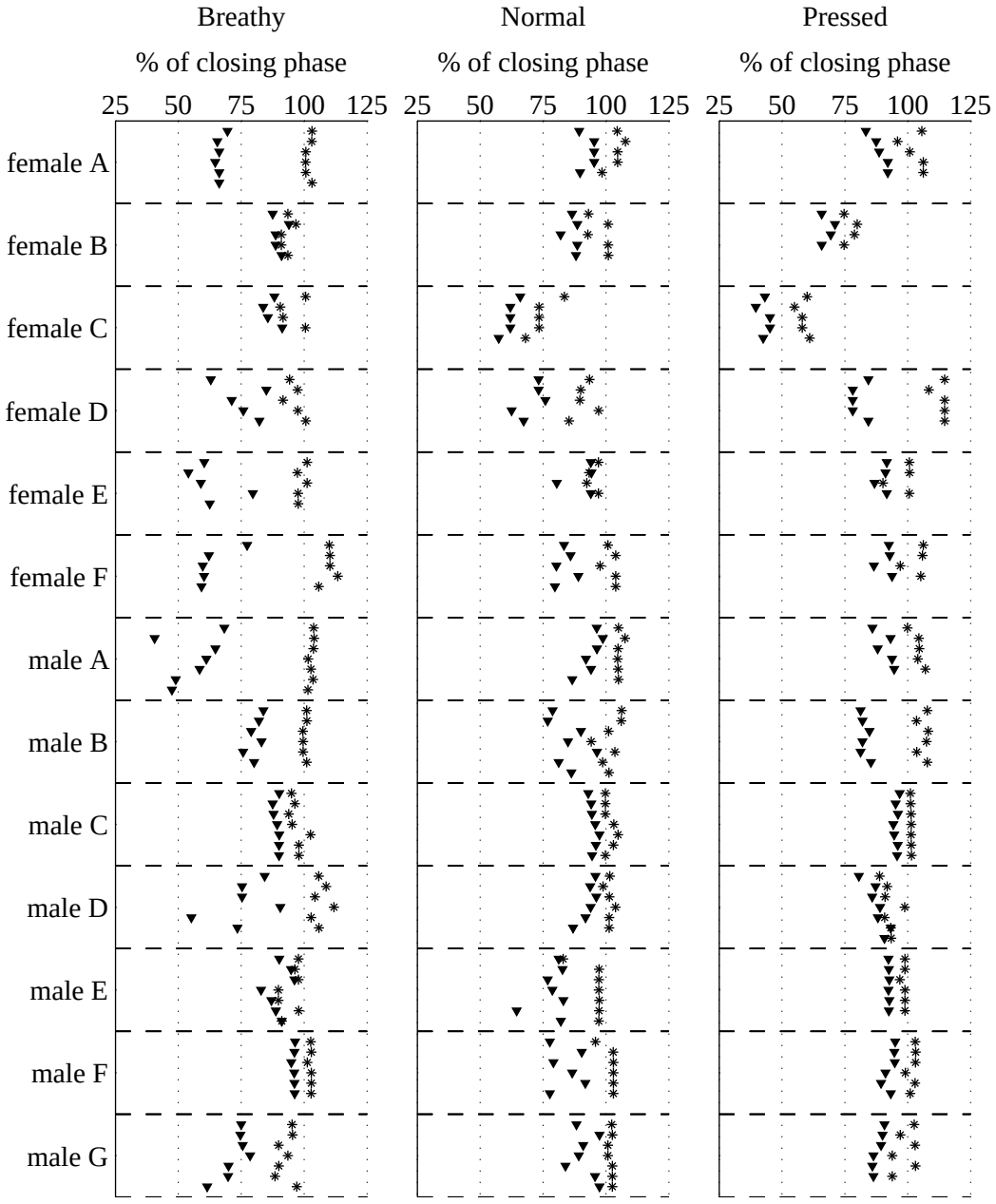

Figure 5.12: Positions of minima in flow derivative and closing peaks in DEGG during the closing phase. Each row indicates the instants of the minimum of flow derivative (▼) and the negative DEGG peak (✳) within one glottal cycle. The horizontal axis denotes the time scale of the closing phase as shown in Figure 5.11.

The position of the minimum in the differentiated flow waveform within the closing phase was examined in more detail. Figure 5.13 shows the average position of this instant for each subject and phonation mode separately. The uncertainty of each mean value is indicated by the 95 % confidence interval derived from the standard error of the mean (SEM), see Section 4.3.6 for details. The use of SEM for this small number of samples requires the assumption of normal distribution. In this case, that seems to be a reasonable approximation.

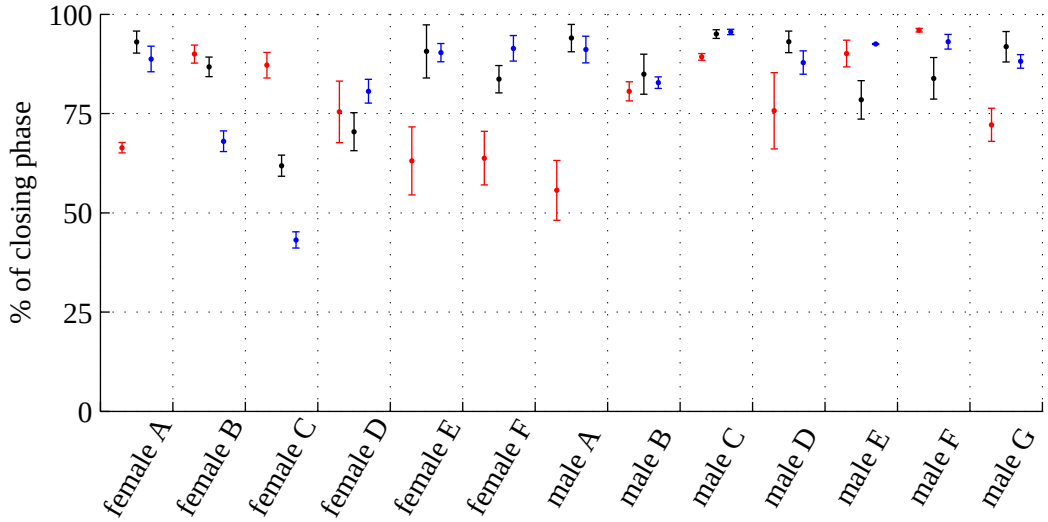

Figure 5.13: Position of the minimum flow derivative within the closing phase. The vertical axis denotes the time scale of the closing phase as shown in Figure 5.11. Breathy phonation is drawn in red, normal phonation in black, and pressed phonation in blue. Vertical lines indicate 95 % confidence intervals derived from the measurements.

No clear trends can be seen in Figure 5.13 except that the maximum excitation occurs in most cases during the last 25 % of the closing phase.

Finally, the relative timing of the minima in the flow derivative and the EGG derivative was studied. Figure 5.14 illustrates the time difference Δt that was measured from each glottal cycle. The average time difference for every subject and phonation mode is shown in Figure 5.15 in milliseconds and in Figure 5.16 using the time scale normalized to the closing phase length as illustrated in Figure 5.11. The uncertainty of each mean value is indicated by the 95 % confidence interval derived from the standard error of the mean. The time differences are assumed to be normally distributed.

No general rules can be found to predict how this time difference changes when the pressedness of phonation is increased. However, the difference is positive in all but one

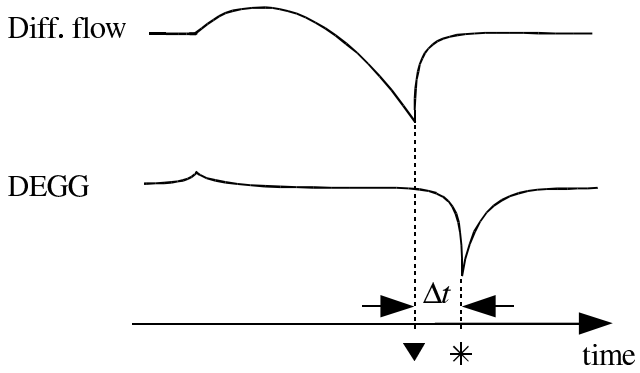

Figure 5.14: Time difference between the closing peaks in the differentiated flow waveform and the differentiated electroglottogram. Positive Δt indicates that the instant of minimum flow derivative precedes the instant of minimum DEGG.

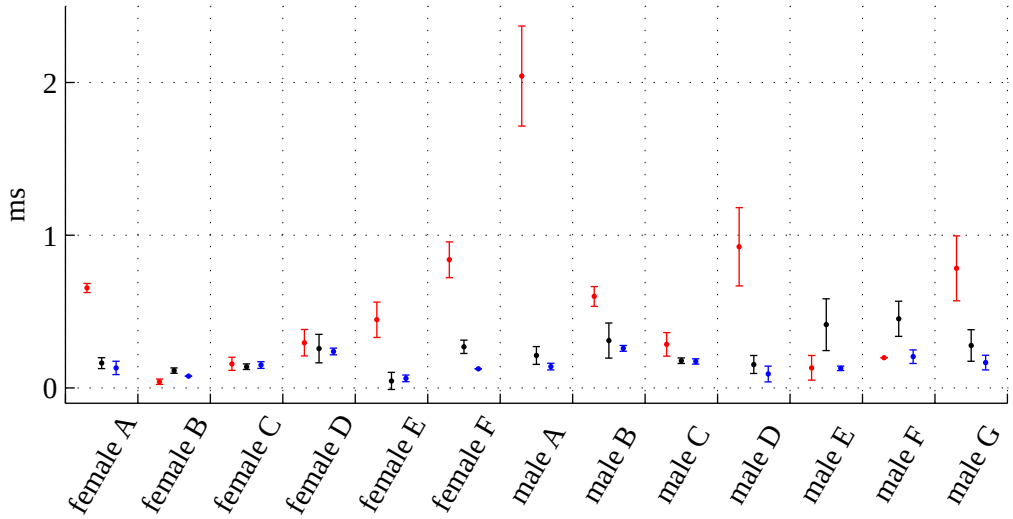

Figure 5.15: Time difference between the minimum of flow derivative and the minimum of DEGG in milliseconds. Breathy phonation is drawn in red, normal phonation in black, and pressed phonation in blue. Vertical lines indicate 95 % confidence intervals derived from the measurements.

case. The closing peak in DEGG thus seems to occur after the minimum flow derivative.

This hypothesis was tested statistically by performing Student's t-tests (Laininen, 2000).

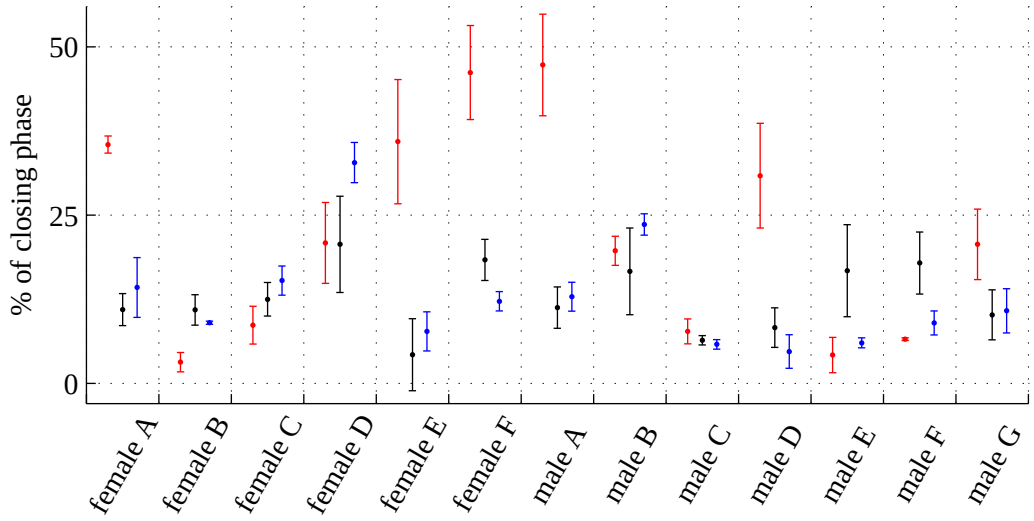

Figure 5.16: Time difference between the minimum of flow derivative and the minimum of DEGG. The time scale is normalized to the closing phase length, see Figure 5.11. Breathy phonation is drawn in red, normal phonation in black, and pressed phonation in blue. Vertical lines indicate 95 % confidence intervals derived from the measurements.

The time difference Δt was assumed to be normally distributed with unknown variance. The null hypothesis was $H_0 : \Delta t \leq 0$ and the alternative hypothesis was $H_1 : \Delta t > 0$. Significance level of 5 % was chosen.

Each phonation mode was tested separately. Furthermore, the test was applied to absolute time differences in milliseconds, and to time differences normalized by the duration of the closing phase. P values acquired by the tests are shown in Table 5.6. In each case, the P value was very small and the null hypothesis was rejected at the 5 % significance level. Thus, the maximum excitation in the flow was found to occur before the closing peak in the differentiated EGG signal.

Table 5.6: P values obtained from the t-tests of the time difference between the instants of minimum flow derivative and minimum EGG derivative.

Phonation mode	P (difference in ms)	P (difference in %)
Breathy	3.3^{-14}	4.7^{-19}
Normal	4.0^{-22}	5.5^{-26}
Pressed	8.9^{-30}	4.5^{-20}

5.3 Observations on Inverse Filtering

5.3.1 Primary and Secondary Opening

As remarked in Section 4.3.4, unexpected two-stage opening behavior was often encountered in the inverse filtered glottal flow waveforms. This phenomenon was analyzed quantitatively by calculating two sets of parameters based on primary and secondary opening instants.

To further examine the two-stage opening behavior, the phonation Male1-06-normal of the Huddinge material was selected for further analysis because it exhibited prominent primary and secondary openings and a clean inverse filtered flow waveform. The microphone signal of this phonation was inverse filtered using the following two additional methods:

- Inverse filtering based on closed-phase covariance analysis (Wong *et al.*, 1979). The beginning of a closed phase of glottal vibration was detected from the derivative of the EGG signal, and a covariance analysis window was located closely after this point. The method was implemented and applied to the signal by professor Paavo Alku.

- Manual inverse filtering using the custom software DeCap developed by Svante Granqvist (Granqvist *et al.*, 2003). The software allows the operator to adjust manually the frequencies and bandwidths of formant filters and displays the resulting flow signal and its spectrum in real time. The test signal was inverse filtered by Eva Björkner, who is an experienced user of the DeCap software.

Figure 5.17 illustrates the obtained inverse filtered signals together with the original microphone signal, electroglottogram and its derivative, and the glottal area signal estimated from the high-speed image sequence.

The closed-phase covariance analysis gave a flow waveform that is very similar to the one obtained by the IAIF method. Primary and secondary opening instants are evident in the flow pulses. The glottal flow estimate acquired using the DeCap software also shows distinct knees at the positions of primary and secondary opening found in the IAIF-based flow. However, the slope of the DeCap flow signal is different: the flow decreases until the time instant where the primary opening occurs in the IAIF-based waveform, and notable increase of flow in the DeCap estimate begins only at the instant of secondary opening in the IAIF signal. Thus, the DeCap waveform suggests an interpretation that the knee at the instant of primary opening is caused by some phenomena during the closed phase and that considerable increase of flow does not begin before the instant of secondary opening. The peaks of the differentiated EGG signal as well as the area waveform support this view.

It is worth pointing out that the flow waveform given by the IAIF method can be made resemble the DeCap signal in Figure 5.17 by tuning the lip radiation parameter. The result-

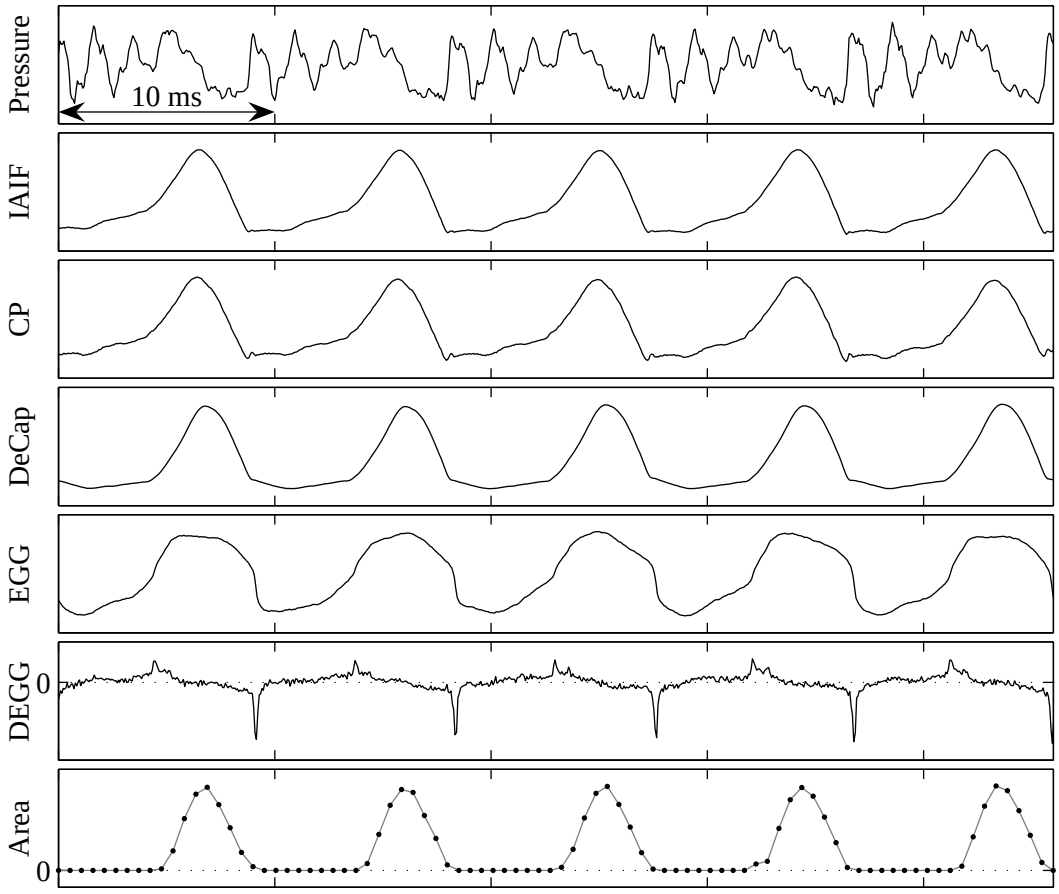

Figure 5.17: Comparison of flow waveforms obtained using different inverse filtering methods. The figure shows the following signals from top to bottom: original speech pressure signal captured by a microphone, flow waveform obtained using the IAIF method, flow waveform obtained by closed-phase covariance analysis, flow waveform obtained using the DeCap software, EGG, differentiated EGG, and glottal area extracted from the high-speed image sequence.

ing waveform thus depends on the preferences of the user of the inverse filtering system. In the IAIF case in the figure, a maximally flat flow waveform after the closure has been preferred to a long closed phase.

Figure 5.18 shows another example where the closed phase of the inverse filtered flow waveform is changed remarkably by modifying inverse filtering parameters. Both flow waveforms were obtained by inverse filtering the phonation FemaleD-pressed with the HUT

IAIF Toolbox software. The high-pass filter cut-off frequency was set to 183 Hz and the maximum number of formants to 11 in both cases. These same parameters were used to inverse filter that phonation for the analysis of the flow waveform in this study. However, the lip radiation parameter was set to two extreme values to get the waveforms in Figure 5.18: it was 0.97 in the case (a) and 1.00 in the case (b).

Waveform (b) shows a hump at the beginning of the closed phase. Hertegård *et al.* (1992) and Hertegård & Gauffin (1995) analyzed this kind of characteristic of the flow waveform and related it to the existence of a mucosal wave, i.e. vertical phase difference along the vocal folds during the closing phase.

Waveform (a), on the other hand, shows a short, flat closed phase and a long opening phase with gradually increasing slope. The shape of the pulses resembles some flow waveforms with a two-stage opening encountered in this study.

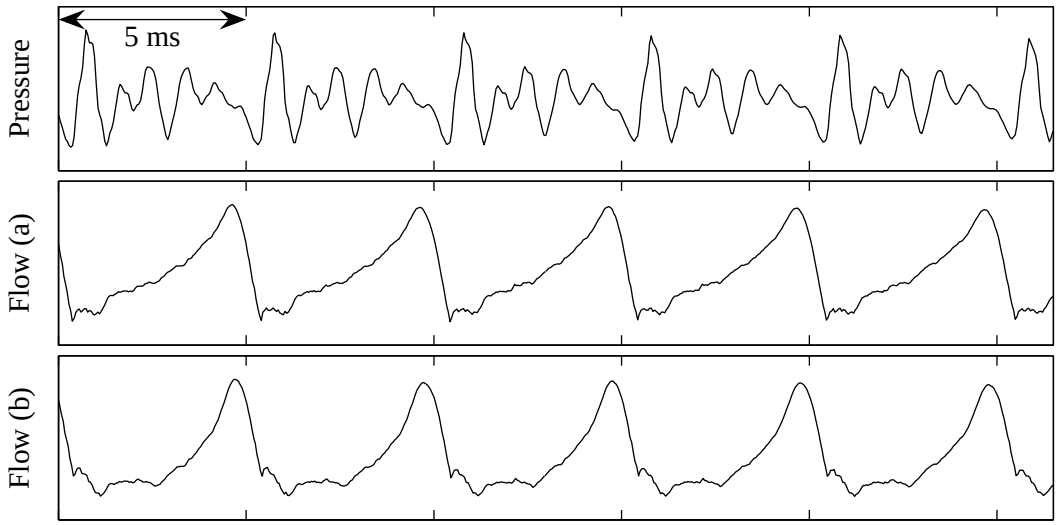

Figure 5.18: Flow waveforms obtained by inverse filtering a pressed female phonation with the IAIF method using two different lip radiation coefficients, 0.97 in (a) and 1.00 in (b). All other parameters were identical in these two cases.

Speculation arises whether the hump could be more generally converted into a two-phase opening and vice versa by tuning the inverse filtering parameters, and whether these two characteristics of the flow pulse might be caused by the same underlying physiological or acoustical phenomena.

Changes in the Flow Waveform

Figure 5.19 illustrates a portion of the phonation Male1-06-breathy. The microphone signal is shown in the top panel, and the two panels below it contain alternative glottal flow estimates. Flow (a) is obtained using IAIF with proper high-pass filtering at 101 Hz, maximum number of formants 9, and lip radiation coefficient 0.995. Flow (b) is acquired by using the same high-pass filtering and setting the maximum number of formants to 7 and the lip radiation coefficient to 0.99.

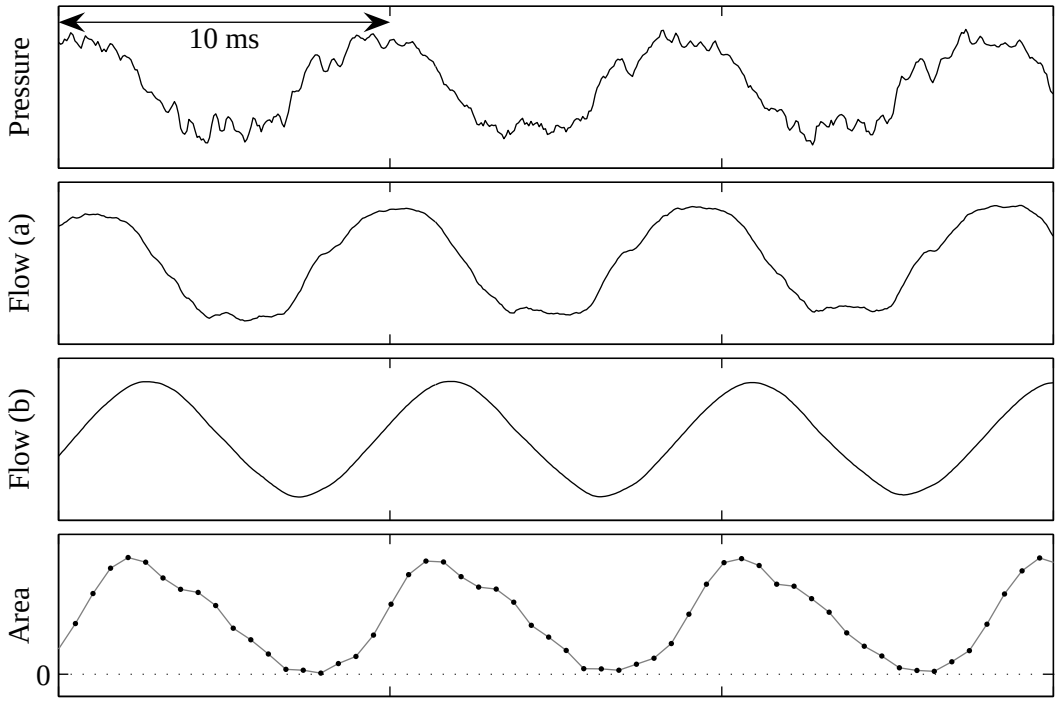

Figure 5.19: Two different flow waveforms (a) and (b) are obtained from the pressure signal at the top by using different inverse filtering parameters. The glottal area function is shown for comparison at the bottom.

Flow (a) shows a nearly flat and relatively long closed phase, which in many cases is a typical feature of an expected flow pulse waveform. Flow (b) is almost sinusoidal without any flat closed phase. The waveforms differ drastically even though they have both been achieved using parameter values that are within the range commonly used in this study.

The bottom panel of Figure 5.19 shows the related glottal area signal. Its individual values are not very reliable but it indicates clearly that there was no complete closure during these glottal cycles. This observation was verified by visual inspection of the high-speed

images. The flat closed phase present in flow (a) is thus not supported by the area function. Furthermore, the flow (a) does not appear to be in phase with the area variation. Consequently, flow (b) seems to be a more plausible estimate of the behavior of the glottal volume velocity in this breathy phonation than flow (a) even though flow (a) resembles the waveforms commonly encountered in normal and pressed phonations.

This example illustrates the significance of the choices made by the operator of the inverse filtering system. It also demonstrates the uncertainty related to the waveforms attained by inverse filtering and to the pulse parameters derived from those waveforms.

Inability to Achieve a Plausible Flow Waveform

Among the almost one hundred segments of pressure signals that were inverse filtered within this study, one signal turned out to be especially problematic for the HUT IAIF Toolbox implementation of the IAIF method. When inverse filtering the phonation MaleApressed, the software failed to produce a plausible flow waveform. No significant improvement was achieved by changing the parameters of the method. Finally, reducing the length of the analysis window slightly changed the resulting flow signal into an expected waveform. Figure 5.20 shows the pressure signal of this phonation, the flow estimate obtained from the entire segment, and the more appropriate flow waveform achieved by leaving approximately one period out at the end of the segment but using exactly the same inverse filtering settings.

Besides, the flow estimate (b) in Figure 5.20 is another example of a flow waveform that could have been made to have a hump after the closure and a long, nearly flat closed phase by tuning the lip radiation coefficient.

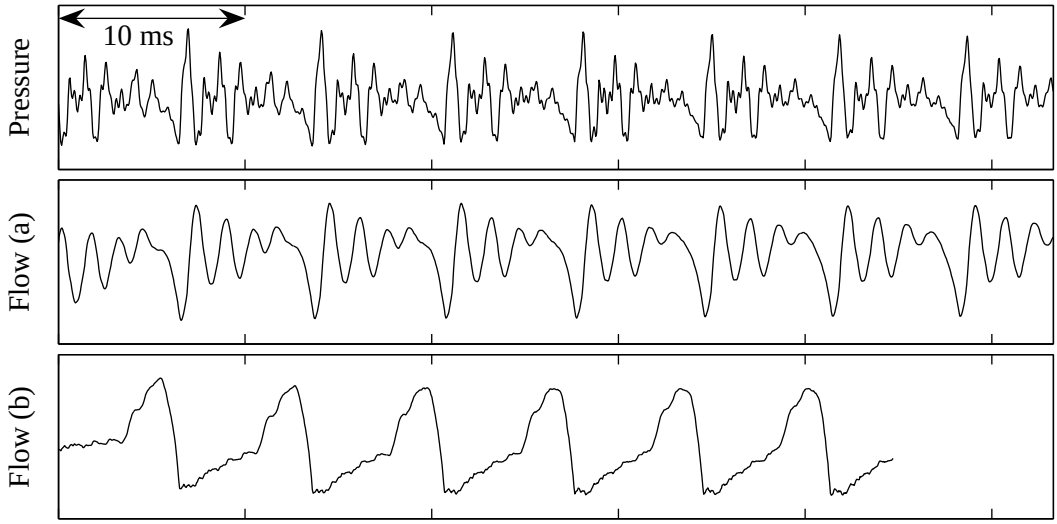

Figure 5.20: Problematic signal segment for inverse filtering. The two panels on the bottom show inverse filtered flow estimates obtained from the microphone signal in the top panel. Flow (a) resulted from inverse filtering the entire signal segment, and flow (b) was acquired by reducing the length of the analysis window by approximately one glottal cycle. All the inverse filtering parameters were identical.

Chapter 6

Conclusions

This chapter concludes the thesis by presenting the most relevant results of the project and relating them to the results of earlier research. The most interesting detailed findings of this study are also described. Finally, some suggestions are provided that might be useful in future work within this field.

Due to the nature of this field of research, the results cannot be regarded as exact patterns that exist uniformly in all examined cases. However, general observations can be found from the material, and interesting details of observed behavior can be pointed out.

6.1 Conclusions about the Inverse Filtering Method

The primary goal of this study was to evaluate the inverse filtering method IAIF by comparing the flow estimates obtained using it to information attained simultaneously by high-speed imaging and electroglottography. Data collected in the Huddinge experiment provided the possibility of comparing inverse filtered flow waveforms with simultaneously recorded image sequences of the vibrating vocal folds as well as EGG waveforms. The material of the HUT experiment, on the other hand, allowed comparisons between flow and EGG waveforms with more reliable temporal synchronization and better EGG signal quality.

Based on the examined material, it can be stated in general that the inverse filtering method produced mostly reasonable estimates of glottal flow waveform.

The user-adjustable parameters of IAIF had a considerable effect on the obtained flow waveforms. Not all parameter settings gave plausible flow estimates. Therefore, the role of the operator of the inverse filtering software is crucial. Knowledge and experience on human speech production and inverse filtering is required for reliable utilization of the inverse filtering system.

The Huddinge material was recorded in a clinical room environment without specific sound-absorbing arrangements. This did not seem to cause problems with inverse filtering. However, the effect of room reflections on the inverse filtered flow waveforms was not explicitly evaluated in this study.

6.2 Detailed Observations

6.2.1 Incomplete Closure of Vocal Folds

Examination of the high-speed image material of the Huddinge experiment revealed that the vocal folds were not completely closed in the breathy phonations of any of the subjects. For the female subject, a minor anterior and posterior gap was commonly encountered in all but the loudest and most pressed phonations. The male subjects, in general, had a complete closure in all but the breathy phonations. Hertegård *et al.* (1992) observed similar behavior. Their subjects were asked to phonate at different frequencies mostly in the normal phonation mode, and complete closure of vocal folds was found in all phonation samples of the male subjects but in none of the samples of the female subjects.

6.2.2 Pulse Skewing

Closing quotients of glottal area waveforms were found to be generally greater than those of glottal flow pulses. This indicates that the closing phase of the area pulse is longer than the closing phase of the corresponding flow pulse, and the flow pulse is thus more skewed to the right. This corroborates earlier theoretical and empirical findings (Rothenberg, 1973, 1981a; Stevens, 1998). The acoustic mass of the airways slows down the increase of the volume velocity when the glottal area is increasing and causes a more rapid decrease of flow in the closing phase (Stevens, 1998). The air displaced by vocal folds may also contribute to the skewing of the flow pulse (Rothenberg, 1973, 1981a).

6.2.3 Flow Waveform in the Closed Phase and the Opening Phase

A two-stage opening phase was commonly encountered in the flow waveforms obtained in this study. After an abrupt closure, a short, flat closed phase was found, followed by a moderately rising flow segment beginning at the instant of primary opening. At a later point of time, the flow suddenly started to increase more rapidly. This instant was referred to as the secondary opening.

Examination of the flow and EGG signals of the HUT experiment showed that the opening peak of the differentiated EGG signal often coincided with the automatically detected instant of secondary opening in the flow waveform in cases where the DEGG peak and the

secondary opening of flow were evident. Consequently, in waveforms with clear primary and secondary opening, the secondary opening seemed to correspond to the instant of rapid opening of the vocal folds as detected from the EGG signal. This finding was supported by visual examination of some phonations of the Huddinge experiment having pronounced primary and secondary openings in the flow waveform: the instant of glottal opening, as observed visually in the image sequence, occurred near the position of the secondary opening in the flow waveform. The secondary opening thus appeared to be related to the physiological opening of the vocal folds.

The increase of glottal flow between the primary opening and the secondary opening could be explained by the piston effect, which means the upward movement of the vocal folds during the closed phase. Another explanation might be the leakage of air between the vocal folds before a pronounced opening of the vocal folds occurs. Both of these explanations have been suggested as reasons for non-zero DC air flow during the closed phase of the glottal cycle (Rothenberg, 1973, 1981a; Hertegård *et al.*, 1992).

The two-stage opening phase of the flow waveform could also be caused by slightly incorrect inverse filtering settings. A case study in Section 5.3.1 showed that tuning the integration coefficient of the inverse filtering method could change the tilt of the closed phase of the flow signal so that a waveform with a short, flat segment in the beginning of the closed phase followed by a moderately rising slope was converted into a short segment of decreasing flow after the closure followed by a longer, almost horizontal closed phase. The latter flow waveform could be described as having a hump in the beginning of the closed phase, and it resembled those observed by Hertegård *et al.* (1992) and Hertegård & Gauffin (1995). They explained the hump after the closure by a mucosal wave traveling vertically along the vocal folds and by the displacement of intraglottal air volume. The signal examined in Section 5.3.1 was particularly suitable for this kind of demonstration, and this result may thus not valid in general.

6.2.4 Closing Phase Phenomena

Two characteristics of the glottal closing phase were studied in detail from the HUT recordings. Firstly, the instant of steepest descent in the glottal flow waveform was located. It was found to vary within the last half of the closing phase, most commonly occurring during the last 25 % of the closing phase. This result is in line with many models of the glottal volume velocity waveform, including the LF model (Fant *et al.*, 1985), which allow the minimum of the flow derivative to occur at an adjustable point of time before the instant of closure.

Secondly, the time difference between the instants of steepest flow descent and the closing dip in the differentiated EGG waveform was examined. The maximum excitation in the flow was found to occur before the closing peak in DEGG. This is in agreement with

the observations by Rothenberg (1981b). He stated that the termination of the flow pulse is typically accompanied by the onset of a sharp drop in the EGG waveform, and that the flow pulse terminates closely before the closure of lower vocal fold margins, which is indicated by the beginning of the steep descent in the EGG waveform. Childers *et al.* (1983) found that the absolute minimum of the differentiated EGG aligned with the instant of glottal closure. In one of their figures (Childers *et al.*, 1983, page 211), the minimum of differentiated volume velocity waveform occurs after the minimum of DEGG, but this may be caused by timing errors of tape recorders also mentioned in their article. In two other figures (Childers *et al.*, 1983, pages 211 and 214), the signal minima seem to be simultaneous or the DEGG minimum occurs slightly later.

6.3 Sources of Error and Uncertainty

6.3.1 Signal Synchronization

In the recordings made in the Huddinge experiment, the synchronization of signals from different sources appeared to be less accurate than was expected. Comparisons between closure instants detected from microphone, glottal flow, EGG, and area signals suggested that the compensation of sound propagation delay from the glottis to the microphone should be smaller than that calculated from the vocal tract length and the microphone distance. This may be partly explained by the experimental setting: Glottal imaging requires that the subject leans the head forward and the camera operator gently pulls the subject's tongue. This might cause the effective vocal tract length to be reduced in comparison to a normal speaking position. At least, it certainly draws the subject's attention from controlling the distance between the mouth and the microphone.

The closure instants located in the different signals are not related to exactly the same physiological events, which may cause some error in this evaluation of synchronization accuracy. Some uncertainty was also involved in the alignment of the image sequence relative to the other signals. However, the time difference between the detected instants of closure was larger on average than expected and it consistently suggested that compensation of propagation delay should be smaller.

A similar calculation of sound propagation delay was used by e.g. Baer *et al.* (1983) and Granqvist *et al.* (2003). The same compensation scheme also yielded better agreement between detectable signs of glottal closure in the flow and EGG signals of the HUT material.

Consequently, the alignment of the signals in the Huddinge material was considered unreliable to some extent, and detailed temporal comparisons between the signals were not made on those recordings.

6.3.2 Estimation of Glottal Area

The detection of the area of glottal opening from high-speed image material is far from trivial. Even by visual examination, it is often difficult to find the exact position of the vocal fold edges that form the boundaries of the glottal opening. Furthermore, especially in pressed phonations, the visibility to the vocal folds is often limited by supraglottal tissues that hide the glottis partially.

An automatic detection algorithm does not provide an ultimate solution to this difficult task. The High-Speed Toolbox software utilized for automatic area detection in this study had problems particularly in finding the edges of the glottis when the opening was narrow. Additionally, in cases with suboptimal illumination, dark areas around the glottis were often detected as a part of the glottal opening. The automatically detected area function was also affected by the values of user-adjustable area detection parameters. Therefore, it was found necessary to check visually the instants of opening, maximum area, and closure in the image sequences in order to achieve as accurate parameters of the area pulses as possible.

6.3.3 Time Resolution of High-Speed Image Sequences

The digital high-speed imaging system produced image sequences with approximately 1900 frames per second. The fundamental frequency of speech was around 100 Hz in most phonations of the male subjects, which yielded approximately 20 image frames per glottal cycle or less.

In cases with high fundamental frequency, however, the number of frames per cycle was much smaller. Especially in the loud phonations of the female subject with f_0 around 300 Hz and OQ approximately 0.5, no more than 3–4 frames were available of the open phase of each cycle. This was obviously not enough for making useful cycle-by-cycle estimates of area pulse parameters from the image data.

Area pulse parameters were determined using the following convention: the instant of opening was marked at the last frame with no visible opening, and the instant of closure was set at the first frame showing complete closure. Consequently, the open phase length was likely to be overestimated. This effect was emphasized by low temporal resolution.

Knowing these limitations of the glottal area data, it was essential to consider the error limits of the pulse parameters derived from the detected time instants.

An estimate of the glottal area pulse with a larger number of measurement points within a cycle could be achieved by combining the information from several successive cycles. A simple method would be estimating first the fundamental frequency of vibration and shifting a few consecutive area pulses by multiples of the glottal period length to make the pulses overlap in time. This approach was experimented briefly within the study. Due to the

difficulty of defining exactly repeatable area detection criteria, and probably also because of varying illumination conditions and differences between successive cycles of vocal fold vibration, overlapping area estimates of consecutive area pulses did not always provide an unambiguous waveform but there were differences between successive pulses. Furthermore, this approach has the same inherent limitation as stroboscopy: detailed information about the glottal activity during a single cycle is not achieved if the glottal pulse shape is estimated from several cycles.

Assuming accurate estimates of glottal area, it would be possible to estimate the instant of maximum opening at higher time resolution than the sampling interval by interpolating the area waveform between the points of highest sample values. The simplest method for peak interpolation would be fitting a parabola to the three highest sample points and estimating the peak position and amplitude as the maximum of this parabola. The method lacks theoretical and physiological relation to vocal fold movement, but might improve the precision of the position of the area pulse peak.

Some kind of extrapolation scheme would be necessary to improve the temporal precision of instants of opening and closure as well. Linear extrapolation from the two non-zero samples closest to the opening or closure would be simple but does not seem to yield satisfying results, especially if the number of samples available from the open phase is small, in which case the benefit of extra precision would be greatest.

Better results might be achieved by fitting a model of the glottal area pulse to the observations and estimating the pulse parameters from the model.

6.3.4 Estimation of Pulse Parameters

Pulse parameters were estimated from glottal flow and area signals by locating time instants of specific events. In this approach, noise in the signals may distort the resulting parameter values severely, and the sampling frequency also affects the results. Furthermore, manual detection of such instants may have subjective bias, and automatic implementation of event detection easily leads to complex heuristic rules that lack theoretical and physiological basis.

An alternative approach would be to fit a mathematical model to the data and estimate parameters from the fitted model. This would allow estimating amplitudes and time points between sample values, and the estimates would be more robust (Strik, 1996). A disadvantage of this approach is that fitting a predefined model to the data does not allow studying signal features that are not included in the chosen model.

6.3.5 Suggestions for Technical Improvements

This section presents a list of practical suggestions that could improve the outcome of a similar research project in the future.

- The microphone should be fastened to the subject in the recording setting to prevent changes in the microphone distance and to avoid speculations about the microphone distance as a potential source of synchronization error.
- The quality of the EGG signal should be controlled before and during a recording session. If the signal is found to be weak or noisy, adjustments should be made to improve the signal quality if possible.
- More specific measurements should be carried out to evaluate possible delays and inaccuracies in the Huddinge measurement equipment. This would be necessary to improve the reliability and to decrease the uncertainty of the synchronization of the different signal sources.
- The algorithm of automatic glottal area detection could be improved to better trace the glottis when the opening is narrow.
- Methods for improving the time resolution of glottal area function should be considered. A modern camera system would be capable of recording images at a higher frame rate. But with the existing equipment, interpolation methods or utilization of several cycles for determining the pulse shape might improve the temporal precision.

6.4 Concluding Remarks

In this study, an combination of the following three voice analysis methods was utilized: inverse filtering, high-speed imaging, and electroglottography. Information obtained simultaneously by these methods was used to evaluate the inverse filtering method IAIF. The results suggest that IAIF produces reasonable estimates of glottal volume velocity waveform. However, experience is needed in the inverse filtering task.

The material of this study was also used to examine the behavior of the human voice source. The glottal flow waveform was found to be more skewed to the right than the corresponding glottal area pulse, which corroborates the results of earlier studies.

A two-stage opening phase was often encountered in the flow waveforms. In many such cases, the flow estimate increased from the base level before the opening of the vocal folds was indicated by high-speed images or the electroglottogram.

Finally, two details of the closing phase were studied. The minimum of the differentiated glottal flow waveform was found to take place mostly in the last 25 % of the closing phase, and it was also found to occur before the minimum of the differentiated EGG waveform.

Bibliography

Airas, M. (2004), 'Matsig - an object-oriented signal processing class library for MATLAB', web page. Referenced 22 December 2004.
URL `http://matsig.sourceforge.net/`

Airas, M. & Alku, P. (2004), 'Emotions in short vowel segments: Effects of the glottal flow as reflected by the normalized amplitude quotient', *in* E. André, L. Dybkjær & W. Minker, eds., 'Proceedings of Affective Dialogue Systems', Kloster Irsee, Germany, pp. 13–24.

Alku, P. (1992), 'Glottal wave analysis with pitch synchronous iterative adaptive inverse filtering', *Speech Communication*, vol. 11, pp. 109–119.

Alku, P., Bäckström, T. & Vilkman, E. (2002), 'Normalized amplitude quotient for parametrization of the glottal flow', *The Journal of the Acoustical Society of America*, vol. 112, no. 2, pp. 701–710.

Alku, P., Tiitinen, H. & Näätänen, R. (1999), 'A method for generating natural-sounding speech stimuli for cognitive brain research', *Clinical Neurophysiology*, vol. 110, pp. 1329–1333.

Ananthapadmanabha, T. & Yegnanarayana, B. (1975), 'Epoch extraction of voiced speech', *IEEE Transactions on Acoustics, Speech, and Signal Processing*, vol. ASSP-23, no. 6, pp. 562–570.

Baer, T., Löfqvist, A. & McGarr, N. S. (1983), 'Laryngeal vibrations: A comparison between high-speed filming and glottographic techniques', *The Journal of the Acoustical Society of America*, vol. 73, no. 4, pp. 1304–1308.

Baken, R. J. (1992), 'Electroglottography', *Journal of Voice*, vol. 6, no. 2, pp. 98–110.

Bäckström, T., Alku, P. & Vilkman, E. (2002), 'Time-domain parametrization of the closing phase of glottal airflow waveform from voices over a large intensity range', *IEEE Transactions on Speech and Audio Processing*, vol. 10, no. 3, pp. 186–192.

Cheng, Y. M. & O'Shaughnessy, D. (1989), 'Automatic and reliable estimation of glottal closure instant and period', *IEEE Transactions on Acoustics, Speech, and Signal Processing*, vol. 37, no. 12, pp. 1805–1815.

Childers, D., Smith, A. & Moore, G. (1984), 'Relationships between electroglottograph, speech, and vocal cord contact', *Folia Phoniatrica*, vol. 36, pp. 105–118.

Childers, D. D., Naik, J. M., Larar, J. N., Krishnamurthy, A. K. & Moore, G. P. (1983), 'Electroglottography, speech, and ultra-high speed cinematography', *in* I. R. Titze & R. C. Scherer, eds., 'Vocal Fold Physiology, Biomechanics, Acoustics and Phonatory Control', The Denver Center for The Performing Arts, Denver, pp. 202–220.

Claes, T., Dologlou, I., ten Bosch, L. & Compernolle, D. V. (1998), 'A novel feature transformation for vocal tract length normalization in automatic speech recognition', *IEEE Transactions on Speech and Audio Processing*, vol. 6, no. 6, pp. 549–557.

Colton, R. H. & Conture, E. G. (1990), 'Problems and pitfalls of electroglottography', *Journal of Voice*, vol. 4, no. 1, pp. 10–24.

de Cheveigné, A. & Kawahara, H. (2002), 'YIN, a fundamental frequency estimator for speech and music', *The Journal of the Acoustical Society of America*, vol. 111, no. 4, pp. 1917–1930.

Doebelin, E. O. (1975), *Measurement Systems, Application and Design*, McGraw-Hill, revised edn.

El-Jaroudi, A. & Makhoul, J. (1991), 'Discrete all-pole modeling', *IEEE Transactions on Signal Processing*, vol. 39, no. 2, pp. 411–423.

Eysholdt, U., Tigges, M., Wittenberg, T. & Pröschel, U. (1996), 'Direct evaluation of high-speed recordings of vocal fold vibrations', *Folia Phoniatrica et Logopaedica*, vol. 48, pp. 163–170.

Fabre, P. (1940), 'Sphygmographie par simple contact d'électrodes cutanées, introduisant dans l'arterè de faibles courants de haute fréquence détecteurs de ses variations volumétriques', *Comptes Rendus Soc Biol*, vol. 133, pp. 639–641.

Fabre, P. (1957), 'Un procédé électrique percutané d'inscription de l'accolement glottique au cours de la phonation: Glottographie de haute fréquence', *Bulletin de l'Académie Nationale de Médicine*, vol. 141, pp. 66–69.

Fant, G. (1960), *Acoustic Theory of Speech Production*, Mouton, The Hague.

Fant, G., Liljencrants, J. & Lin, Q. (1985), 'A four-parameter model of glottal flow', *Speech Transmission Laboratory Quarterly Progress and Status Report (STL-QPSR), Royal Institute of Technology, Stockholm*, vol. 4, pp. 1–13.

Farnsworth, D. (1940), 'High-speed motion pictures of the human vocal cords', *Bell Laboratories Record*, vol. 18, pp. 203–208.

Flanagan, J. L. (1972), *Speech Analysis Synthesis and Perception*, Springer-Verlag, second edn.

Fritzell, B. (1992), 'Inverse filtering', *Journal of Voice*, vol. 6, no. 2, pp. 111–114.

Gobl, C. & Chasaide, A. N. (2003), 'The role of voice quality in communicating emotion, mood and attitude', *Speech Communication*, vol. 40, no. 1–2, pp. 189–212.

Granqvist, S., Hertegård, S., Larsson, H. & Sundberg, J. (2003), 'Simultaneous analysis of vocal fold vibration and transglottal airflow; exploring a new experimental setup', *Speech, Music and Hearing, Quarterly Progress and Status Report (TMH-QPSR), Royal Institute of Technology, Stockholm*, vol. 45, pp. 35–46.

Henrich, N., d'Alessandro, C., Doval, B. & Castellengo, M. (2004), 'On the use of the derivative of electroglottographic signals for characterization of nonpathological phonation', *The Journal of the Acoustical Society of America*, vol. 115, no. 3, pp. 1321–1332.

Hertegard, S. & Gauffin, J. (1992), 'Acoustic properties of the rothenberg mask', *Speech Transmission Laboratory Quarterly Progress and Status Report (STL-QPSR), Royal Institute of Technology, Stockholm*, vol. 2–3, pp. 9–18.

Hertegård, S. & Gauffin, J. (1995), 'Glottal area and vibratory patterns studied with simultaneous stroboscopy, flow glottography, and electroglottography', *Journal of Speech and Hearing Research*, vol. 38, pp. 85–100.

Hertegård, S., Gauffin, J. & Karlsson, I. (1992), 'Physiological correlates of the inverse filtered flow waveform', *Journal of Voice*, vol. 6, no. 3, pp. 224–234.

Hertegård, S., Gauffin, J. & Åke Lindestad, P. (1995), 'A comparison of subglottal and intraoral pressure measurements during phonation', *Journal of Voice*, vol. 9, pp. 149–155.

Hertegård, S., Larsson, H. & Wittenberg, T. (2003), 'High-speed imaging: applications and development', *Logopedics Phoniatrics Vocology*, vol. 28, pp. 133–139.

Holmberg, E., Hillman, R. & Perkell, J. (1988), 'Glottal airflow and transglottal air pressure measurements for male and female speakers in soft, normal, and loud voice', *The Journal of the Acoustical Society of America*, vol. 84, no. 2, pp. 511–529.

Holmes, J. (1962), 'An investigation of the volume velocity waveform at the larynx during speech by means of an inverse filter', *in* 'Proceedings of the 4th International Congress on Acoustics', Copenhagen.

Hunt, M. J., Bridle, J. S. & Holmes, J. N. (1978), 'Interactive digital inverse filtering and its relation to linear prediction methods', *in* 'Proceedings of the IEEE International Conference on Acoustics, Speech, and Signal Processing (ICASSP '78)', vol. 3, pp. 15–18.

Javkin, H. R., Antonanzas-Barroso, N. & Maddieson, I. (1987), 'Digital inverse filtering for linguistic research', *Journal of Speech and Hearing Research*, vol. 30, pp. 122–129.

Karjalainen, M. (2000), *Kommunikaatioakustiikka*, Otamedia Oy.

Kiritani, S., Honda, K., Imagawa, H. & Hirose, H. (1986), 'Simultaneous high-speed digital recording of vocal fold vibration and speech signal', *in* 'Proceedings of the IEEE International Conference on Acoustics, Speech, and Signal Processing', vol. 11, Tokyo, Japan, pp. 1633–1636.

Kiritani, S., Imagawa, H. & Hirose, H. (1990), 'Vocal cord vibration and voice source characteristics – observations by a high-speed digital recording', *in* 'Proceedings of the International Conference on Spoken Language Processing (ICSLP '90)', Kobe, Japan, pp. 61–64.

Klaucke, D., Sunderland, N., Gogstad, E. & Wren, S. (2004), 'Standard deviation and standard error of the mean', web page. Referenced 24 January 2005.
URL `http://www.cdc.gov/epo/dih/MiniModules/sd_sem/page01.htm`

Krishnamurthy, A. & Childers, D. (1981), 'Vocal fold vibratory patterns: Comparison of film and inverse filtering', *in* 'Proceedings of the IEEE International Conference on Acoustics, Speech, and Signal Processing (ICASSP '81)', vol. 6, pp. 133–136.

Laininen, P. (2000), *Tilastollisen analyysin perusteet*, 597, Otatieto, Helsinki, second edn.

Larsson, H., Hertegård, S., Lindestad, P. & Hammarberg, B. (2000), 'Vocal fold vibrations: High-speed imaging, kymography, and acoustic analysis: A preliminary report', *The Laryngoscope*, vol. 110, pp. 2117–2122.

Laukkanen, A.-M. & Leino, T. (1999), *Ihmeellinen ihmisääni*, Gaudeamus.

Lauri, E.-R., Alku, P., Vilkman, E., Sala, E. & Sihvo, M. (1997), 'Effects of prolonged oral reading on time-based glottal flow waveform parameters with special reference to gender differences', *Folia Phoniatrica et Logopaedica*, vol. 49, pp. 234–246.

Lecluse, F., Brocaar, M. & Verschuure, J. (1975), 'The electroglottography and its relation to glottal activity', *Folia Phoniatrica*, vol. 27, pp. 215–224.

Lehto, L., Airas, M., Björkner, E., Sundberg, J. & Alku, P. (2005), 'Comparison of two inverse filtering methods for determining the normalized amplitude quotient and closing quotient - voice source characteristics in different phonation types', *Journal of Voice*. Manuscript in preparation.

Ma, C., Kamp, Y. & Willems, L. F. (1994), 'A frobenius norm approach to glottal closure detection from the speech signal', *IEEE Transactions on Speech and Audio Processing*, vol. 2, no. 2, pp. 258–265.

Marasek, K. (1997), 'EGG & voice quality', web page. Referenced 20 December 2004.
URL `http://www.ims.uni-stuttgart.de/phonetik/EGG/`

Markel, J. E. & Gray, A. (1976), *Linear Prediction of Speech*, Springer-Verlag.

Merriam-Webster (2004), 'Merriam-Webster OnLine', web page. Referenced 30 November 2004.
URL `http://www.webster.com/`

Miller, R. (1959), 'Nature of the vocal cord wave', *The Journal of the Acoustical Society of America*, vol. 31, no. 6, pp. 667–677.

Owens, R. (1997), 'Classical feature detection', web page. Referenced 23 December 2004.
URL `http://homepages.inf.ed.ac.uk/rbf/CVonline/LOCAL_COPIES/OWENS/LECT6/node2.html`

Pindyck, R. S. & Rubinfeld, D. L. (1998), *Econometric Models and Economic Forecasts*, McGraw-Hill, fourth edn.

Rabiner, L. R. & Gold, B. (1975), *Theory and Application of Digital Signal Processing*, Prentice-Hall.

Rosenberg, A. E. (1971), 'Effect of glottal pulse shape on the quality of natural vowels', *The Journal of the Acoustical Society of America*, vol. 49, no. 2, pp. 583–590.

Rothenberg, M. (1973), 'A new inverse-filtering technique for deriving the glottal air flow waveform during voicing', *The Journal of the Acoustical Society of America*, vol. 53, no. 6, pp. 1632–1645.

Rothenberg, M. (1981a), 'Acoustic interaction between the glottal source and the vocal tract', *in* K. Stevens & M. Hirano, eds., 'Vocal fold physiology', University of Tokyo Press, Tokyo, pp. 305–323.

Rothenberg, M. (1981b), 'Some relations between glottal air flow and vocal fold contact area', *in* C. Ludlow & M. Hart, eds., 'Proceeding of the conference on the assessment of vocal pathology', vol. 11, American Speech-Language-Hearing Association, Rockville, MD, pp. 88–96.

Sakakibara, K.-I., Imagawa, H., Konishi, T., Kondo, K., Murano, E. Z., Kumada, M. & Niimi, S. (2001), 'Vocal fold and false vocal fold vibrations in throat singing and synthesis of khöömei', *in* 'Proceedings of the International Computer Music Conference 2001', International Computer Music Association, pp. 135–138.

Sakakibara, K.-I., Kimura, M., Imagawa, H., Niimi, S. & Tayama, N. (2004), 'Physiological study of the supraglottal structure', *in* 'Proceedings of the International Conference on Voice Physiology and Biomechanics', Association de Formation et de Recherche en Orthophonie Phoniatrie.

Scarborough, J. (1955), *Numerical Mathematical Analysis*, The Johns Hopkins Press, Baltimore, 3rd edn.

Scherer, R. C., Druker, D. G. & Titze, I. R. (1988), 'Electroglottography and direct measurement of vocal fold contact area', *in* O. Fujimora, ed., 'Vocal Physiology: Voice Production, Mechanisms and Functions', Raven Press, New York, pp. 279–291.

Schutte, H. K. & Miller, D. G. (2001), 'Measurement of closed quotient in a female singing voice by electroglottography and videokymography', *in* 'Proceedings of the 5th International Conference on Advances in Quantitative Laryngoscopy, Voice and Speech Research', Groningen.

Smits, R. & Yegnanarayana, B. (1995), 'Determination of instants of significant excitation in speech using group delay function', *IEEE Transactions of Speech and Audio Processing*, vol. 3, no. 5.

Stevens, K. N. (1998), *Acoustic Phonetics*, The MIT Press.

Story, B. H. (2002), 'An overview of the physiology, physics and modeling of the sound source for vowels', *Acoustical Science and Technology*, vol. 23, no. 4, pp. 195–206.

Strik, H. (1996), 'Comments on "Effects of bandwidth on glottal airflow waveforms estimated by inverse filtering" [J. Acoust. Soc. Am. 98, 763–767 (1995)]', *The Journal of the Acoustical Society of America*, vol. 100, no. 2, pp. 1246–1249.

Strik, H. (1998), 'Automatic parametrization of differentiated glottal flow: Comparing methods by means of synthetic flow pulses', *The Journal of the Acoustical Society of America*, vol. 103, no. 5, pp. 2659–2669.

Strube, H. W. (1974), 'Determination of the instant of glottal closure from the speech wave', *The Journal of the Acoustical Society of America*, vol. 56, no. 5, pp. 1625–1629.

Švec, J. G. & Schutte, H. K. (1996), 'Videokymography: High-speed line scanning of vocal fold vibration', *Journal of Voice*, vol. 10, no. 2, pp. 201–205.

Södersten, M., Håkansson, A. & Hammarberg, B. (1999), 'Comparison between automatic and manual inverse filtering procedures for healty female voices', *Logopedics Phoniatrics Vocology*, vol. 24, pp. 26–38.

The MathWorks (2004), 'Matlab®7.0.1', web page. Referenced 22 December 2004. URL `http://www.mathworks.com/products/matlab/`

Titze, I. R. (1990), 'Interpretation of the electroglottographic signal', *Journal of Voice*, vol. 4, no. 1, pp. 1–9.

Titze, I. R. (1994), *Principles of Voice Production*, Prentice-Hall.

Titze, I. R., Story, B. H., Burnett, G. C., Holzrichter, J. F., Ng, L. C. & Lea, W. A. (2000), 'Comparison between electroglottography and electromagnetic glottography', *The Journal of the Acoustical Society of America*, vol. 107, no. 1, pp. 581–588.

Vaari, J. (1994), *Fysiikan laboratoriotyöt*, Suomen Fyysikkoseura, Jyväskylä.

Veldhuis, R. (1998), 'A computationally efficient alternative for the Liljencrants–Fant model and its perceptual evaluation', *The Journal of the Acoustical Society of America*, vol. 103, no. 1, pp. 566–571.

Vilkman, E., Lauri, E.-R., Alku, P., Sala, E. & Sihvo, M. (1997), 'Loading changes in time-based parameters of glottal flow waveforms in different ergonomic conditions', *Folia Phoniatrica et Logopaedica*, vol. 49, pp. 247–263.

Weinberger Vision (2004), 'Weinberger vision', web page. Referenced 23 December 2004. URL `http://www.weinbergervision.com/`

Wittenberg, T., Bloss, H., Gick, S., Heppner, W., Tigges, M., Popp, I. & Schmidt, R. (2001), 'Some thoughts about color-high-speed-cameras', *in* 'Proceedings of the 5th International Conference on Advances in Quantitative Laryngoscopy, Voice and Speech Research', Groningen.

Wittenberg, T., Tigges, M., Spinnler, K. & Eysholdt, U. (2000), 'Some thoughts about 3D and stereo in laryngoscopy', *in* 'Proceedings of the 4th International Workshop on Advances in Quantitative Laryngoscopy, Voice and Speech Research', Jena, pp. 116–123.

Wong, D. Y., Markel, J. D. & Gray, A. H. (1979), 'Least squares glottal inverse filtering from the acoustic speech waveform', *IEEE Transactions on Acoustics, Speech, and Signal Processing*, vol. ASSP-27, no. 4, pp. 350–355.

Appendix A

Huddinge Data

This appendix contains graphical illustrations of the pulse parameters derived from all examined flow and area pulses of the Huddinge material. Parameters are shown with error bounds that indicate the uncertainty due to limited time resolution.

For each examined sequence of five consecutive glottal periods, the inverse filtered flow waveform and the area pulse of the third of the five cycles are also shown. The flow and area pulses thus originate from the same glottal cycle, but they are not synchronized accurately in these illustrations.

In some cases, the area waveforms show obvious errors that are caused by incorrect tracing of the vocal fold edges by the automatic detection algorithm. Additionally, many individual area values were modified manually by tuning the area detection parameters for those image frames. This was done primarily in order to make the maximum of each area pulse coincide with the image frame that indicated maximum opening by visual inspection. In addition, the instants of opening and closure in the area waveforms were treated similarly to make them agree better with visual observations. This tuning of individual area values occasionally caused noticeable discontinuities in the overall pulse shapes. Consequently, the area pulses adjusted with this procedure cannot always be considered fully reliable.

Due to obvious detection errors and especially the inability of the area estimation software to detect very narrow openings, the area pulse parameters were, after all, calculated from manually marked instants of opening, maximum area, and closure. Thus, the parameters are not directly based on the area waveforms.

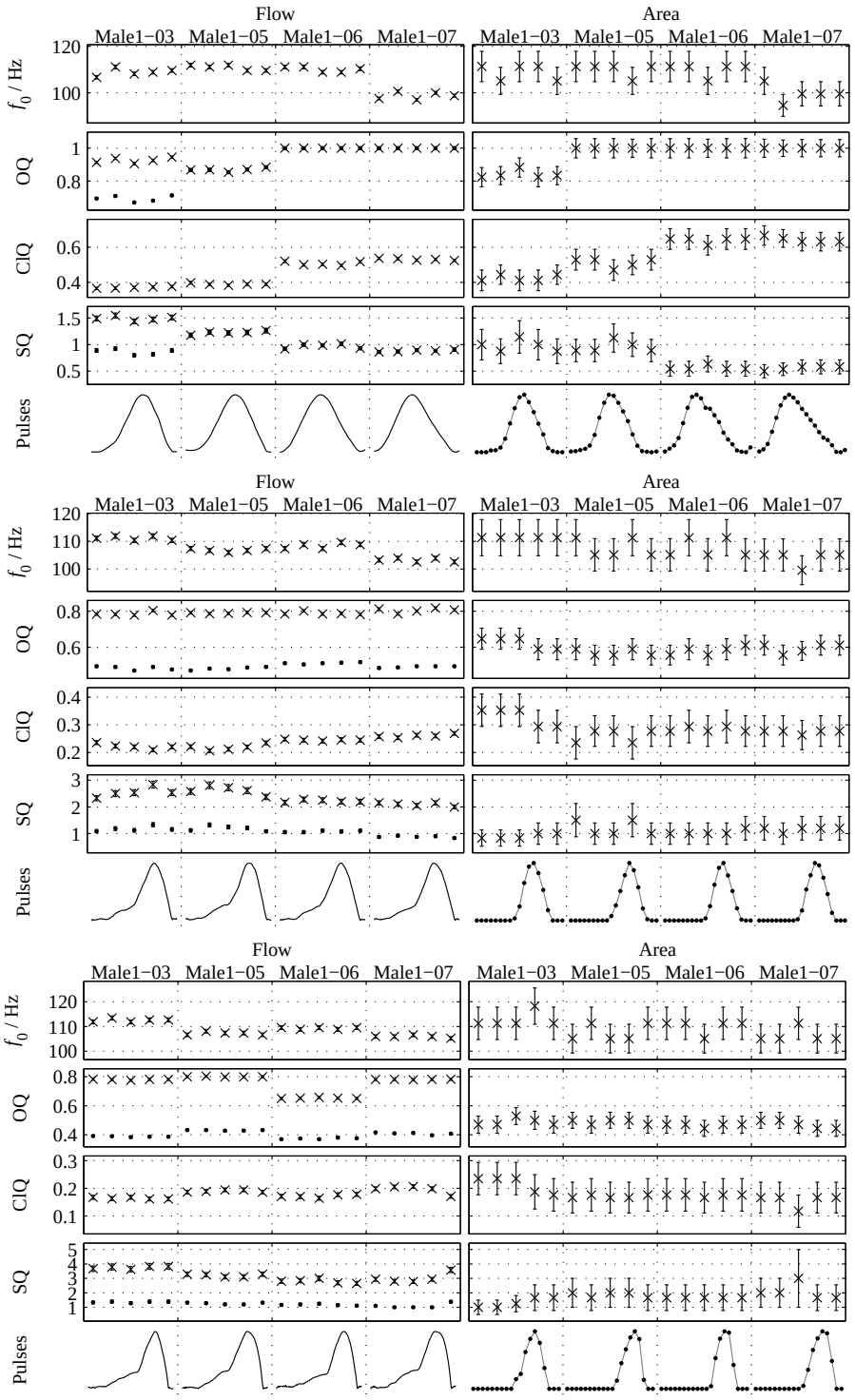

Figure A.1: Parameters estimated from breathy (top), normal (middle), and pressed (bottom) phonations of the subject Male 1. Each column with five values of each parameter corresponds to one recording from which five successive glottal periods have been analyzed. For OQ and SQ, cross ($\times$) denotes primary opening and dot ($\bullet$) denotes secondary opening. Vertical lines indicate estimated error boundaries due to limited time resolution. A sample pulse is shown for each phonation.

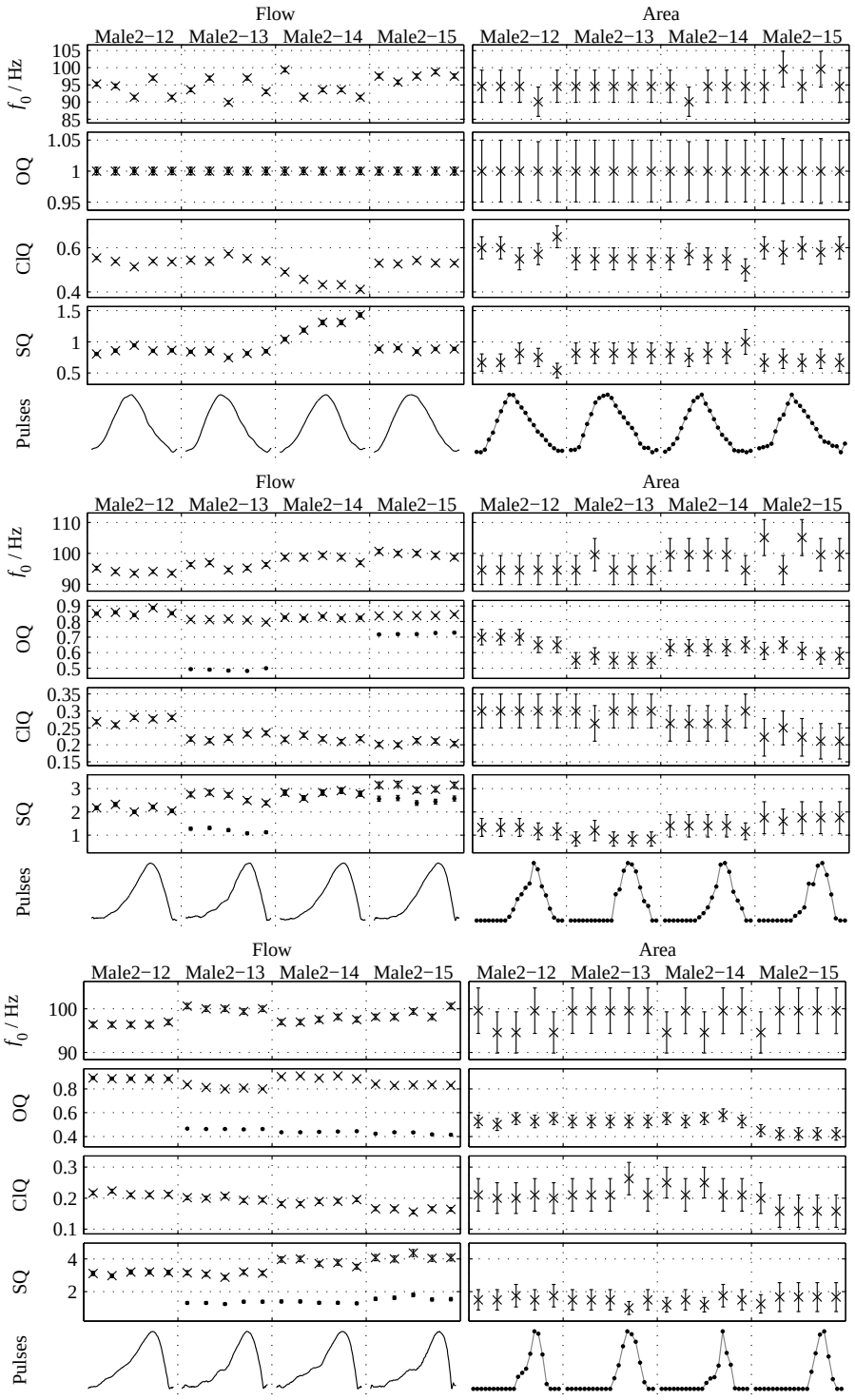

Figure A.2: Parameters estimated from breathy (top), normal (middle), and pressed (bottom) phonations of the subject Male 2. Each column with five values for each parameter corresponds to one recording from which five successive glottal periods have been analyzed. For OQ and SQ, cross ($\times$) denotes primary opening and dot ($\bullet$) denotes secondary opening. Vertical lines indicate estimated error boundaries due to limited time resolution. A sample pulse is shown for each phonation.

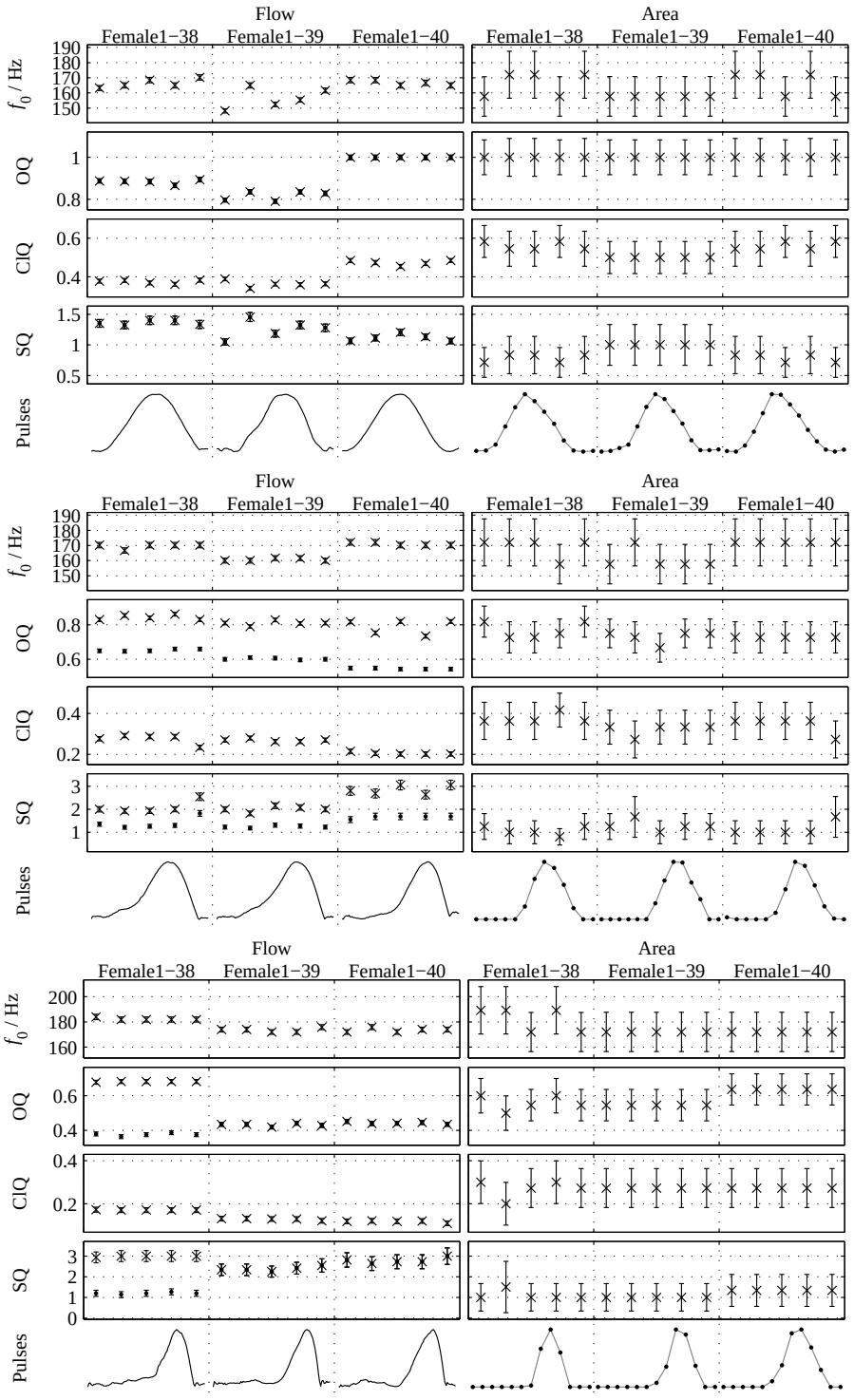

Figure A.3: Parameters estimated from breathy (top), normal (middle), and pressed (bottom) phonations of the subject Female 1. Each column with five values of each parameter corresponds to one recording from which five successive glottal periods have been analyzed. For OQ and SQ, cross (×) denotes primary opening and dot (•) denotes secondary opening. Vertical lines indicate estimated error boundaries due to limited time resolution. A sample pulse is shown for each phonation.

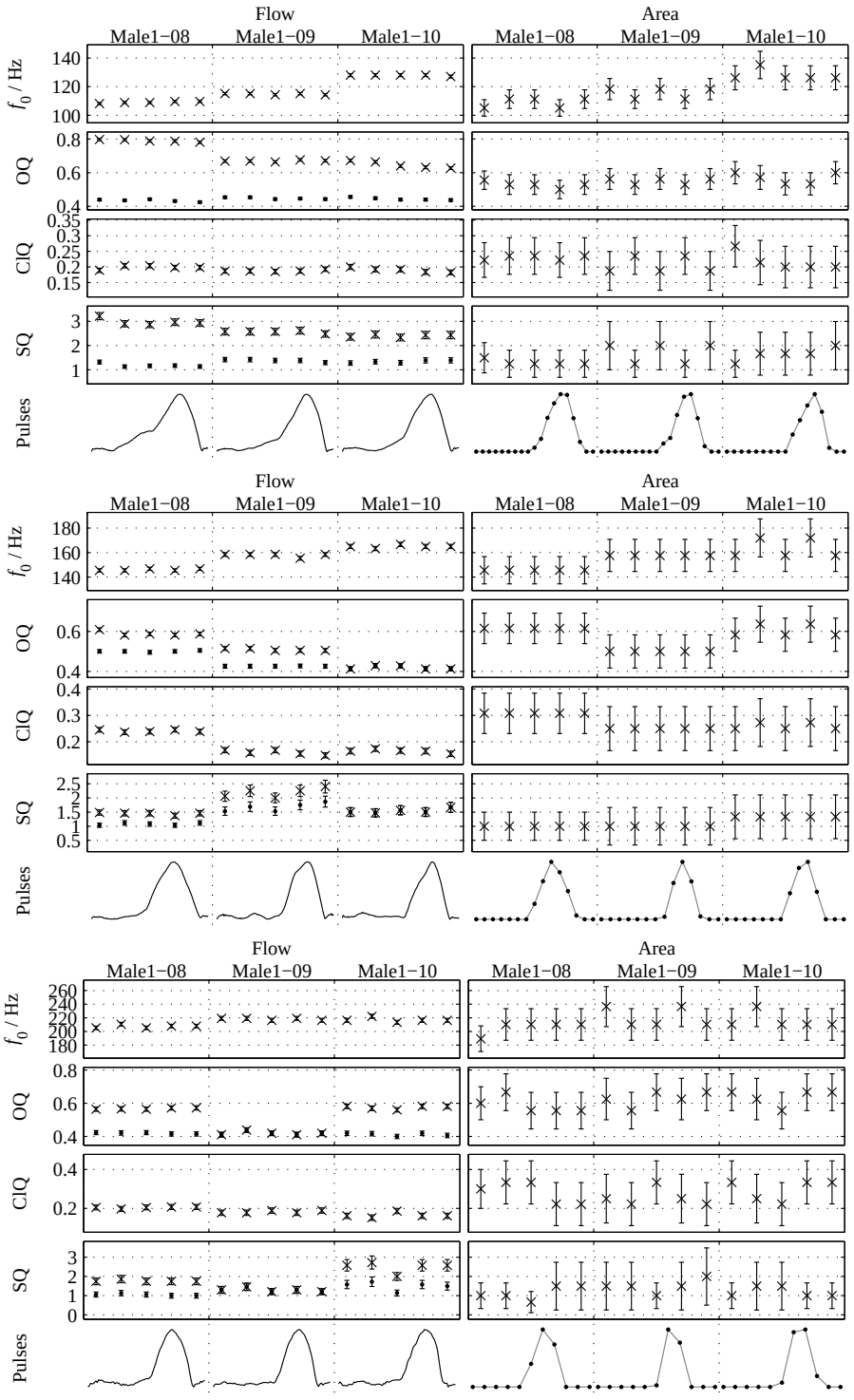

Figure A.4: Parameters estimated from soft (top), normal (middle), and loud (bottom) phonations of the subject Male 1. Each column with five values of each parameter corresponds to one recording from which five successive glottal periods have been analyzed. For OQ and SQ, cross (×) denotes primary opening and dot (•) denotes secondary opening. Vertical lines indicate estimated error boundaries due to limited time resolution. A sample pulse is shown for each phonation.

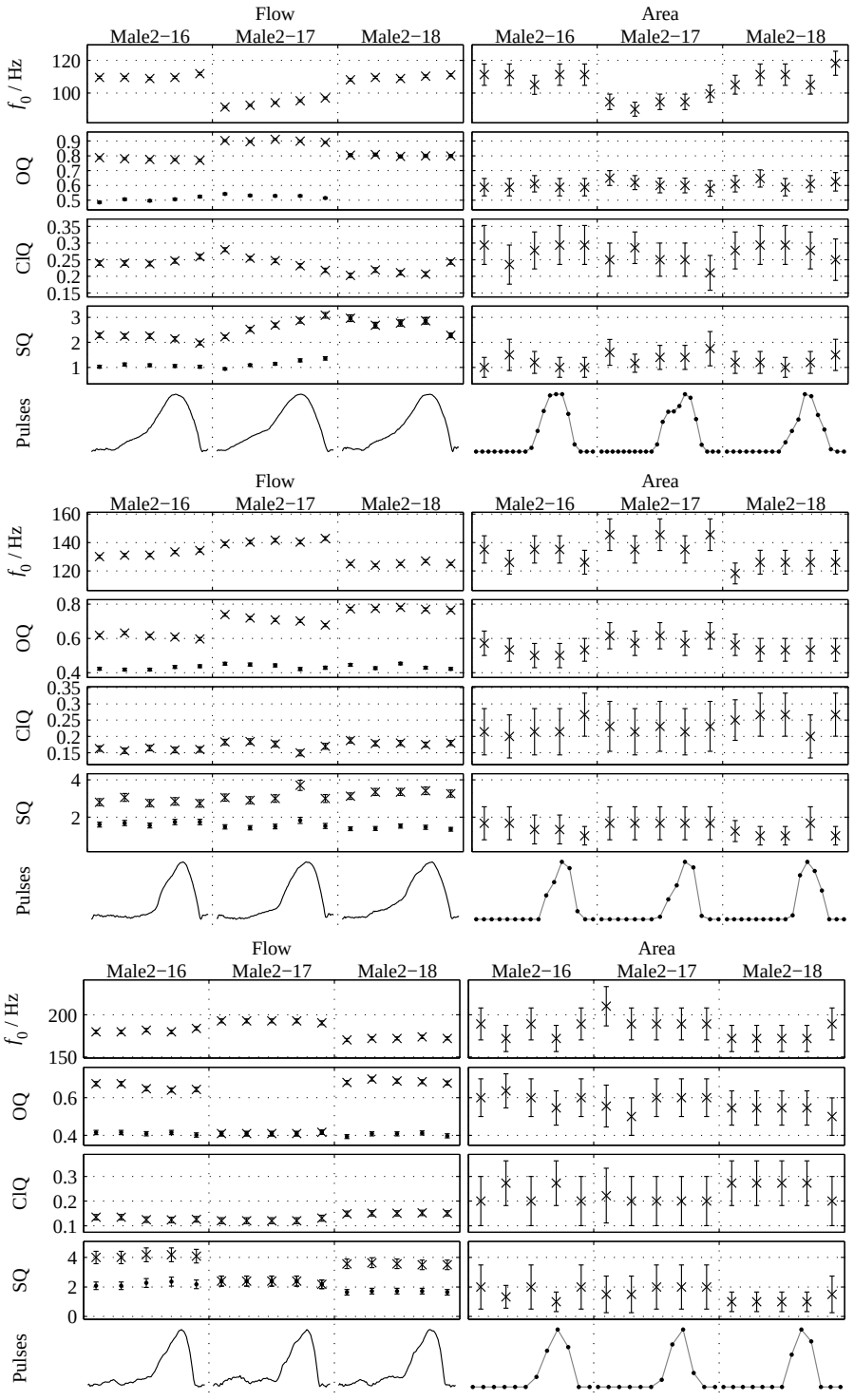

Figure A.5: Parameters estimated from soft (top), normal (middle), and loud (bottom) phonations of the subject Male 2. Each column with five values of each parameter corresponds to one recording from which five successive glottal periods have been analyzed. For OQ and SQ, cross (×) denotes primary opening and dot (•) denotes secondary opening. Vertical lines indicate estimated error boundaries due to limited time resolution. A sample pulse is shown for each phonation.

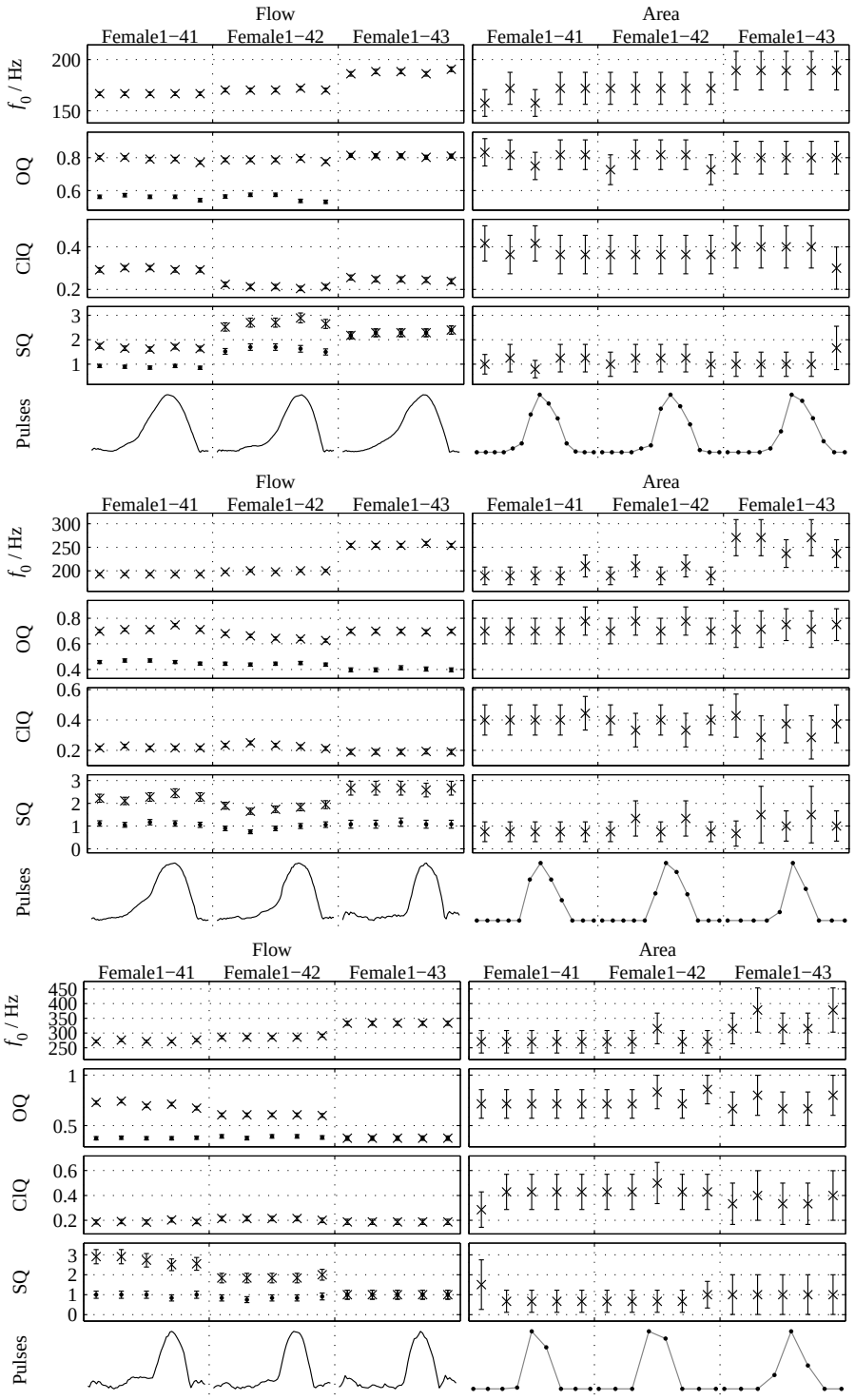

Figure A.6: Parameters estimated from soft (top), normal (middle), and loud (bottom) phonations of the subject Female 1. Each column with five values of each parameter corresponds to one recording from which five successive glottal periods have been analyzed. For OQ and SQ, cross (×) denotes primary opening and dot (•) denotes secondary opening. Vertical lines indicate estimated error boundaries due to limited time resolution. A sample pulse is shown for each phonation.